Secteur des Sciences de la Santé
Louvain Drug Research Institute
Groupe de Recherches en Résonance
Magnétique Biomédicale

Focus on tumor oxygen consumption: development of methods to measure oxygen consumption and evaluation of innovative co-treatment for radiotherapy

Caroline Diepart

Promoteur :
Professeur B. Gallez

Co-promoteur :
Professeur B. Jordan

Thèse présentée en vue de l'obtention du grade de Docteur en Sciences Biomédicales et Pharmaceutiques

2010

Si j'en suis arrivée là aujourd'hui, c'est bien par la patience, la disponibilité, les précieux conseils des gens qui ont croisé mon chemin.

Tout d'abord, je ne pourrais pas commencer les remerciements sans évoquer la personne qui m'a proposé le sujet de thèse et qui m'a encadré tout au long de ces 4 années: le professeur Bernard Gallez. Merci pour sa grande disponibilité à discuter des résultats obtenus, à lire les articles et abstracts, et à nous faire répéter pour les comités d'encadrement et congrès.
Je tiens également à remercier tout particulièrement Bénédicte Jordan, ma co-promotrice d'avoir toujours été disponible pour remédier aux manips foireuses, répondre à mes nombreuses questions, d'avoir passé de nombreuses heures à lire articles, abstracts, pour ces précieux conseils lors de la rédaction de ma thèse et enfin, pour le barbec annuel.
Merci à Julie pour sa patience lors de mon apprentissage à l'IRM et Matlab, à Philippe pour la résolution des problèmes informatiques, à Mickaël pour son aide aux différentes manips. Merci aussi à tous les autres membres de l'unité REMA : Kim, Oussama, Quentin, Pierre, Anne-Catherine, Linda qui chacun à leur manière contribue à la bonne ambiance du labo. Merci aussi aux anciens de l'unité REMA pour leur aide et conseils lors de mon apprentissage au labo : Nicolas, Mous et Nathalie.

Merci aux laboratoires FATH, PMNT et IMRE, particulièrement aux Professeurs Olivier Feron, Pedro Buc Calderon et Vincent Grégoire pour leur collaboration. Merci aussi à Julien Verrax pour ses nombreux conseils, sa patience et sa disponibilité lors de nos collaborations.

Je remercie tous les membres de mon Jury, c'est-à-dire Nathalie Delzenne, Vincent Grégoire, Olivier Feron, Samuel Valable et Mark De Ridder pour avoir lu et commenté mon manuscrit.

Je remercie également l'ARC et le Télévie pour le financement de cette thèse.

Et enfin, un grand merci à ma famille et mes amis (surtout à Julie avec qui j'ai parcouru ces 4 années de thèse) qui m'ont soutenu tout au long de cette thèse.

En mémoire de mon
petit frère, Romain

Table of contents

Abbreviations list

AA	ascorbic acid
APL	acute promyelocytic leukemia
As_2O_3	arsenic trioxide
ATRA	all-trans retinoic acid
BOLD	blood oxygen dependent level
BSO	buthionine sulfoxide
CDK	cyclin-dependent kinase
CBF	cerebral blood flow
CBV	cerebral blood volume
$CMRO_2$	cerebral metabolic rate of oxygen utilization
COX	cyclooxygenase
dHB	deoxyhemoglobin
EPR	electron paramagnetic resonance
EPRI	electron paramagnetic resonance imaging
FMISO	F-18-fluoromisonidazole
fMRI	functional magnetic resonance imaging
FREDOM	fluorocarbon relaxometry using for dynamic oxygen mapping
GPx	glutathione peroxidase
GRE	gradient recalled echo
GSH	gluthatione
GST	glutathione-S-transferase
Gy	Gray (unit of radiation dose)
Hb	hemoglobin
HbO2	oxygenated hemoglobin
HFB	hexafluorobenzene
HIF-1	hypoxia-inducible factor-1
KCl	potassium chloride
LiPc	lithium phtalocyanine
MIBG	meta-iodobenzylguanidine
MRI	magnetic resonance imaging
NAC	N-acetyl-L-cysteine

NIRS	near-infrared spectroscopy
NMR	nuclear magnetic resonance
NO	nitric oxide
NOS	nitric oxide synthase
NSAID	non steroidal anti-inflammatory drugs
OEF	oxygen extraction fraction
O_2-FET	oxygen field effect transistor
PET	positron emission tomography
PFC	perfluorocarbon
PG	prostaglandin
PML	promyelocytic leukemia
pO_2	oxygen partial pressure
qBOLD	quantitative blood oxygen dependent level
RAR	retinoic acid receptor
ROS	reactive oxygen species
SNAP-IR	snapshot inversion recovery
TCD 50	tumor control dose 50
TNF- α	tumor necrosis factor- α
VEGF	vascular endothelial growth factor

Abstract

Response to cancer treatment is largely influenced by the tumor microenvironment. One of the most important factors playing a crucial role in this process is the existence of hypoxia in solid tumors. It has been shown to decrease the therapeutic efficacy of radiation treatment, surgery and some forms of chemotherapy. Several studies have shown improved outcomes for cancer patients whose tumors have lower hypoxic fractions. Tumor hypoxia also promotes metastasis, selects cells with malignant phenotypes, and promotes angiogenesis.

Since inadequate tumor oxygenation is a considerable obstacle in the successful therapy of some human tumors, one relevant approach is the improvement of the O_2 status of hypoxic tumors or hypoxic areas during cytotoxic therapies. A number of strategies to improve tumor oxygenation and increase its uniformity have been considered. These include enhancing O_2 availability and/or reducing cellular respiration rate, parameters that crucially determine the O_2 status of a given tissue. Tumor oxygenation is a matter of supply and demand of the respiring cancer cells. However, modulation of O_2 consumption seems to be a much more efficient way of affecting the oxygenation status than modification of the O_2 availability through elevating blood flow. Several pharmacological drugs that inhibit cellular oxygen consumption have been characterized for their potential to increase tumor oxygenation and thereby enhance radiosensitivity.

In view of its clinical importance, several techniques have been developed to measure oxygenation status in tissues and tumors in living animals and humans, but methods to measure rates of oxygen consumption *in vitro* and *in vivo* are more limited. The literature was lacking of a systematic comparison between techniques able to measure oxygen consumption *in vitro*. For that reason, one of the thesis objectives was to compare the sensitivity of the methods for determining oxygen consumption (see chapter 3.I). Most of the *in vivo* methods available are not applicable in tumors (see chapter 1.IV.2). Consequently, we intended to develop new methods to measure the oxygen consumption of tumor cells non invasively (see chapter 3. II).

Arsenic trioxide (As_2O_3) has been demonstrated as potent antitumor agent against acute promyelocytic leukemia (APL) and more recently solid tumors, and could inhibit mitochondrial respiration function. We therefore made the hypothesis that As_2O_3

could be an important modulator of tumor oxygenation by affecting the oxygen consumption of tumor cells. The several effects of As_2O_3 are described in the introduction and its effects on oxygen consumption will be part of our research in the last chapter.

Chapter 1: Introduction

I. Tumor hypoxia

Solid tumors constitute approximately 90% of all known cancers. They develop from a single mutated cell and lead to significant morbidity and mortality, either by invading normal tissue or by metastatization to vital organs, such as liver, lung, or brain. The process of tumor progression (proliferation, local invasion, and distant metastasis) is characterized by rapid cellular growth accompanied by alterations of the microenvironment of the tumor cells. This results in poorly vascularized tumors characterized by hypoxia and low pH. To survive in this hypoxic microenvironment, tumor cells co-opt adaptative mechanisms to switch to glycolysis, promote malignant progression, become resistant to apoptosis and induce changes in the proteome and genome of neoplastic cells. Moreover, hypoxia hinders the efficacy of anti-tumor treatments such as radiation therapy and chemotherapy (Vaupel, 2004d, c; Vaupel, 1989; Ruan, 2009; Fukumura and Jain, 2007a, b).

1. Tumor vasculature and blood flow

To grow beyond a diameter of approximately 1mm, newly developing tumors must form their own vascular network and blood supply, which they accomplish either by incorporating pre-existing host vessels or by forming new microvessels through the influence of tumor angiogenic factors. The vascular endothelial growth factor (VEGF) plays a major role in physiological blood vessel formation and pathological angiogenesis in tumor growth. However, the newly formed vascular network differs greatly from that found in normal tissues. Normal microvessels consist of differentiated units such as arterioles, capillaries and venules, and form a well-organized architecture with dichotomous branching and hierarchic order (Jain, 2003). In contrast, tumor vessels are dilated, saccular, tortuous, and heterogeneous in their spatial distribution. Tumor vasculature is disorganized and has trifurcation and branches with uneven diameters (Figure 1). The walls of tumor vessels may have fenestrations, discontinuous or absent basement membranes and fewer pericytes than walls of normal vessels and may lack perivascular smooth muscle cells (Tredan, 2007). In addition, cancer cells may be integrated into the vessel wall. These abnormalities tend to make tumor vessels leaky,

although their permeability varies both within and among the tumors. The molecular mechanisms causing these abnormal vascular architectures are not well understood, but the imbalance of pro- and anti-angiogenic factors is considered to be a key contributor (Fukumura and Jain, 2008).

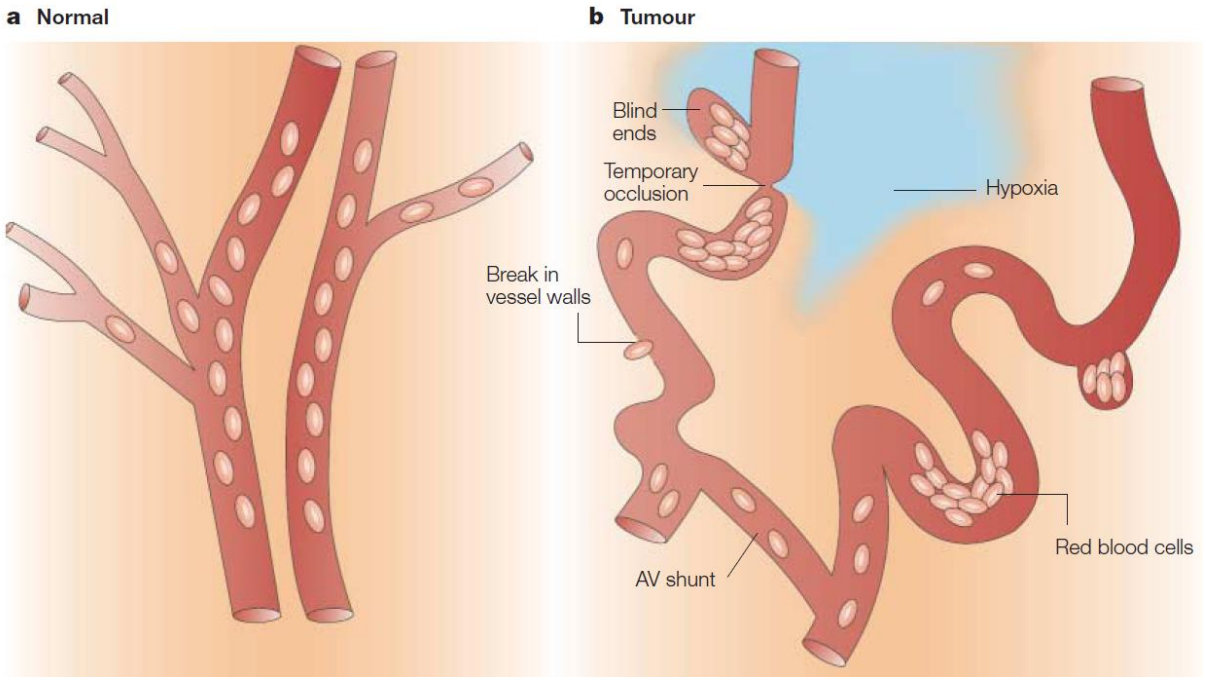

Figure 1: The vascular network of normal versus tumor tissue (Brown and Wilson, 2004).

Because of these features, blood flow in many tumors is disorganized and heterogeneous (Carmeliet, 2000). In a vascular network, flow rate is directly proportional to the difference in pressure between the arteries and the veins and inversely proportional to the viscous and geometric resistance. In tumors, the difference in pressure between arterioles and venules is reduced and viscous and geometric resistance is increased. These abnormalities, as well as the compression of blood vessels by cancer cells, increase resistance to blood flow and impair blood supply to the tumor (Tredan, 2007). In addition, vascular morphology and rates of blood flow may vary with location and with time, even in the same tumor (Gillies, 1999). As a result, there is reduction in delivery of nutrient metabolites and in the clearance of breakdown products of metabolism, leading to hypoxic and acidic regions in tumors (Tatum, 2006). Delivery of anticancer drugs is similarly compromised (Tredan, 2007).

Tumors exhibit interstitial hypertension while the interstitial fluid pressure in normal tissue is around zero mmHg (Fukumara and Jain, 2007b). The abnormal

structure and function of blood and lymphatic vessels in tumors cause the interstitial fluid pressure elevation. Tumor vessels lack permanent selectivity due to the high vascular permeability. As a result, the hydrostatic and oncotic pressures become almost equal between the intravascular and extravascular spaces (Boucher and Jain, 1992). The interstitial fluid pressure is uniformly high throughout a tumor and drops precipitously in the tumor margin (Boucher, 1990). Fluid convection or bulk flow is negligible inside tumors due to the lack of interstitial pressure gradients. Thus, the uniformly elevated interstitial fluid pressure compromises the delivery of the therapeutic agents both across the blood vessel wall and interstitum in tumors. On the other hand, the interstitial fluid oozes out from the tumor periphery into the surrounding normal tissue, carrying angiogenic, lymphangiogenic growth factors, and/or metastazing tumor cells with it. This may facilitate tumor invasion and metastasis (Fukumura and Jain, 2007a, b).

The normal lymphatic network maintains tissue interstitial fluid balance by draining excess fluid of the tissue. Proliferating tumor cells in a confined space create mechanical stress which compresses intra-tumor lymphatic vessels. Consequently, there are no functional lymphatic vessels inside solid tumors. The absence of functional lymphatics is another contributor of elevated tumor interstitial fluid pressure (Fukumura and Jain, 2008; Tredan, 2007).

2. Causes and consequences of tumor hypoxia

Molecular oxygen (O_2) is required for aerobic metabolism to maintain intracellular bioenergetics and to serve as an electron acceptor in many organic and inorganic reactions. Hypoxia occurs in a variety of pathological conditions, including stroke, tissue ischemia, inflammation and the growth of solid tumors. Here, hypoxia will be considered in the case of solid tumor development in which it plays an important function.

In 1955, Thomlinson and Gray showed the presence of hypoxic areas in the human lung tumors. Since, it has been suggested that most human tumors present regions of low levels of oxygen (Thomlinson and Gray, 1955; Tatum, 2006). Moreover, investigations have demonstrated that tumor hypoxia diminishes the radio- and chemotherapeutic efficacy, and plays a pivotal role in malignant progression (Bertout, 2008).

2.1. Oxygen status of tumors

Tissue oxygenation is determined by the balance between oxygen delivery to the tissue and oxygen consumption by the tissue. In normal tissues, this balance is maintained by normally distributed vascular networks, intact vascular signalling pathways, and direct alterations in oxygen consumption, all resulting in a normoxic environment. However, solid tumors are unable to maintain this balance, resulting in regions of decreased oxygenation. Ambient air is 21% O_2 (160 mmHg); however, most mammalian tissues exist at 2%-9% O_2 (on average 40 mmHg). Clinical investigations have demonstrated that the prevalence of hypoxic areas, for example areas with pO_2 values of 2.5 mmHg or less, is a characteristic pathophysiological property of locally advanced solid tumors and that these areas have been found in a wide range of human malignancies, including cancers of the breast, uterine cervix, head and neck, prostate, rectum,...(Tatum, 2006).

Accumulating evidences show that up to 50-60% of locally advanced solid tumors may exhibit heterogeneously distributed hypoxic and/or anoxic tissue areas within the tumor mass. The pretherapeutic oxygenation status assessed in cancers of the breast, uterine cervix, and head and neck is poorer than that assessed in the respective normal tissues, and it is independent of clinical size, stage, histology, grade, nodal status, and several other tumor characteristics or patients demographics (Vaupel, 2001; Tatum, 2006).

2.2. Causes of hypoxia

Hypoxia emerges in solid tumors as a result of several factors (Vaupel, 2004a; Tatum, 2006):

- Perfusion-limited oxygen delivery or **acute hypoxia** consists in transient fluctuation in the red cells flux and is caused by severe structural and functional abnormalities in the tumor microvessels. Perfusion-related hypoxia leads to ischemic hypoxia, which is often transient.
- Diffusion-limited oxygen delivery or **chronic hypoxia** is caused by an increase in diffusion distances with tumor expansion. This results in an inadequate O_2 supply for cells distant (>70 μm) from the nutritive blood vessels. Diffusion-related hypoxia may also be caused by deterioration of diffusion geometry, for example,

concurrent versus countercurrent blood flow within the tumor microvessel network.

- Anemic hypoxia is caused by reduced O_2 transport capacity of blood subsequent to tumor-associated or therapy-induced anemia.

In reality, the hypoxia concepts are more complex processes. There both consist in spatial and temporal fluctuations in oxygenation. Two types of oxygen gradients within tumors have been identified: radial gradients, resulting from oxygen diffusion limitations, and longitudinal gradients, resulting from depletion of oxygen from hemoglobin as it progresses from the arterial to the venous circulation (Cardenas-Navia, 2007). One of the factors affecting oxygen gradients within tumors is the irregular vascular network that exists in tumors. Imbalanced expression of various cytokines results in the classic characteristics of tumor vasculature (Hardee, 2009).

Tumor oxygen consumption can also contribute to the hypoxic microenvironment, even though tumor cells do not have drastically increased oxygen consumption rates compared to that of normal tissues. However, there is clearly an imbalance between consumption rates and oxygen delivery that will result in hypoxic conditions (Thews, 1999). The tumor oxygenation is also unsteady and can change in part due to remodelling of tumor vasculature. Transient blood flow has been demonstrated in animal models, not only in terms of temporal fluctuations in blood flow, but also heterogeneity in the magnitude and frequency of these fluctuations (Durand, 1995; Chaplin and Hill, 1995; Dewhirst, 2008). Intravascular hypoxia resulting from longitudinal O_2 gradients has also been demonstrated. The overall oxygenation state of tumors varies with the average magnitude of oxygen delivery and the instability in red cell flux of surrounding microvessels (Dewhirst, 1999; Hardee, 2009).

2.3. Consequences of hypoxia

2.3.a. Impact on tumor metabolism

The tumor hypoxic microenvironment, resulting from inadequate and disordered neo-vasculature, selects for tumor cells that could respond and adapt to oxygen deficiency. The hypoxia-inducible factor-1 (HIF-1) permits tumor cells to adapt by inducing hypoxia responsive genes. HIF-1 is a heterodimeric transcription factor consisting of two subunits: HIF-1α and HIF-1β. The first one is independent of O_2 tension

and the second one is responsive to O_2 levels. Under hypoxic conditions, HIF-1α subunits translocate to the nucleus, where they heterodimerize with HIF-1β subunits. The resultant product is an active HIF-1 protein that binds to specific hypoxic response elements present in target genes, ultimately activating transcription of these genes which encode for glucose transporters, enzymes in glycolytic pathway, erythropoietin and vascular endothelial growth factor (VEGF). HIF-1 is involved in processes associated with cancer progression, such as angiogenesis and invasion. In most cases, increased HIF-1 expression clearly correlates with poor clinical outcomes: high mortality rate, poor response to radiation and chemotherapy, and metastasis (Carmeliet, 1998; Kim, 2007; Vaupel, 2004d; Ruan, 2009).

Under normoxic conditions, cells generate ATP via oxidative phosphorylation. However, in the expanding tumor mass, which is generally characterized by a limited O_2 supply and high glucose consumption rate, anaerobic glycolysis can become the predominant pathway of ATP generation. The high rate of glycolysis typically displayed by cancer cells is known as the Warburg effect (Warburg, 1956) (Figure 2). Warburg found that cancer cells tend to "ferment" glucose into lactate even in the presence of sufficient oxygen to support mitochondrial oxidative phosphorylation (Fang, 2008; Vander Heiden, 2009). The lactate produced when oxidative phosphorylation is switched to glycolysis to maintain energy production causes an acidic microenvironment to occur in tumor cells (Schmaltz, 1998). Pyruvate, a glucose metabolite, is converted into lactate instead of undergoing oxidative phosphorylation in the mitochondria due to the lack of oxygen, the final electron acceptor after the mitochondrial electron transport chain. Recent findings showed that lactate produced by hypoxic tumor cells may diffuse and be taken up by oxygenated tumor cells which thus spare glucose, making it more easily available for hypoxic tumor cells located far from blood vessels (Feron, 2009). HIF-1 has been known as a major transcription factor for the induction of virtually all genes encoding glucose transporters and glycolytic enzymes, which allows hypoxic tumor cells to take up the glucose more efficiently and metabolize pyruvate to lactate (Semenza, 2006; Denko, 2008). HIF-1 activation correlates with an accelerated glycolytic flux under hypoxic conditions, which contributes to restoration of ATP levels and tumor growth (Carmeliet, 1998).

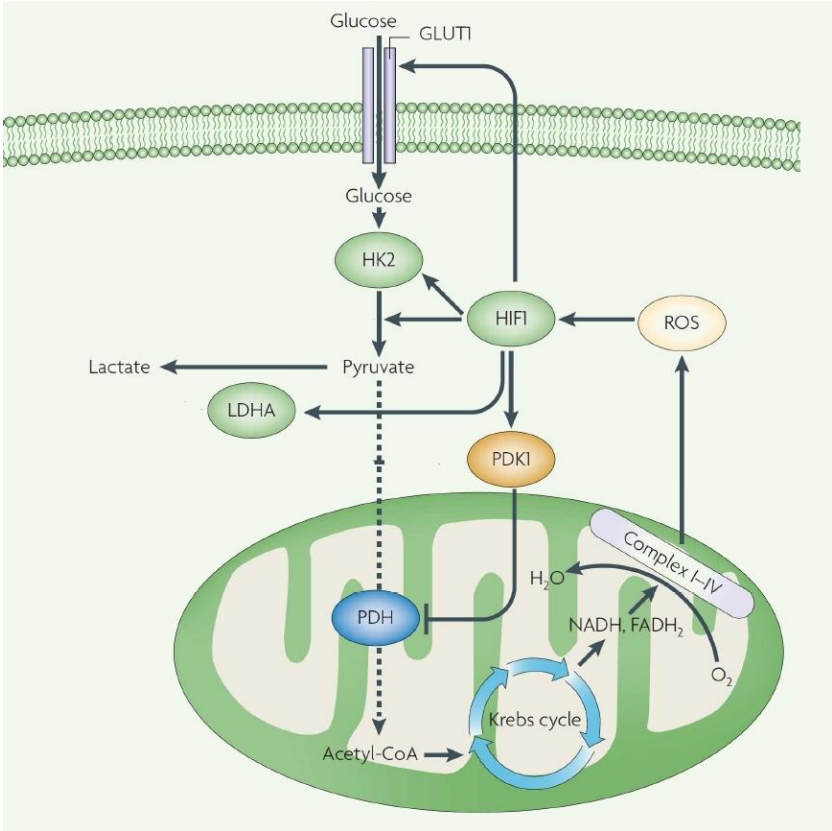

Figure 2: Molecular aspects of the Warburg effect and HIF-1 interactions. Glucose is shown transported across the plasma membrane. Hypoxia-inducible factor 1 (HIF-1) activates hexokinase 2 (HK2) and pyruvate dehydrogenase kinase 1 (PDK1), resulting in enhanced conversion of glucose to lactic acid. HIF-1 activates the glucose transporter GLUT1 and lactate dehydrogenase A (LDHA). All of this contributes to the Warburg effect. PDH, pyruvate dehydrogenase; ROS, reactive oxygen species (adapted from Dang, 2008).

Although glycolysis and the production of lactic acid in cancer cells can lower the pH in tumors, carbonic anhydrase might also be involved. These enzymes catalyse the reversible hydration of CO_2 to carbonic acid and are upregulated by HIF-1 under hypoxic conditions (Helmlinger, 2002). Recent findings showed an important role of carbonic anhydrase 9 in regulating the pH of tumors (Swietach, 2009). Interestingly, high-resolution measuring techniques have shown that hypoxic and acidic conditions do not need to occur concomitantly in tumors (Helmlinger, 1997). This is probably due to the disordered blood flow within a tumor, with vessels closing and re-opening, meaning transient hypoxia can occur in a region where the pH is normal (Helmlinger, 1997; Schmaltz, 1998). A study showed that tumor cells were able to survive under hypoxic

and buffered conditions. However, apoptosis occurred when the tumor cells were tested under hypoxic and non-buffered conditions (Schmaltz, 1998). Lowering of pH may therefore, be a more important factor than hypoxia in tumor cell death (Harris, 2002). These experiments indicate that when hypoxia is uncoupled from acidosis, as occurs in areas of tumors with disordered blood flow, tumor cells survive in conditions where normal cells would not, leading to treatment resistance and a subsequent growth advantage (Schmaltz, 1998).

Since fatty acid is one of the key components for the biosynthesis of membrane, it is speculated that increased fatty acid synthesis may confer tumor cell proliferation and survival under hypoxic conditions. Intriguingly, fatty acid synthase, a key enzyme that is involved in the novo fatty acid synthesis, is implicated in many types of human tumors and is induced by a hypoxic and/or acidic microenvironment (Kuhajda, 2006). Inhibition of the fatty acid synthase induced cancer cell death *in vitro* and tumor regression *in vivo* (Pizer, 1996). The modulation of lipid metabolism is independent of HIF induction.

2.3.b. Tumor hypoxia and malignant progression

Hypoxia can influence tumor cells by acting as a stressor that impairs growth or causes cell death or by serving as a factor that results in malignant progression and increases resistance to radiation therapy and other cancer treatments (Figure 3). Furthermore, sustained hypoxia can change the cell cycle distribution and the relative number of quiescent cells. The degree of inhibition of cell proliferation depends on the severity of duration of hypoxia, on the coexistence of other microenvironmental inadequacies (e.g., acidosis, glucose depletion), and on the cell line investigated (Höckel, 2001a). The response of cells exposed to hypoxia in terms of the cell cycle is in most cases a G1/S-phase arrest. Hypoxia levels necessary to induce a disproportionate lengthening of G_1 or an accumulation of cells in this cycle phase are in the range of 0.2-1 mmHg (Amellem, 1994; Vaupel, 2004b). Above this hypoxic threshold, the environmental O_2 status appears to have only negative effects on the proliferation rate. Under anoxia, most cells undergo immediate arrest in whichever phase of the cell cycle they are in.

Hypoxia can induce programmed cell death (apoptosis) both in normal and in neoplastic cells. p53 accumulates in cells under hypoxic conditions and induces apoptosis involving Apaf-1 and caspase-9 as important downstream effectors (Soengas,

1999). However, hypoxia also initiates p53-independent apoptosis pathways, including those involving genes of the Bcl-2 family and others. Below a critical energy state, hypoxia/anoxia may result in necrotic cell death, a phenomenon seen in many human tumors and experimental tumor models. Hypoxia-induced proteome changes leading to cell cycle arrest, differentiation, apoptosis, and necrosis may explain delayed recurrences, dormant micrometastases, and growth retardation in large tumor masses (Prehn, 1991; Holmgren, 1995; Vaupel, 2004b).

Accumulating evidences suggest that hypoxia may lead to malignant progression by means of genomic changes in the tumor cells and clonal selection. Hypoxia, with or without reoxygenation, promotes genomic instability through point mutations, gene amplification, and chromosomal rearrangement (Rofstad, 2000). The frequency of mutations in the cells within the murine tumors was found to be five times that of the comparator culture cells. Exposure of cultured cells to hypoxic conditions produced an elevated mutation frequency and a mutation pattern similar to those observed in the tumor-grown cells (Yuan, 1998). Point mutations may develop in tumor cells exposed to hypoxia and reoxygenation through several mechanisms, including insufficient DNA repair, errors in DNA replication, or both (Reynolds, 1996; Yuan, 2000). Several studies have demonstrated that hypoxia followed by reoxygenation can lead to gene amplification, which, together with chromosomal rearrangement, can be caused by DNA strand breaks or decreased repair of DNA strand breaks (Rofstad, 2000). Hypoxia-induced point mutations, chromosomal rearrangement, and gene amplification may, in turn, promote development of metastatic disease by several mechanisms, including inactivation of metastasis suppressor genes or increased expression of oncogenes involved in the metastasis process, for example encoding for angiogenesis and growth factors (Vaupel, 2004d).

It has also been suggested that hypoxia exerts a strong selection pressure on malignant cells. Tumor cell variants with adaptations favourable to survival under hypoxic conditions (e.g., decreased capacity for cell-cycle arrest, differentiation, or apoptosis, or increased angiogenic potential) may have selection advantages over nonadapted cells in the hypoxic microenvironment and expand through clonal selection. The expansion of cell clones with favourable proteomic and genomic adaptative changes can, in turn, exacerbate tumor hypoxia, thereby establishing a vicious circle of increasing hypoxia and subsequent malignant progression. At the clinical level, the consequences of

this vicious circle are translated into more local recurrences, locoregional spread, and distant tumor metastases, and greater resistance to radiation therapy and certain form of chemotherapy (Höckel, 1999; Höckel, 2001b; Vaupel 2004d).

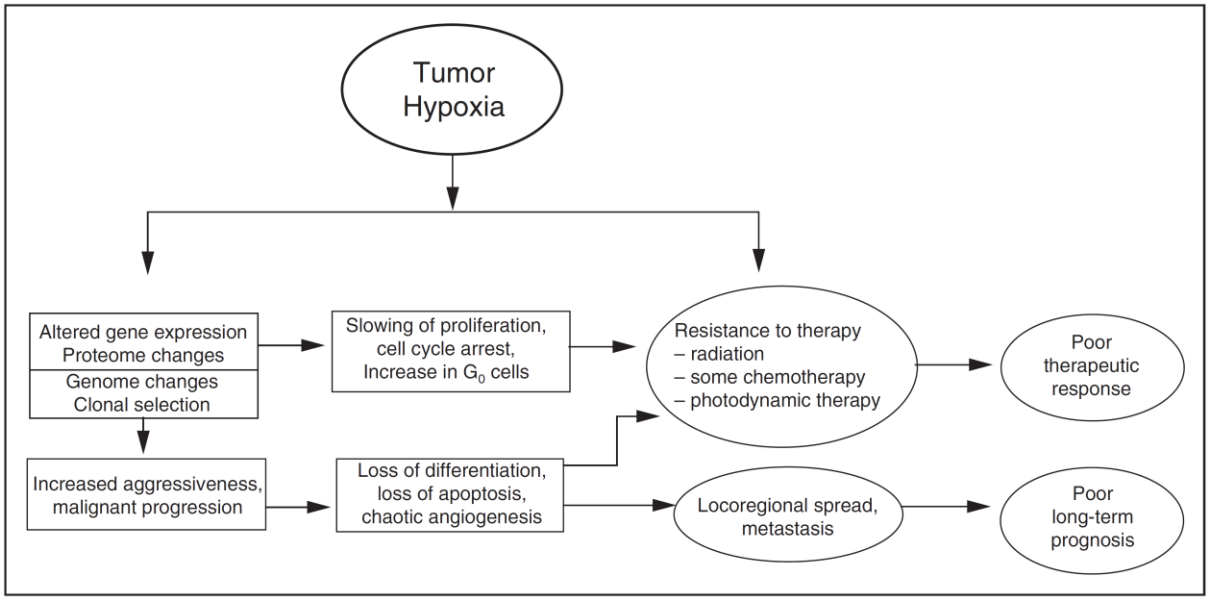

Figure 3: Schematic representation of the consequences of hypoxia (Vaupel, 2004a).

A model for tumor invasion has been proposed by Gillies and Gatenby (Nature reviews in cancer). The stages of tumor growth and their physiological states are illustrated in the figure 4. Normal epithelial cells (grey) become hyperproliferative (pink) following induction. As they reach the oxygen diffusion limit, they become hypoxic (blue), which can either lead to cell death (apoptotic cells shown with blebbing) or adaptation of a glycolytic phenotype (green), which allows cells to survive. As a consequence of glycolysis, lesions become acidic, which selects for motile cells (yellow) that eventually breach the basement membrane. As cancer progression proceeds, the mutations in cells increase (nuclei shown as light orange for one mutation and darker oranges for more mutations) (Gatenby and Gillies, 2004; Fang, 2008).

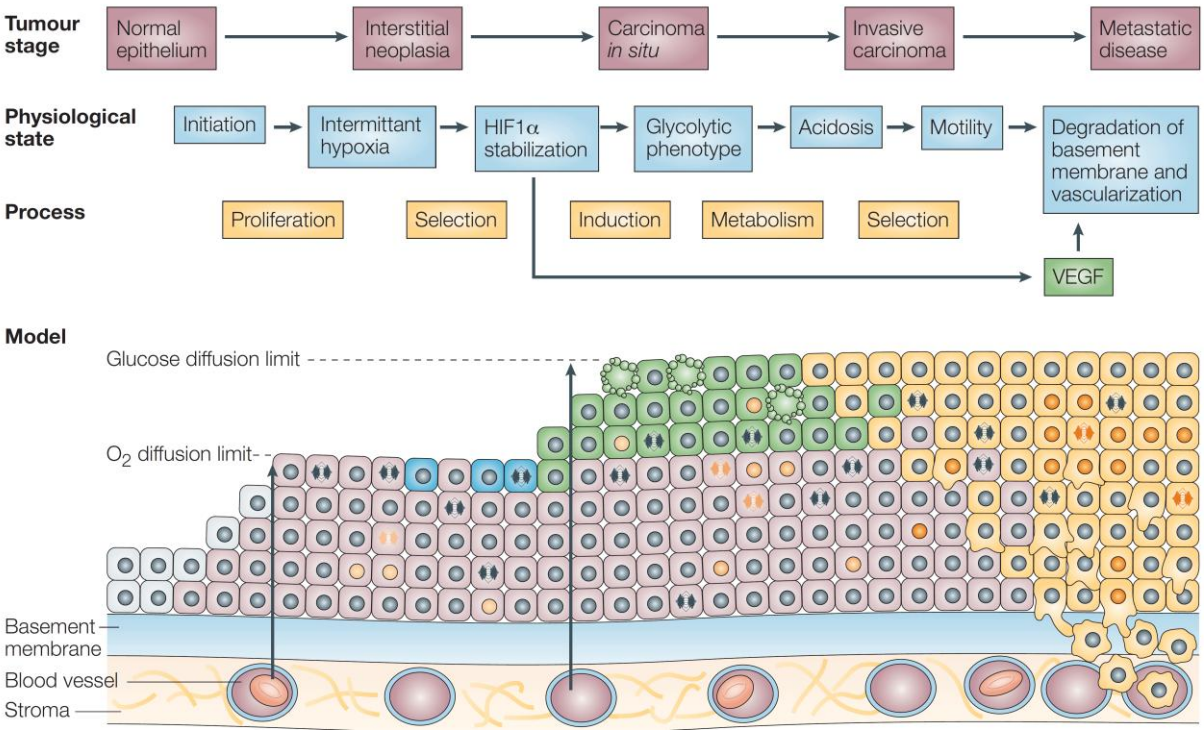

Figure 4: Model for tumor invasion (Gatenby and Gillies, 2004). Early carcinogenesis proceeds from normal tissues through initiation to a hyperplastic state to interstitial neoplasia, progressing to carcinoma in situ. Following breakdown of the basement membrane, cells gain access to existing and newly formed blood and lymphatic vascular routes for metastasis. The stages of tumor growth and their associated physiological states are diagrammed, showing that progression from one stage to the next is governed by state processes.

2.4. Therapeutic implications

2.4.a. Radiation response

Ionizing radiation, such as that used in radiotherapy, kills cells by producing DNA damage, particularly DNA double strand breaks. This damage results from ionizations on or very close to the DNA that produce a radical on the DNA (DNA$^{\bullet}$). This radical then enters into a competition for oxidation, primarily by oxygen (which fixes, or makes permanent, the damage) or reduction, primarily by –SH-containing compounds that can restore the DNA to its original form (see figure 5, part a). Therefore, DNA damage is less in the absence of oxygen. This effect of oxygen in sensitizing cells to radiation is illustrated in the cell-survival curve (see figure 5, part b) and is quantitated as the ratio of dose in the absence of oxygen to dose in the presence of oxygen needed to obtain the

same surviving fraction of cells. For mammalian cells, this ratio is usually 2.5-3.0 (see horizontal dotted line). Cells that are anoxic during irradiation are about three times more resistant to radiation than cells that are well oxygenated at the time of irradiation. Clinical trials, particularly with head and neck cancers for which control of the primary tumor is the main problem, have demonstrated that the more hypoxic tumors (typically those with a median pO_2 less than 10 mmHg) are more redioresistant than the less hypoxic tumors (Brown and Wilson, 2004; Brizel, 1999; Nordsmark, 2005).

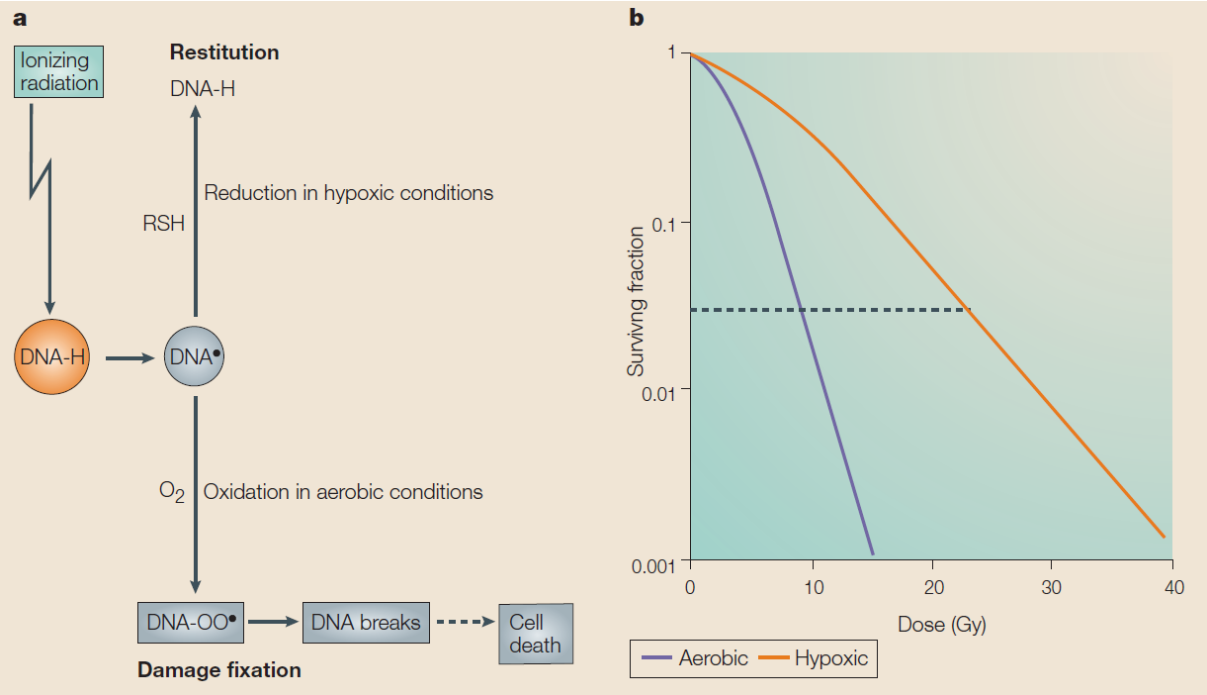

Figure 5: Radiation resistance of hypoxic cells (Brown and Wilson, 2004).

The radiosensitivity of the cells increases rapidly as the oxygen tension rises from anoxia to ~10 mmHg. At higher concentrations of O_2, similar to those found in venous blood, the radiosensitivity plateaus does not increase greatly as the oxygen tension rises to that of cells equilibrated with air or with 100% O_2 at normal atmospheric pressure or even hyperbaric pressure (Figure 6). The pO_2 that produces sensitivity midway between the oxic and hypoxic response is approximately 3 mmHg. Because the underlying chemical reactions are essentially completed within a few milliseconds after irradiation, O_2 must only be present during irradiation to produce full radiosensitization; the presence of oxygen before and after irradiation is irrelevant to this mode of radiosensitization (Figure 6) (Rockwell, 2009).

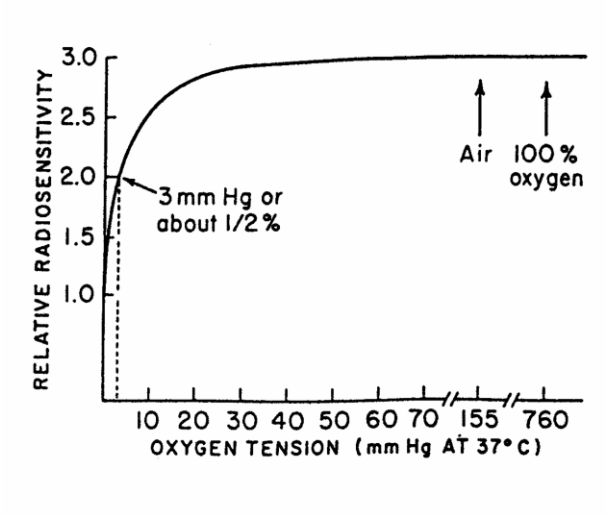

Figure 6: Relationship between radiosensitivity and oxygen tension (adapted from Elkind, 1963).

Evidences suggest that hypoxia-induced proteome and genome changes may also have substantial impact on radioresistance by increasing the levels of heat shock proteins or by increasing the number of cells in a tumor with diminished apoptotic potential or increased proliferation potential, both of which have been linked to radioresistance (Höckel, 2001a).

2.4.b. Effectiveness of chemotherapy

Under hypoxia, a reduced activity has been demonstrated for a variety of chemotherapeutic substances. A limited penetration of anti-cancer agents would result in lower efficacy. It has indeed been shown that the drug toxicity falls off as a function of distance from blood vessels (Durand, 1994). As a result of decline in nutrient and oxygen availability, cells further away from the vascular system would be dividing at a reduced rate and thus would be protected from the effects of chemotherapeutic agents whose activity is selective for rapidly dividing cell populations (Tannock, 1968). Multiple mechanisms are probably also involved in the hypoxia-induced resistance to chemotherapeutic agents, including a hypoxia-induced decreased cytotoxicity of some agents, and tissue acidosis, which is often observed in hypoxic tumors with a high glycolytic rate (Durand, 1994; Teicher, 1990). Furthermore, hypoxic stress proteins and the loss of apoptotic potential can impart resistance to certain chemotherapeutic drugs (Sakata, 1991; Höckel, 2001a). Finally, fluctuating hypoxia has significant implications

for the delivery of chemotherapeutic agents, cellular responsiveness to those agents, and the regrowth potential of the surviving tumor cells (Durand, 2001).

Hypoxia also conditions the activity of bioreductive drugs such as tirapazamine. Indeed, a novel approach to inducing tumor-specific toxicity is the use of cytotoxic drugs which are active only under limited O_2 conditions. Tirapazamine is a bioreductive cytotoxin. Intracellular reductases convert the drug to a cytotoxic radical that produces DNA single-strand and DNA double-strand breakages under hypoxic conditions (Siim, 1996). In aerobic cells, this cytotoxicity of the tirapazamine radical is greatly reduced as O_2 causes back-oxidation of the radical to the non-toxic parent compound (Peters, 2001). Although *in vitro* studies with tirapazamine showed that the drug is highly effective in killing cells under hypoxic conditions, clinical trials did not achieve significant results with tirapazamine as a sole agent. Tirapazamine has been shown to potentiate the effect of both radiation and cisplatin. When administered before chemo/radiotherapy, tirapazamine added synergistically to the killing effect of both radiation and cisplatin (Rischin, 2001; Von Pawel 2000; Marcu, 2006; Tatum, 2006). However, a recent phase III trial showed no improvement in locoregional control, failure-free survival and overall survival with the addition of the tirapazamine to cisplatine and radiation in patients with locoregionally advanced head and neck cancer. Morevover, the combination of tirapazamine and cisplatin with radiation was associated with important toxicity (Rischin, 2010).

2.5. Conclusion

pO_2 is an important determinant of tumor growth, metabolism, and response to a variety of therapies. Oxygen is an important actor in radiation therapy. Hypoxia in solid tumors significantly reduces their radiation sensitivity and is also associated with resistance to some chemotherapeutics. Furthermore, exposure to hypoxia renders tumor cells to be highly invasive and metastatic. The hostile metabolic environment in tumors selects tumor cells that are more malignant, aggressive and genetically unstable, and less susceptible to apoptosis, thus rendering them resistant to various therapies. Adequate techniques for rapidly determining the local pO_2 in tumors *in vivo* are crucial for the assessment of radiobiologically relevant hypoxia.

II. *In vivo* methods to measure hypoxia

As demonstrated above, the assessment of tumor oxygenation may have profound therapeutic implications in oncology. Understanding of tumor hypoxia could lead to the discovery of diagnostic and prognostic markers for malignant progression, and identification of novel therapeutic targets. Hence, a non invasive technique that could accurately and repetitively measure tumor oxygenation would find broad application in clinical and basic research. Actually, there is no gold standard to measure hypoxia. But different methods are available to measure tumor pO_2. The advantages and disadvantages of the currently available methods are presented.

1. Polarographic oxygen electrodes

The most commonly used commercial system for the measurement of tissue oxygenation *in vivo* is an electrode designed for rapid assessment of oxygen distribution throughout a tissue: the Eppendorf pO_2 histograph. This method depends on measurement of the current formed at the cathode upon ionization of oxygen at -0.7V. The attractiveness of this method lies with the linear response between pO_2 and current generated and the sensitivity of the method (Dewhirst, 2000). The current generated by the electrode and the subsequent perturbation of the oxygen field are highly dependent upon the size of the cathode type. The system has a computerized driver that moves the electrode through the tissue to minimize compression artefact on the tissue and consumption of oxygen by the electrode. Consequently, it cannot repeat measurements in the same position because it must be moved to minimize oxygen consumption by the electrode itself. The oxygen consumption occurs by electrochemical reduction and can introduce underestimation to the oxygen value (Collingridge, 1997). The method also suffers from signal-to-noise problems at low oxygen tension because the pO_2 is directly proportional to the current generated at the cathode. This is an important issue in tumors, since they are hypoxic, relative to most normal tissues. There is uncertainty regarding which current actually represents zero oxygen. First, it is difficult to obtain a calibration *ex vivo* that matches the circuit created *in vivo*. The second problem is that the signal-to-noise ratio decreases at low oxygen tension, which is the result of the positive correlation between current and pO_2 (Dewhirst, 2000). Despite the different disadvantages of the method, it has been extensively used to measure oxygen tension in tissues (Dewhirst, 1996; Lanzen, 1998; Braun, 1999) and oxygen consumption in tumors

(Dewhirst, 1994). Polarographic oxygen electrode systems were commercially available for clinical applications and have been used to characterize the oxygenation of human tumors in several studies (Vaupel, 1991; Nordsmark, 1994).

2. Oxylite

The oxylite is an instrument capable of continuous, quantitative measurement of dissolved partial pressure of oxygen (pO_2) and temperature in tissues, physiological fluids, cell cultures and *in vitro* samples (Figure 7B). Light pulses carried by an optical fibre induce pulsatile fluorescence of ruthenium luminophor or platinum incorporated into a silicone rubber polymer at the probe tip (Figure 7A). The lifetime of the fluorescent pulses is inversely proportional to the oxygen tension in the tip. This rapidly equilibrates with the pO_2 in the surrounding medium, so a continuous readout of tissue pO_2 can be obtained. Measured pO_2 is dependent on the local temperature, thus quantification requires temperature correction, which is accomplished by thermocouples attached to the fibre-optic probes. The calibrations are stable and the sensitivity is highest at lower pO_2 values (Griffiths, 1999). The spatial distribution is limited to the number of probes inserted and the method is invasive. Some studies have compared the Oxylite system with polarographic electrodes and showed a good correlation between the two systems (Seddon, 2001; Wen, 2008). However, Oxylite tends to overestimate the hypoxic fraction compared to polarographic electrodes (Braun, 2001). The two probes differ in many respects, including the mechanism of pO_2 measurement, and the tissue volume sensed by the probe tip, the speed and process of pO_2 readings. Finally, it has been described that the relationship of the Oxylite sensor response versus oxygen concentration is nonlinear (Griffiths, 1999). Therefore, errors in determining fluorescence lifetime are more serious at high oxygen concentrations than at low concentrations. Another limitation of the method is the impossibility to record pO_2 from the same site over days. Any clinical studies have been carried out with the oxylite.

A. ***B.***

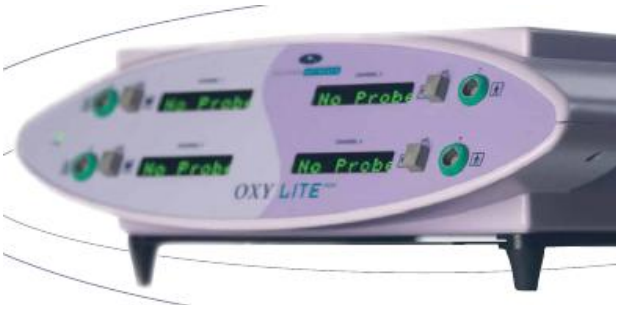

Figure 7: *Optical probe induces pulsatile fluorescence (A) and Oxylite device capable of continuous, quantitative measurement of dissolved partial pressure of oxygen (B).*

3. Positron emission tomography (PET)

Positron emission tomography (PET) allows the *in vivo* measurement and quantification of physiological processes using short-lived positron emitting radiopharmaceutical. PET is based on the detection of very small quantities of biological substances which are labelled with positron emitter. Most commonly used are carbon 11, oxygen 15, nitrogen 13, and fluorine 18. Advantages of positron labelled substances are their very high specificity (molecular targeting), the possibility of using biological active substances without changing their behaviour by the label. Target structures of these molecules are e.g. glucose metabolism, receptor binding potential, catecholamine transport, amino acid transport, or protein synthesis. All the above mentioned nuclides have very short radioactive half-lives, which necessitates a nearby cyclotron and radiochemistry facility. Imaging of regional tracer concentration is accomplished by the unique properties of positron decay and annihilation. After the emission from the parent nucleus, the energetic positron traverses a few millimeters through the tissue until it becomes thermalized by electrostatic interaction between the electrons and the atomic nuclei of the media and combines with a free electron to annihilate. The annihilation generates a pair of gamma rays which travel in nearly opposite direction with an energy of 511 keV each. The opposed photons from the positron decay can be detected by using pairs of aligned detectors in coincidence. PET consists of multiple, closely packed rings of detectors that enable simultaneous imaging of several image planes (Ziegler, 2005).

PET offers the possibility of *in vivo* mapping of regional tumor hypoxia with adequate anatomical resolution as well as monitoring of therapy through follow up mapping of hypoxia. Derivatives of misonidazole (an azomycin-based hypoxic cell sensitizer) that was introduced in radiation oncology decades ago have been successfully labelled with positron emitters. F-18-fluoromisonidazole (FMISO) is a radiopharmaceutical directly derived from the misonidazole and is the most extensively studied PET agent for hypoxia. FMISO has a high accumulation in hypoxic tissue that is proportional to the hypoxic fraction of the tumor. FMISO accumulates in tissues by binding to intracellular macromolecules when $pO_2 < 10$ mmHg. FMISO is only sensitive to the presence of hypoxia in viable cells; FMISO is not retained in necrosis because the electron transport chain that reduces the nitroimidazole to a bioreductive alkylating agent is no longer active. FMISO is a highly stable radiopharmaceutical that can be used to visualize and to quantify hypoxia (Rajendran, 2003). It is easy to synthesize and has a high safety profile. Typically, FMISO is injected intravenously and scanning is performed 90 to 120 min after injection. FMISO distribution immediately after injection will reflect blood flow but later distribution purely reflects tissue-plasma partitioning. Thus, the tissue concentration that represents partitioning, rather than hypoxic-specific uptake can be subtracted from the image (Tatum, 2006). Analysis of the collected data gives a tissue/blood ratio or tumor/muscle ratio, which is used for interpretation of the oxygen status in tumors (Koh, 1992; Yeh, 1996). Several studies have shown that a tissue/blood ratio of >1.2 reliably identifies the presence of hypoxia.

FMISO PET presents some disadvantages. The range of fractional hypoxic volume is scattered across tumor types, which precludes a standard correlation of hypoxic volume with that of the tumor. Although serial measurements can be preformed with FMISO PET, they have to be performed at least with one day interval. Thus, the ability of FMISO PET to monitor temporal heterogeneity is limited. FMISO PET has been validated in several studies using various animal models and human disease conditions, and its signal is independent of other factors associated with hypoxia, such as regional glucose concentration, glutathione levels, other transporters, and pH (Tatum, 2006). However, FMISO PET has been compared with that of polarographic needle electrodes and it was concluded that PET does not measure hypoxia to the same extent as that reported by electrode measurements (Bentzen, 2003).

The pharmacokinetics properties of FMISO are not optimal for hypoxia imaging. FMISO has relatively high lipophilicity, which leads to reduced accumulation of radioactivity in hypoxic tissue and slow clearance of radioactivity from normoxic tissue, contributing to a relatively low target-to-back ground contrast. To overcome the problems of the sub-optimal pharmacokinetics of FMISO several less lipophilic analogues nitroimidazoles have been developed. These include fluoroazomycin arabinoside (FAZA), fluoroerythronitromidazole (FETNIM), EF5, EF3 and fluoroetanidazole (FETA) (Minn, 2008). It remains unclear whether any of the alternative 2-nitroimidazoles provides sufficient advantages over FMISO for a dominant role in clinical trials using nuclear imaging, given the substantial human experience with FMISO (Krohn, 2008). PET is widely used in clinical oncology using the metabolic tracer [^{19}F] FDG (Cohade and Wahl, 2003; Gambhir, 2002).

4. Near-infrared spectroscopy (NIRS)

NIRS is widely used as a research tool to investigate dynamic changes in tissue oxygenation by measuring hemoglobin (Hb) saturation. NIRS uses visible light (700-1000 nm) in the near-infrared region which passes readily through biological tissues, bone, and muscle (Boushel, 2000). The energy in this range is absorbed by Hb, myoglobin, and cytochrome c oxidase. The NIRS signal is obtained primarily from the absorption of light by hemoglobin in the vasculature. Since the absorption spectra of oxyhemoglobin and deoxyhemoglobin are different, the concentrations of these species can be determined by recording the spectral changes and then fitting relative absorbances to the spectra of the chromophores (Dunn, 1998).

NIRS is non invasive, with excellent temporal resolution and low cost. The biggest advantage is the ability to perform real-time measurements and their repeatability, so that treatment as well as progression of the pathologic condition can be investigated (Intes, 2005). One drawback of the NIRS method is that it does not measure tissue pO_2. It provides information on vascular oxygenation (oxygen saturation) which indicates the balance between oxygen delivery and oxygen consumption. The light scatter and path-length may be constant within a subject, but there might be inter-subject variability. Also, modelling is required to estimate the path-length and consequently, the absorption coefficient of the tissue (Boushel, 2001). In addition, there are issues with the estimation

of path-length and modelling for heterogeneous tissues. The spatial resolution of NIRS is limited due to diffuse light measurements (Dunn, 1998).

NIRS is used for clinical studies of peripheral vascular disease and studies involving muscle oxygenation, especially in the area of physiology. In the clinical setting, NIRS is used for cerebral oxygenation and blood flow measurements (Vikram, 2007). But this technology can provide an efficient approach for monitoring tumor oxygenation and blood flow measurements (Liu, 2000). Moreover, good correlation was found between NIRS and other methods measuring tumor oxygenation (Xia, 2006; Dunn, 1998; Kida, 1996).

5. EPR oximetry

Electron paramagnetic resonance (EPR) specifically responds only to atoms or molecules with unpaired electrons, including free radicals, free electrons in some types of matrices, and some valence states of metal ions. The phenomenon that is observed in EPR is the transition (resonance absorption of energy) between the two energy states than can occur in an unpaired electron system placed in a magnetic field. The magnetic field separates the energy states associated with the two possible spin states of an unpaired electron (spin ½ system). The presence of other unpaired electron species can affect the EPR spectrum, by introducing a fluctuating magnetic field. Of particular importance to EPR oximetry is the fact that the ground state of molecular oxygen has two unpaired electrons. Nevertheless, it cannot be detected directly by EPR at ambient conditions due to fast relaxation of spins from the excited state, resulting in broad and low–amplitude EPR spectrum. However, it can be measured indirectly from the oxygen-induced changes in the EPR spectrum of other paramagnetic probes in the system. From oxygen-induced EPR line broadening, one can quantitate the oxygen concentration (Figure 8A). EPR line broadening occurs due to the Heisenberg spin-spin exchange between molecular oxygen and the spin probe. This exchange shortens the relaxation time of the spin probe, causing an increase in the peak-to-peak width in the first-derivative EPR spectrum. This spin exchange occurs when a collision between molecular oxygen and spin probe occurs. As the number of such a collision increases, the spin exchange increases proportionately, resulting in proportionately increased EPR line widths. While this effect occurs with all paramagnetic materials, it is much larger in some materials, and these have been selected for use for EPR oximetry. The EPR signal

arising from these materials can be a sensitive report of the pO_2 or $[O_2]$ at the location. Typically, the spectra line width (the peak to peak splitting along the magnetic field axis) is measured and converted to pO_2 or $[O_2]$ using an appropriate calibration curve (Figure 8B) (Swartz, 2004a; Ilangovan, 2004).

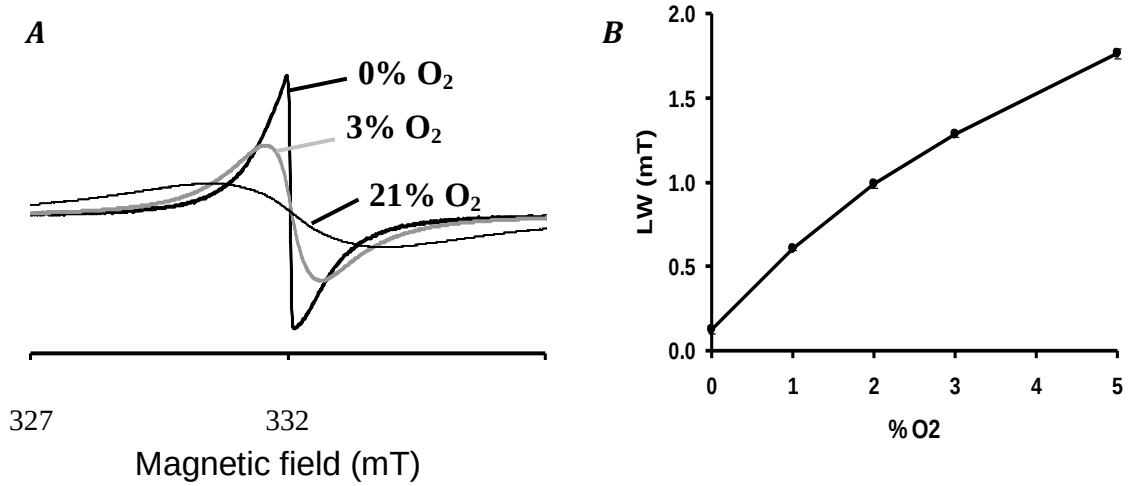

Figure 8: EPR spectra recorded under different oxygen atmospheres and hypoxia (A). Calibration curve (EPR line width as a function of the pO_2) (B).

Major endogenous paramagnetic species are present in insufficient amounts to be detected directly by EPR *in vivo*. The short half-life of most free radicals is another source of difficulty in the study of paramagnetic species. Therefore, the paramagnetic substance has to be introduced as a probe into the system (Figure 9), which can cause problems with sensitivity and toxicity. The main requirements in a paramagnetic probe suitable for oximetric applications are: a few narrow EPR lines, a good stability in the biological media, and no toxicity (Gallez, 2004).

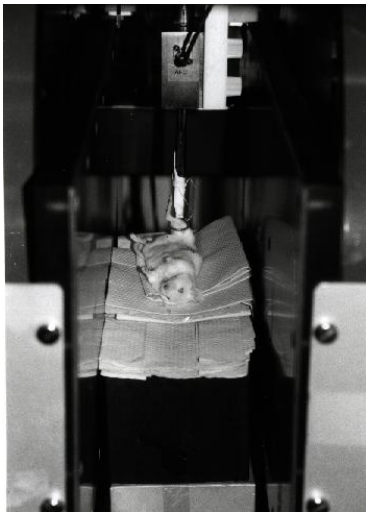

Figure 9: After placing an oxygen-sensitive paramagnetic material, the hind leg is placed on a surface detector to measure pO_2.

- **Soluble paramagnetic materials**

Among soluble paramagnetic materials, two types of structures are particularly interesting: the nitroxides and the triaryl methyl radicals (see Gallez, 2004). However, the soluble paramagnetic materials lack in sensitivity and are susceptible to bioreduction/oxidation by the cells *in vivo* (Ilangovan, 2004), resulting in instability of the probe.

- **Particulate paramagnetic materials**

These substances all exhibit very strong, nearly Loretzian EPR line shapes which broaden reproducibly in the presence of oxygen. These materials have several features which are not available in the soluble free radicals. They can have high spin density combined with much larger sensitivity to oxygen in terms of the magnitude of changes of the line widths per unit of oxygen. These materials also tend to be very unreactive, being stable to oxidation, reduction, large changes in pH and unaffected by the presence of other paramagnetic materials. The advantages of these materials reside in their capability of providing repeated sensitive and accurate measurements of pO_2. This is particularly useful for observing changes in pO_2 induced by physiological modulations or by pharmacological agents (Swartz, 1998). Two coals were identified by our group and had considerable stability and sensitivity for oximetry purpose (Jordan, 1998). In our studies, we preferentially used coals. Indeed, the calibration curve for the coals possessess a curvilinear response, with higher sensitivity to oxygen at low pO_2 (Gallez, 1999) compared for example to lithium phtalocyanine (LiPc) which presents a linearity

of response. The signal to noise ratio for LiPc is particularly high at low pO_2 due to the narrowness of the line width, but the line width at high pO_2 remains sufficiently narrow to get a reasonable signal to noise ratio in these conditions and is very valuable for measuring dramatic changes in pO_2 (Liu, 1993) (Figure 10).

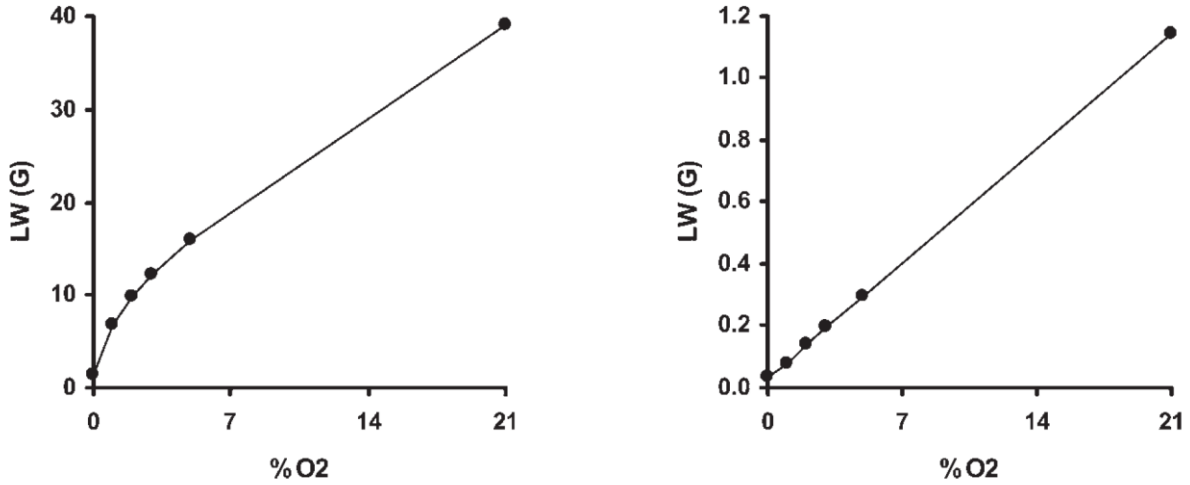

Figure 10: Calibration curve (line width as a function of the pO_2). Note the linearity of the response for the lithium phthalocyanine while the charcoals possess a curvilinear response, with a higher sensitivity to oxygen at low pO_2. Note also the order of magnitude of difference in terms of the line widths observed when comparing both materials (Gallez, 2004).

The development of *in vivo* EPR has been technically challenging for several reasons, but especially because of the non-resonant absorption of the electromagnetic radiation by the liquid water of the biological samples. The simplest solution to the problem of non-resonant absorption is to go to lower frequencies where the loss is not as severe. Unfortunately, this results in a significant loss in sensitivity. Consequently, *in vivo* EPR studies require the experimenter to make difficult trade-offs between sensitivity and depth of penetration.

The highest frequency that has been used for EPR oximetry is about 1.2 GHz (compromise between depth of penetration, which increases inversely with frequency, and sensitivity, which increases directly with frequency). This early limits the experimental conditions which can be used because the practical limits of depth are 5-10 mm. In small animals such the mouse, this depth allows studies in virtually any

region or the whole body. There is no limitation on the size of animal that can be studied, but without the use of invasive techniques, the technique is limited to regions close to the surface. In spite of this limitation, EPR oximetry at 1.2 GHz has been used extensively and successfully (Swartz, 1998).

To make measurements at greater depths, Swartz at al., use an implantable resonator. With this system, a small detection loop containing highly sensitive oximetric material, such as LiPc, is implanted in the tumor and covered in a gas-permeable coating. The implanted resonators extend the ability to make measurements to depths of at least several centimeters while achieving very high sensitivity (Swartz, 1998; Tatum, 2006; Li, 2010).

EPR oximetry based on spectroscopy of particulates offers several advantages, one of which is simplicity. This approach provides a direct measure of pO_2 without consuming oxygen and uses readily measured changes in spectra. This approach resolves pO_2 of less than 1 mmHg, does not need to be recalibrated during the experiment, is reproducible over time, and is not affected by the local environment, except for magnetic gases. The method can make measurements for periods of hours or more, make repeated measurements from the same sites for periods of years, and make multiple simultaneously measurements (Tatum, 2006). Currently, EPR is not used in clinic but clinical applications of *in vivo* EPR are now underway, with some results obtained with volunteers (Swartz, 2004b; Williams, 2010). However, it should be noted that EPR oximetry techniques using particulate materials are unlikely to be able to resolve microscopic heterogeneity in the pO_2. Indeed, EPR method measures only a single point in the tumor corresponding to about ~10 mm^3 and does not provide a paramagnetic map of the pO_2.

6. ^{19}F NMR spectroscopy/imaging

^{19}F nuclear magnetic resonance (NMR) spin-lattice relaxation rate (R_1) of perfluorocarbon (PFCs) probes could be used for imaging tumor pO_2 *in vivo*. PFCs are highly hydrophobic and offer exceptional oxygen solubility. It was demonstrated that the ^{19}F NMR spin-lattice relaxation rate is highly sensitive to oxygen. Indeed, the ^{19}F spin-lattice relaxation rate of PFCs varies linearly with the dissolved oxygen concentration. Intravenous administration of biocompatible emulsions allowed measurements of vascular oxygenation, and subsequent tissue uptake and sequestration

facilitated pO_2 measurements in tissues (Mason, 1994; Tatum, 2006). Although this approach continues to be used by some investigators, systemic delivery leads to extensive uptake by the reticuloendothelial system, including liver, spleen, and bone marrow, with potential hepatomegaly. Vascular delivery of PFCs, however, also biases the delivery to well perfused, and hence, well oxygenated regions (Mason, 1994; McIntyre, 1999; Tatum, 2006). Thus the most effective approach to achieving representative interrogation of a tumor is direct intratumoral delivery of reporter molecules.

Several PFCs have been used for NMR oximetry, but hexafluorobenzene (HFB) has been identified as the best pO_2 reporter. HFB gives a single, narrow ^{19}F NMR signal (Mason, 1996). It is also advantageous for pO_2 measurements because of its high sensitivity to oxygen concentration and lack of temperature dependence compared to the rest of the PFCs (Mason, 1996). In addition, a long spin-spin relaxation time (T_2), availability, low cost, and easy storage contribute to HFB being the most used PFC in ^{19}F MRI imaging. HFB is retained in the tumor for hours, so repeated and dynamic measurements are possible. HFB must usually be reintroduced after 24h if further measurements are needed (Mason, 1996). The group of Mason developed an oximetry procedure, called fluorocarbon relaxometry using echo planar imaging for dynamic oxygen mapping (FREDOM), which includes intratumoral injection of HFB and generates a relaxation map that is directly proportional to interstitial pO_2. FREDOM is minimally invasive, allows repeated measurements and reveals heterogeneity in a precise manner (Hunjan, 2001; Zhao, 2001a).

Recently, our group developed a new MRI fluorocarbon oximetry technique using snapshot inversion recovery. The SNAP-IR pulse sequence allows to sample tumor oxygenation with an effective in-plane spatial resolution similar to that of FREDOM. The acquisition time was 1.5 min, which is shorter than that of FREDOM (6.5 min). The method shows an important sensitivity to changes in tumors pO_2 with respect to respiratory challenge and is particularly relevant in terms of temporal resolution compared to FREDOM (Figure 11) (Jordan, 2009).

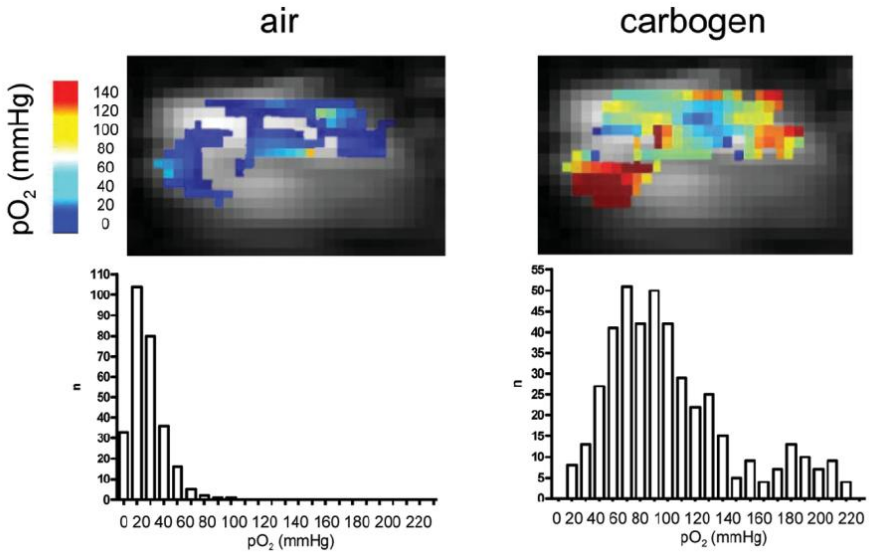

Figure 11: Typical oxygen maps of a tumor under air and carbogen breathing conditions and their corresponding histograms (Jordan, 2009).

The ^{19}F MRI oximetry has been compared with the polarographic needle electrodes (Mason, 1999). It was found that basal tumor pO_2 using ^{19}F oximetry was higher than those reported by the electrodes. However, direct intratumoral administration of PFCs has produced histograms comparable to those produced by electrodes (McIntyre, 1999). ^{19}F MRI oximetry has also been compared with the fibre optic measurement system Oxylite, which is a method for point measurement of pO_2 but not imaging (see above) (Zhao, 2001b; Jordan, 2009). It was found that both methods were similar when the mice were breathing oxygen or carbogen. A comparison with NIRS in a tumor model has also been reported and it was found that changes in vascular oxygenation were more rapid compared to tumor pO_2 measurement using ^{19}F MRI (Xia, 2006). Currently, no clinical application of PFC oximetry has been carried out due to the invasiveness and biocompatibility issues of intra-tumoral implantation of PFCs (Robinson and Griffiths, 2003).

7. BOLD imaging

The blood oxygen level-dependent (BOLD) MRI for tissues was first described for imaging the blood oxygen level in rat brains (Ogawa, 1990). BOLD images reflect the changes in the amount of oxygen bound to hemoglobin in blood. Deoxyhemoglobin is paramagnetic while oxyhemoglobin is not. In deoxyhemoglobin, the iron (Fe^{2+}) is in a paramagnetic high spin state as four out of six outer electrons are unpaired. The

deoxyhemoglobin content in blood can cause differences in susceptibility (i.e., changes in the local magnetic field) around the blood vessels. This affects the relaxation properties of the surrounding protons. Thus, a decrease in MRI image signal intensity reflects a decrease in the blood oxygenation. In terms of relaxation parameters, the spin-spin relaxation parameters R_2 (=$1/T_2$) and R_2* (=$1/T_2^*$) (where R_2^* incorporates local field inhomogeneities) are both affected by changes in oxygenation (Mason, 2006; Vikram, 2007). R_2* maps minimize, but do not completely eliminate, inflow effects that can contribute to contrast on single-echo gradient-echo images while retaining sensitivity to oxygenation changes that may be caused by alterations in blood flow (Howe, 2001; Robinson, 1999). Most of the applications of BOLD have been in the field of functional MRI (fMRI). In the brain, blood vessel size, density and distribution are well characterized, in contrast to tumors. The assumption used in models to describe BOLD contrast of fMRI in brain cannot therefore be applied to tumors. However, a study reported a good estimation of the SO_2 (oxygen saturation of hemoglobin) values in brain tumors (thesis of Christen, 2009). Gradient echo imaging, which provides BOLD contrast, has been used to investigate parameters related to tumor vasculature, such as perfusion, blood oxygenation, blood vessel development, remodelling and function, as well as to monitor the effects of therapy changing the tumor oxygenation.

Studies compared BOLD MRI with different methods to evaluate hypoxia. An apparent lack of correlation between BOLD MRI and pO_2 histography was observed during carbogen breathing (Robinson, 1999). However, a good one was found between the average increase in the T_2^* signal and pO_2 measured using microelectrodes and ^{19}F MRI in a tumor model (Al-Hallaq, 1998; Zhao, 2009). Baudelet at al. have compared BOLD contrast with pO_2 in tumors. The pO_2 was measured using Oxylite and it was found that while the BOLD signal temporally correlated with changes in pO_2, there was no correlation of the amplitude of the BOLD signal with absolute pO_2 in the tumors (Baudelet, 2002; Jordan, 2006a). Information afforded by the BOLD imaging technique is therefore qualitative in nature. If an absolute measurement of pO_2 is needed, it should be combined with another technique capable of providing an absolute measurement of pO_2.

The BOLD MRI technique offers several advantages. It does not require externally administered contrast agent medium or radioactive isotopes and it can be repeated as necessary. BOLD MRI is a non invasive method with high spatial resolution and real-time detection of fluctuations. The real-time evolution of changes in oxygenation and/or

perfusion can be mapped, and the tumor heterogeneity response can be taken into account (Baudelet, 2004; Baudelet, 2003a, b). In addition, BOLD MRI potentially can predict radiation response. However, the major disadvantage of this method is that it does not provide quantitative tumor oxygenation information (Baudelet, 2002). It measures the changes in blood oxygenation, but not the absolute oxygen concentration in tissue. The data are also affected by other factors such as the macroscopic field inhomogeneities and R_2 relaxation process. The deoxyhemoglobin content can be affected by the local blood flow and volume, and this must be taken into account when interpreting the data (Baudelet, 2002; Mason 2006). In addition, hematocrit concentration, pH, and temperature can change the fraction of deoxyhemoglobin as a function of pO_2 (Mason, 2006). Functional MRI based on the BOLD signal has a growing role in clinical neuroimaging (Hennig, 2003; Kessler, 2003) and is under investigation in clinical studies of human tumors (Taylor, 2001; Rijpkema, 2002).

8. Conclusion

Although it is not really obvious to define which parameters are the best to describe hypoxia, some standards should be considered for the evaluation of methods to measure hypoxia (see table below). The methods should be evaluated on their ability to measure oxygen directly or not, their ability to assess heterogeneity of tumors. The volume sampling required, the interval time between two measurements and their ability to repeat the measurement should also be considered. For clinical application, the invasiveness is an important parameter and finally, the cost of an examination is not a negligible factor.

9. Comparative table of methods to measure oxygen *in vivo*

	Eppendorf	***Oxylite***	***PET***	***NIRS***	***EPR (with particulates)***	***^{19}F-MRI***	***BOLD-MRI***
Tumor volume	300 µm	230µm	Whole tumor	Whole tumor	10 mm^3	Whole tumor	Whole tumor
Direct measurement	Yes 0-150mmHg	Yes 0-100mmHg	No <10mmHg	No	Yes 0-150mmHg	Yes 0-150mmHg	No
Quantitative measurement	Yes	Yes	No	No	Yes	Yes	No
O_2 mapping	No	No	Yes	Yes	No	Yes	Yes
Repeatability	No	No	Yes (±)	Yes	Yes	Yes	Yes
Rapidity	1.4sec	1sec	20-30min	15sec	>20sec	1.5min	15sec
Invasiveness	Yes	Yes	Non invasive	Non invasive	Minimally invasive	Minimally invasive	Non invasive
Mode of operation	Spatial distribution	Spatial and temporal	Spatial and temporal	Temporal	Temporal	Spatial and temporal	Spatial and temporal
Cost	Inexpensive	Inexpensive	Expensive	Inexpensive	Expensive	Expensive	Expensive
Clinical application	Yes	No	Yes	Yes	No (but in development)	No	Yes
Advantages	Sensitivity Linear relationship between current and pO_2	Electrode not consumes O_2	Hypoxia mapping Non invasive	Low cost Non invasive	Sensitivity Repeatability	pO_2 map Repeatability	pO_2 map No contrast agent
Disadvantages	Electrode consumes O_2 Not repeatable	No linearity of response Not repeatable	Radiation absorbed dose Indirect measurement	Indirect measurement	No mapping Requires injection	Sensitivity Requires injection	Indirect measurement Flow influence

III. Modulation of oxygen consumption

After the oxygen enhancement effect was discovered, studies were soon underway to find a way to exploit it for therapeutic gain. Since the prevailing thought was that oxygen essentially acts as a direct radio- and chemo-sensitizer, most strategies involved simply trying to increase oxygen availability in the tumor by either increasing the oxygen content in efferent tumors vessels or decreasing tumor oxygen consumption. It had been predicted theoretically that modification of oxygen consumption is much more efficient at alleviating hypoxia than modification of oxygen delivery (Secomb, 1995), a hypothesis that was further validated *in vivo* in experimental models by several groups. This is explicited in the following section that presents the strategies able to decrease tumor oxygen consumption rate. Indeed, several pharmacological drugs that inhibit cellular oxygen consumption have been characterized for their potential to increase tumor oxygenation by decreasing oxygen consumption and thereby enhance radiosensitivity.

1. Inhibitors of mitochondrial respiration

Aerobic respiration takes place in two regions of the cell, glycolysis occurring in the cytoplasm, and Kreb's cycle and electron-transport chain in the mitochondria. Glucose, the primary substrate for cellular aerobic respiration, is converted into pyruvate in the glycolytic phase, which is shunted into the Kreb's cycle for oxidative phosphorylation that is undertaken by electron-transport chain in the mitochondrial inner membrane. Oxygen undergoes a four-electron reduction in the electron-transport chain, thus generating ATP, the ultimate biologic currency of energy. The whole process of cellular aerobic respiration yields 28 ATP molecules as opposed to two ATP molecules that are generated during anaerobic respiration. The electron transport chain is composed of five complexes (complexI-V) and two intermediary substrates (coenzyme Q and cytochrome C) (Bellance, 2009) (Figure 12):

Complex I: NADH dehydrogenase
Complex II: Succinate dehydrogenase
Complex III: Cytochrome C reductase
Complex IV: Cytochrome oxidase
Complex V: ATP synthase

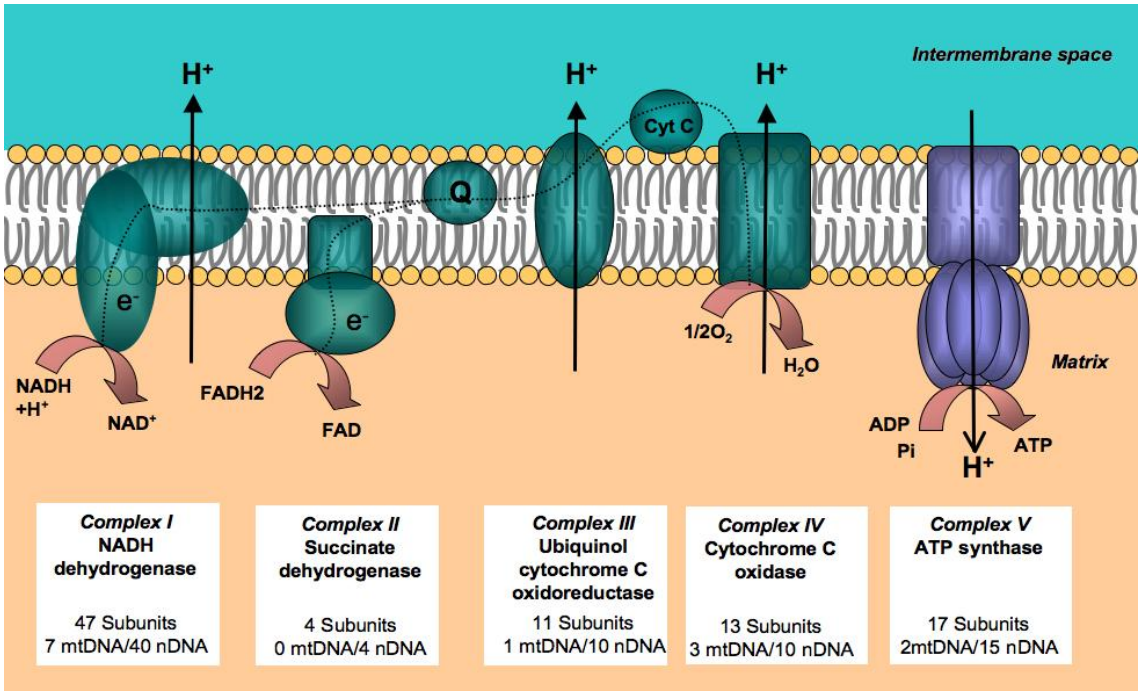

Figure 12: Mitochondrial respiratory chain. The respiratory chain consists of five complexes (complexI-V) and two intermediary substrates (coenzyme Q and cytochrome C) (Bellance, 2009).

Since the mitochondrial membrane potentials in cancer cells are frequently reduced in comparison with those of non-neoplastic cells (Pilkington, 2008), there is an opportunity for agents to enter the tumor cell mitochondria and to reduce oxygen consumption with subsequent increase of tumor pO_2 and enhancement of the efficacy of radiotherapy.

1.1. Meta-iodobenzylguanidine (MIBG)

Meta-iodobenzylguanidine (MIBG) is a functional analogue of the neurotransmitter norepinephrine. Radio-iodinated ^{131}I-MIBG is used clinically as a tumor-target radiopharmaceutical agent in the diagnosis and treatment of adrenergic tumors. MIBG is known to inhibit mitochondrial respiration and ATP production, causing a reactive stimulation of the glycolysis (Loesberg, 1990; Loesberg, 1991). Inhibitory effects of MIBG on the oxygen consumption were demonstrated in 9L glioma tumor cells. MIBG causes the mitochondrial site I electron transfer inhibition of

NAD(P)H oxidation. MIBG also causes earlier changes in tumor metabolism and pH, results which are consistent with the hypothesis that MIBG alters tumor glycolysis by inhibiting oxygen consumption (Biaglow, 1998; Biaglow, 2005).

Administration of glucose reduces tumor pH to various degrees in many rodent and human tumors. The variability in tumor acidification may be attributed to a dose-dependent response to glucose, to reduction in tumor blood flow, and/or to different levels of oxidative metabolism in various tumors. Inhibition of oxidative phosphorylation by administration of MIBG has been proposed as a method of increasing lactate production by tumors cells, hence enhancing tumor acidification (Loesberg, 1990; Biaglow, 1998). By the same way, synergic effects of MIBG and hyperglycemia were observed, resulting in significant acidification of the tumor and a decrease in bioenergetics status. The effects were largely selective for tumors in comparison with normal tissues (Zhou, 2000). Finally, the combined treatment with glucose and MIBG significantly enhanced tumor radiation-induced effect, mainly due to reduction in oxygen utilisation and increase in tumor pO_2 (Lee, 2003).

1.2. Glucocorticoids

Glucocorticoids have been shown to interfere with mitochondrial energy production because of their modulating role in many physiological processes requiring increase in energy expenditure (immune function, homeostasis, stress response and cellular differentiation). Earlier work had demonstrated that the administration of cortisone to rats resulted in both the inhibition of oxygen consumption and the uncoupling of oxidative phosphorylation in liver mitochondria (Kimberg, 1968). Glucocorticoids seem to decrease the cytochrome c oxidase (complex IV) activity of isolated rat kidney mitochondria by a direct mechanism (Simon, 1998; Scheller and Sekeris, 2003). This was observed for different glucocorticoids but the intensity of the inhibition was different between the glucocorticoids studied. Moreover, glucocorticoids can steadily modify respiratory chain by increasing transcription of nuclear and/or mitochondrial-encoded oxidative phosphorylation genes (Desquiret, 2008; Scheller and Sekeris, 2003). Finally, a recent study showed an important increase in tumor oxygenation induced by an effect on oxygen consumption. This decrease in oxygen consumption could be explained by the capacity of glucocorticoids to inhibit cytochrome c oxidase of the mitochondrial respiratory chain. The result of this increase in tumor

oxygenation was an improvement of the radiation efficacy by a factor of 1.7 (Crokart, 2007).

1.3. Anti-inflammatory drugs (NSAIDs)

Non-steroidal anti-inflammatory drugs (NSAIDs) are analgesics, anti-inflammatory and anti-pyretic agents. NSAIDs inhibit inflammation, mainly through their ability to inhibit cyclooxygenase (COX) activity. COX is a key regulatory enzyme involved in prostaglandin (PG) biosynthesis, which is strongly implicated in the induction of inflammation (Jana, 2008). Studies revealed that the prolonged use of NAIDs reduce the risk of cancer. Indeed, several studies have shown overproduction of COX-2 and PG in gastric and colon neoplastic lesions, which suggests that COX-2 overexpression is important during gastric carcinogenesis (Scartozzi, 2004).

Several reports indicate that many NSAIDs uncouple mitochondrial oxidative phosphorylation with important consequences on cell oxygen consumption. However, the behaviour of the drug may be dependent on the dose of the drug; diclofenac may behave as a decoupler at low concentrations and as an uncoupler at high concentrations. The kind of the NSAIDs studied is also important; nabumetone inhibits O_2 uptake, whereas the other NSAIDs stimulate respiration (Moreno-Sanchez, 1999; Krause, 2003). The drugs inhibit electron transfer in complex I, and complexes II plus III, in a concentration dependent manner (Somasundaram, 1997). For the first time, a study reported that the administration of NAIDs induces a dramatic increase in tumor oxygenation explained by a significantly reduced oxygen consumption. A dramatic increase in the tumor response was observed when the irradiation was applied at the time of maximal reoxygenation induced by NSAIDs (Crokart, 2005).

1.4. Insulin

Insulin has long been known to stimulate glucose transport and metabolism in skeletal muscle. This hormone is known to increase blood flow in human skeletal muscle and could be an important modulator of tumor oxygenation. However, a study showed that insulin has a profound effect on tumor oxygenation but it was not because of an increase in tumor blood flow but because of a decrease in tumor cell oxygen consumption. The increase in tumor oxygenation results in an important enhancement in the sensitivity of tumors to irradiation (Jordan, 2002). The likely scenario involves a

stimulation of eNOS (nitric oxide synthase) and thus increases NO release (Jordan, 2002; Jordan, 2004). As NO regulates mitochondrial respiration by virtue of reversible interactions with cytochrome c oxidase (complex IV), an increase in NO release consequently decreases respiration. The study indicates that an important consideration may be the influence of the fasting status of patients before irradiation. Because insulin secretion is dependent on feeding, it is likely that the tumor oxygenation will be modified after a meal (Jordan, 2002). A preclinical study confirmed the increase of tumor oxygenation and radiation sensitivity by insulin, without increase in the radiation toxicity for normal tissues (Jordan, 2006).

1.5. Thyroid hormones

Thyroid hormones are key regulators of growth, development, and metabolism. The development of hyperthyroid state in vertebrates leads to an enhancement in their basal metabolic rate due to an increase in the rate of O_2 consumption in most tissues. Conversely, hypothyroidism has the opposite effects. Mitochondria extracted from the livers of hyperthyroid rats display oxygen consumption rates greater than those recorded in controls, whereas mitochondria from hypothyroid animals have lower oxygen consumption. Similar changes have been observed in hepatocytes isolated from hyperthyroid or hypothyroid animals (Wrutniak-Cabello, 2001). Chronic alteration in thyroid status has also been shown to affect mitochondrial oxygen consumption in skeletal muscle (Gredilla, 2001).

A lot of evidences suggest that thyroid hormones act on tumor growth or incidence. Studies have demonstrated that hypothyroidism slows the neoplastic process, whereas administration of thyroid hormones preparation restores tumor growth rates (Shoemaker, 1979; Theodossiou, 1999; Mishkin, 1981). In humans, several case reports have indicated a prolonged survival in the presence of hypothyroidism (Hercbergs and Leith, 1993; Cristofanilli, 2005). Moreover, a decrease in thyroid function may also serve to favourably influence the response to treatment. Low levels of circulating thyroid hormones result in an increased response to chemotherapy (Shoemaker, 1979) and; in clinical studies, hypothyroidism has been positively correlated with responses to treatment. Patients present an enhanced response rate to chemotherapy and survived significantly longer under hypothyroidism (Hercbergs, 2003). Recently, it was also demonstrated that thyroid status was associated with a significant change in tumor

radiosensitivity since the regrowth delay was increased in hypothyroid mice compared to euthyroid mice. The mechanism was a higher level of tumor oxygenation, induced by a significant inhibition of oxygen consumption in hypothyroid mice (Jordan, 2007).

1.6. Inhibitors of vascular endothelial growth factor

The antiangiogenic drugs prevent the formation of new tumor blood vessels, thus inhibiting tumor growth (Folkman, 2002; Carmeliet, 2000). The early phase effects of an anti-angiogenic agent are likely to involve a transient normalization of the tumor vasculature. This phenomenon results in a transient increase in tumor perfusion and a reoxygenation of the tumor (Jain, 2005; Ansiaux, 2005). The resultant increase in delivery of drugs and oxygen into the tumor enhances the actions of chemotherapy and radiotherapy. SU5416 is an antiangiogenic agent that binds to the VEGF receptor and thereby inhibits the action of VEGF. However, in a study, SU5416 was unable to induce a normalization of tumor vasculature, contrarily to the other antiangiogenic agents. Actually, SU5416 induced tumor reoxygenation by a long-term effect on the oxygen consumption of the tumor cells. This molecule also potentiated tumor response to radiotherapy but not to chemotherapy (Ansiaux, 2006). Similar results were obtained with ZD6474 (Ansiaux, 2009). The exact mechanism of interaction between SU5416 or ZD6474 (or downstream effectors of involved pathways) and the mitochondrial respiratory chain has not been studied yet.

2. Crabtree effect

An alternative to pharmacologic manipulation of oxygen consumption is to invoke the Crabtree effect by exposing tumor cells to elevated glucose. This biochemical phenomenon results in transient reduction in oxygen consumption via respiration in favour of glycolysis (Wojtczak, 1996; Biaglow, 2005; Smolkova, 2010). Several mechanisms have been suggested to explain the Crabtree effect in tumor cells: (a) a glucose-induced increase in cytosolic free Ca^{2+} would inhibit oxidative phosphorylation through the increased association of the inhibitory subunit to the ATP synthase (Wojtczak, 1996); (b) competition between oxidative phosphorylation and glycolysis for ADP and inorganic phosphate; (c) a decrease of the intracellular pH, as a consequence of lactic acid formation; and damage of the mitochondrial membranes by free radicals, produced as a consequence of glucose catabolism (Rodriguez-Enriquez, 2001). However,

unlike cells grown at pH 7.3, cells adapted to growth at pH 6.7 did not exhibit a Crabtree effect with exposure to glucose. On the contrary, exposure of low pH-adapted cells to glucose stimulated the rate of oxygen consumption to 100% of the rate of cells grown at pH 7.3. Glucose-stimulated respiration in cells adapted to growth at pH 6.7 indicates that chronic exposure to low pH induced a metabolic shift in glucose utilization, in that addition of glucose resulted in an increase in pyruvate oxidation rather than lactate production (Burd, 2001). However, the combination of meta-iodobenzylguanidine (MIBG) and glucose can inhibit oxygen consumption and stimulate lactate production. Therefore, hyperglycemia plus MIBG can cause tumor acidification with the added therapeutic benefit of reduced oxygen consumption and increase tumor oxygenation (Burd, 2001; Burd, 2003). The same combination, hyperglycemia and MIBG, leads to improvements in tumor pO_2 and radiation response in the R323Ac tumor model (Lee, 2003). Finally, a study also demonstrated, in a murine tumor model that is sensitive to the Crabtree effect, that the combination of hyperglycemia and hyperoxic gas breathing can lead to significant improvement in tumor pO_2, the increase in oxygen levels was more than the sum of the effects of the two separate treatments (Snyder, 2001; Secomb, 2004).

3. Hypothermia

Hypothermia is associated with reduced metabolism of tissues and especially reduced oxygen consumption by tumors. Studies showed that the hypoxic fraction of tumors can be modulated by whole body hypothermia. Indeed, hypothermia reduces oxygen consumption, which leads to an increase in tumor oxygenation and results to a radiosensitizing effect (Nias, 1988). In a clinical study, patients were treated with hyperbaric oxygen simultaneously with total body hypothermia. They reported that the treatment could be delivery safely. However, the serie was small, so it is difficult to know if their results were any different from the use of radiotherapy alone (Sealy, 1986). Finally, the effect of localized hypothermia has been investigated by cooling by superfusion of the tumor surface with cooled saline solution to 25°C or 15°C. This hypothermia caused progressive decrease in the size of the hypoxic fraction and was explained by a decrease in oxygen consumption (Kelleher, 1998). Recently, it has been shown that during a hyperglycemic challenge, glioma tumors accumulated higher glucose under moderate hypothermia than under normothermia (Simoes, 2009).

IV. Oxygen consumption measurement

In view of its clinical importance, several techniques have been developed to measure oxygenation status in tissues and tumors in living animals and humans, but methods to measure rates of oxygen consumption are more limited. As mentioned above, many studies suggest that decreasing oxygen consumption rate of tumor cells is more efficient at alleviating tumor hypoxia than increasing tumor blood flow. So, development of methods to evaluate tissue oxygen consumption *in vitro* and *in vivo* will be appropriate. Several methods to measure oxygen consumption *in vitro* and *in vivo* are available and are described here. The advantages and disadvantages are also discussed.

1. *In vitro* methods

1.1. Fluorescence Method

The MitoXpress-Xtra assay is based on a phosphorescent oxygen-sensitive probe developed by Luxcel. The assay is based on the ability of O_2 to quench the excited state of the MitoXpress probe. Depletion of O_2 in the surrounding solution is perceived as an increase in probe phosphorescence signal. Changes in oxygen consumption, reflecting changes in mitochondrial activity, are therefore measured as changes in MitoXpress probe signal over time (Figure 13A). Culture cells are harvested and diluted with pre-warmed assay medium to the desired concentration (depending on cell type) and 150µl/well dispensed into 96-well microplates. The probe stock solution is added to each well to achieve the desired concentration. To reduce the effect of atmospheric oxygen, 100µl/well of pre-warmed mineral oil is added to seal the samples. The plate is placed in the pre-warmed plate reader and emission readings are taken at regular interval time. Measured time profiles and initial slopes of the phosphorescent signal reflecting the rates of oxygen uptake are then analyzed and compared to a reference sample (Figure 13B).

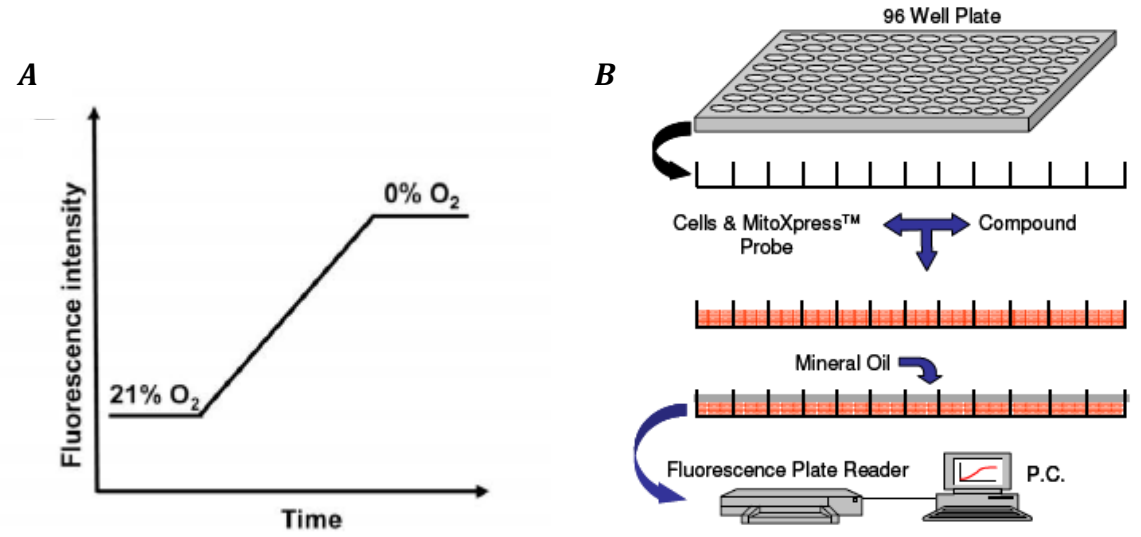

Figure 13: Schematic fluorescence intensity profile of MitoXpress during oxygen consumption assay (A). Schematic of MitoXpress cell-based screening assay (B) (www.luxcel.com).

The advantages of the fluorescence method are the simplicity of the measurement procedure, the high-sample throughout (up to 384-wells), and the low bulk requirements (standard multiwall plates, standard fluorescent reader, and oxygen sensitive probe). However, to achieve the convenience of measurement in a standard microplate, a level of sensitivity is sacrificed. Due to the incomplete sample sealing in the microplate formats and the associated back diffusion of atmospheric oxygen, the rate of change of dissolved oxygen measured using this approach is lower than the consumption rates measured using a sealed system (Hynes, 2006 a, b).

1.2. Clark electrode

The Clark type oxygen electrode has long been the main technique for measuring pO_2 and oxygen consumption, and is still widely used on a laboratory scale. The YSI 5300 Clark-type electrode (Yellow Springs Instrument Co, Yellow Springs, OH) consists of a platinum cathode and a silver anode, both in contact with an electrolyte solution (50% saturated KCl-solution). It is covered at the tip by a semi-permeable membrane which is permeable to gases (Figure 14A). The electrode is placed and fixed on the top of the measuring chamber. A magnetic stirrer is positioned on the bottom of the measuring chamber. To maintain a stable chamber temperature, an additional surrounding chamber is filled with water and connected with a water circulation system (Figure

14B). When a current is applied to the electrodes, the platinum electrode is negatively charged whereas the silver electrode is positively charged. Oxygen diffuses through the Teflon membrane to the platinum electrode where it is reduced. The current produced by the electrode is proportional to the oxygen tension in the solution (Von Heimburg, 2005). Air-saturated medium is introduced into the electrode chamber (capacity of 10 ml) and incubated until a steady baseline is obtained on the chart. Cells can be introduced into the incubation chamber using a syringe.

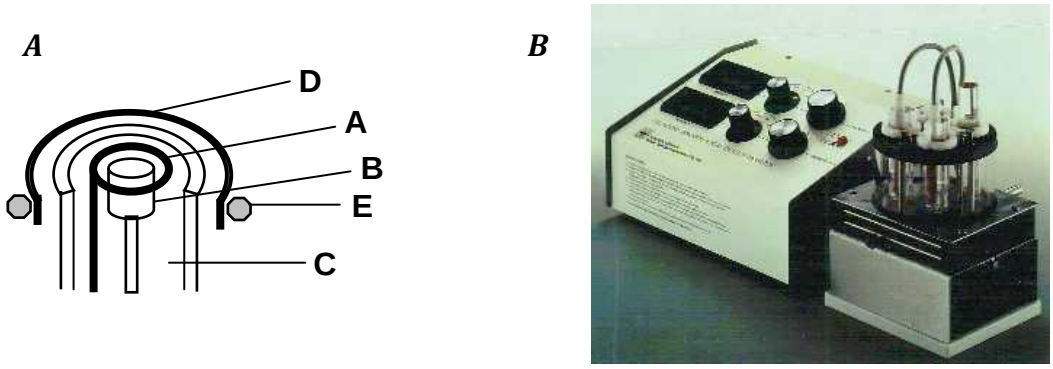

*Figure 14: **A**: The Clark-type electrode consists of a Pt-* (A) *and a reference Ag/AgCl-electrode (*B*) covered by a film of half-saturated KCl electrolyte (*C*) enclosed within a Teflon membrane (*D*) which is held in place by a rubber ring (*E*). **B**: YSI 5300 Clark-type electrode system.*

Although this measurement approach has proved very useful, the methodology is associated with a number of inherent limitations. These include the oxygen consumption by the electrode, the sensitivity to mass exchange (stirring requirements), which may damage the cells during a long experiment, and the need for a large assay volume compared to other techniques.

1.3. EPR oximetry

EPR oximetry (X-band) is being widely used to measure the oxygen consumption of cells. The method is based on the variation of the line width of a paramagnetic material in the presence of oxygen consuming cells in a closed system. The effect of treatments on tumor cell oxygen consumption rate can be measured because of the relationship between EPR line width and pO_2 (Figure 15A). The EPR principle has been described in part II.5. The soluble spin probes used are nitroxides which are very useful

to assess tumor oxygen consumption rate by cells inserted in a close capillary tube (James, 1995). To increase the sensitivity to oxygen, it is convenient to use perdeuterated nitroxides, for which the line width is lower than 200 mGauss. This method has been extensively applied to assess tumor oxygen consumption rate mediated by different treatments (Jordan, 2002; Crokart, 2005; Ansiaux, 2006).

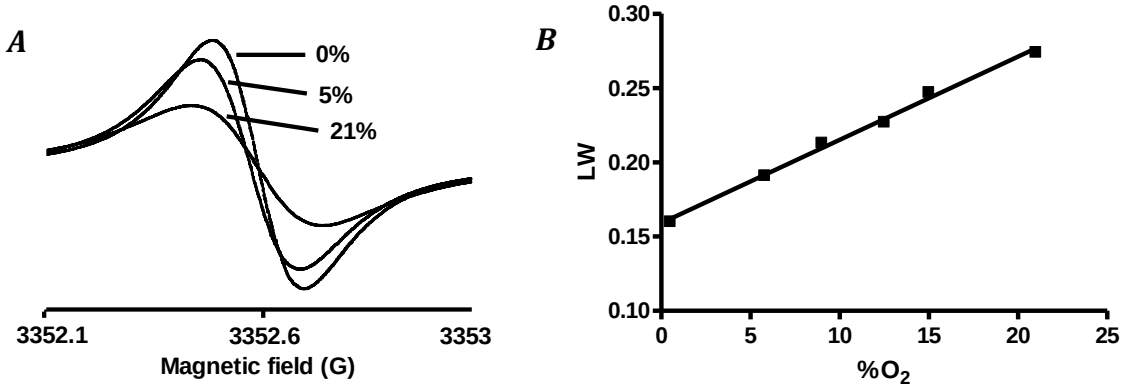

Figure 15: EPR spectra recorded in different oxygen environments (A). Calibration curve (EPR line width as a function of the pO_2) (B).

When it was first introduced for oxygen measurements, several advantages of this method were highlighted including: the fact that the cells and the oxygen sensors are homogeneously distributed throughout the samples and that the spin probe does not consume oxygen, allowing low concentrations of oxygen in solutions to be measured (Presley, 2006). This method has also been shown to be a useful tool for accurate, repeated measurements of local concentrations of oxygenation and respiration in cell suspensions.

1.4. Conclusion

The different methods present some advantages and disadvantages, and it is difficult to determine which technique is the best. It is, therefore, timely to compare the sensitivity of the available methods for determining oxygen consumption. This will be part of our research project in the present thesis.

2. *In vivo* methods

2.1. ^{17}O MRI

^{17}O is the only stable oxygen isotope that has a magnetic moment and can be detected by NMR. Compared with nuclei such as ^{1}H, ^{31}P and ^{13}C that are commonly used for most *in vivo* MR applications, ^{17}O has a spin quantum number of greater than ½ (I=5/2) and possesses an electric quadrupolar moment. The natural abundance of ^{17}O is only 0.037%, which is almost 2700 times lower than that of ^{1}H. Consequently, ^{17}O is introduced into a biological system through inhalation for studying oxidative metabolism. Moreover, ^{17}O presents a relatively small gyromagnetic ratio, a short transverse relaxation time (T_2), and has the lowest value of relative NMR receptivity. This low inherent NMR sensitivity might be the most likely cause of the infrequent use of ^{17}O NMR for *in vivo* MR studies. One unique NMR property of ^{17}O spin is the independence of ^{17}O relaxation times on the magnetic field strength, and this makes it possible to achieve a large sensitivity gain for *in vivo* ^{17}O NMR applications at high fields. *In vivo* ^{17}O NMR has two major applications for studying brain function and cerebral bioenergetics. The first application is to measure the cerebral blood flow (CBF) through monitoring the washout of inert $H_2{}^{17}O$ tracer in the brain tissue following an intravascular bolus injection of the ^{17}O-labeled water. The second application is to determine the cerebral metabolic rate of oxygen utilization ($CMRO_2$) through monitoring the dynamic changes of metabolically generated $H_2{}^{17}O$ from inhaled ^{17}O-labeled oxygen gas in the brain tissue. Each molecule of $^{17}O_2$ consumed in the brain produces two molecules of $H_2{}^{17}O$. One great merit of *in vivo* ^{17}O NMR for the determination of $CMRO_2$ is that only the metabolic $H_2{}^{17}O$ is detectable (Figure 16). Indeed, $H_2{}^{17}O$ metabolically generated can be detected alone without confounding signals from the $^{17}O_2$ molecules either bound to hemoglobin or dissolved in blood and tissue space. The dynamic change in the cerebral $H_2{}^{17}O$ concentration during an $^{17}O_2$ inhalation is determined by three parallel processes: (1) the cerebral oxygen utilization for generating the metabolic $H_2{}^{17}O$ in the brain tissue; (2) blood perfusion resulting in $H_2{}^{17}O$ washout from the brain; and (3) blood flow recirculation bringing the metabolically generated $H_2{}^{17}O$ in the entire living body into the brain (Figure 16) (Pekar, 1991; Zhu, 2005).

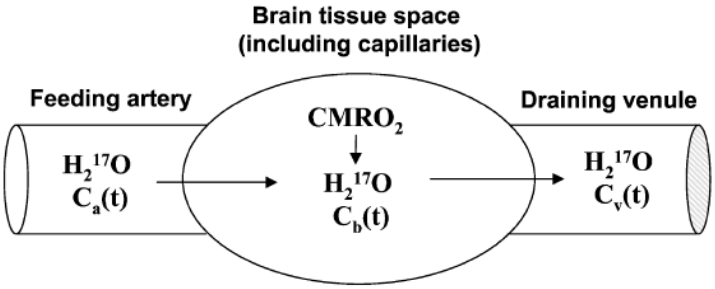

Figure 16: Schematic illustration of a 'complete model' describing the special events in the brain when the ^{17}O-labeled oxygen gas molecules are introduced via an inhalation. In this model, only the ^{17}O-labeled water ($H_2{}^{17}O$) is involved because the ^{17}O-labeled O_2 is invisible in the detected ^{17}O NMR signal (Zhu, 2005).

There are two major NMR approaches for monitoring $H_2{}^{17}O$ *in vivo*, namely direct approach by using ^{17}O NMR detection and indirect approach by using ^{1}H NMR detection for measuring the changes in T_2- or $T_{1\rho}$-weighted proton NMR signals caused by the ^{17}O-^{1}H scalar coupling and proton chemical exchange. Both approaches are suitable for CBF measurements. However, recent studies indicated that the direct *in vivo* ^{17}O NMR approach at high/ultrahigh fields appears to offer significant advantages for quantifying and imaging $CMRO_2$. New developments have further demonstrated the feasibility for establishing a completely non invasive *in vivo* ^{17}O NMR approach for imaging $CMRO_2$ in a rat brain during a brief $^{17}O_2$ inhalation (Zhu, 2002; Tailor, 2004; Mellon, 2009; Zhu, 2009).

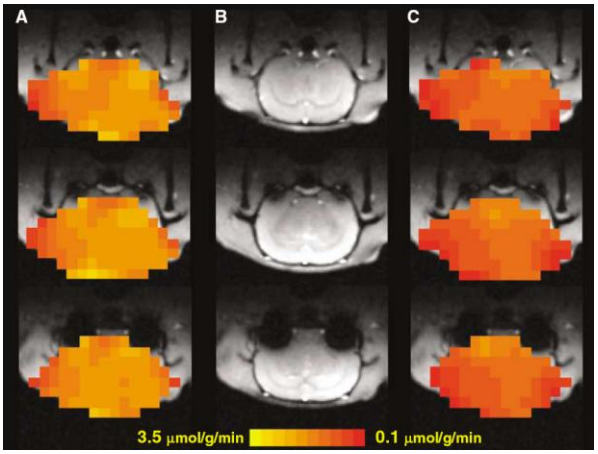

Figure 17: $CMRO_2$ maps of a representative rat brain at (A) normothermia (37°C) and (C) hypothermia (32°C) condition, as well as their corresponding anatomic images (B) (Zhu, 2007).

Finally, the similar approach could potentially be applied to image $CMRO_2$ non invasively in human brain. However, one hurdle for routine application of *in vivo* ^{17}O approaches including both indirect and direct ^{17}O detection for imaging $CMRO_2$ is the cost of $^{17}O_2$. Currently, the cost of the ^{17}O-labeled oxygen gas is high because of the extremely low ^{17}O natural abundance, low production efficiency for achieving high ^{17}O enrichment, and presumably the low demand.

2.2. Microelectrodes

Dewhirst at al. reported determination of oxygen consumption rate in microscopic tumor tissue regions bounded by microvessels. The adenocarcinoma was implanted in a window chamber and the vascular network was visualized by transillumination (Figure 18). The aim of the study was to measure the profiles of tissue pO_2 between two vessel segments in order to provide data for calculation of oxygen consumption rates. The method relies on the identification of an isolated one or two-vessel network where vascular segments are roughly parallel and pO_2 measurements were performed at the wall of each vessel segment and at several interstitial points between the two segments. Distances between measured points were also determined. Theoretical simulations of oxygen diffusion in the regions were made, and consumption rates were estimated for best fit between measured and simulated values (Dewhirst, 1994).

Figure 18: Window chamber showing the vascular network visualized by transillumination.

2.3. NIRS

NIRS can be used to investigate the oxygen dynamics and the oxygen consumption rate in tumors using a mathematical model. NIRS was used to measure changes of oxygenated hemoglobin concentrations ([HbO_2]) before and after potassium chloride (KCl) induced cardiac arrest. The changes in the tumor vascular [HbO_2] and total hemoglobin concentration were continuously monitored during and after cardiac arrest by NIRS. The tumor oxygen consumption rate decreased exponentially with time after KCl administration. The tumor oxygen consumption rate was calculated by fitting the model to the measured Δ[HbO_2] data. Fick's law was applied to extract and quantify the tumor oxygen consumption from the tumor oxygenation dynamics, since the rats died rapidly so that the tumor metabolism or oxygen consumption was not coupled to the tumor blood flow (Song, 2005). Due to the animal sacrifice, it is not possible to repeat the measurement and it constitutes a major disadvantage of the method.

2.4. ^{15}O PET

The introduction of molecular [^{15}O] into the vascular compartment of the body results in the distribution of the labelled oxygen to the tissues, where it is converted to ^{15}O-labeled water of metabolism. The labelled water then redistributes to all tissues by way of the same vascular compartment. Unmetabolized labelled molecular oxygen is removed by respiration. These properties of the [^{15}O] tracer have been incorporated into an equilibrium model that has been used to measure oxygen consumption in the human brain using data from the sequential inhalation to equilibrium of [^{15}O] oxygen and carbon dioxide. Positron emission tomography (PET) allows the quantitative measurement of regional cerebral blood flow (CBF) and the rate of oxygen metabolism ($CMRO_2$) (Figure 19), which is enabled to understand the pathophysiological basis of cerebrovascular disorders.

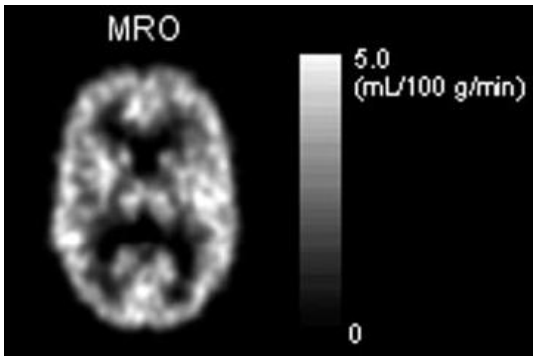

Figure 19: Example of parametric image of $CMRO_2$ (Hattori, 2004).

These measurements are achieved using a protocol involving separate PET scans, one after the administration of each of three distinct ^{15}O-labeled radioactive tracers: $H_2{}^{15}O$ or $C^{15}O_2$ for CBF, $^{15}O_2$ for $CMRO_2$, and $C^{15}O$ for cerebral blood volume (CBV) (Frackowiak, 1980; Lammertsma, 1981; Mintun, 1984). Two common methods are known as the steady-state method and the bolus inhalation method based on a single compartment model (Okazawa, 2009). Authors started the method with continuous inhalation of ^{15}O-labeled gases such as $^{15}O_2$, $C^{15}O_2$ and $C^{15}O$ (Frackowiak, 1980). Lammertsma at al. corrected the effect of blood volume on $CMRO_2$, which is overestimated without cerebral blood volume correction when using the ^{15}O-gas steady-state method. This method requires the continuous inhalation of radioactive gas at a constant rate of concentration during PET scans (Lammertsma, 1981). Only a few samples of arterial blood are required during each scan, which is simple and easier than the bolus tracer administration method. However, patients cannot avoid high exposure to radioactive gas. Mintun at al. proposed a three-step method which includes ^{15}O-water (or $C^{15}O_2$), $^{15}O_2$, $C^{15}O$ scans (Mintun, 1984). Various quantitative methods for measurement of cerebral blood flow using ^{15}O-water PET were also proposed and the three-step method was improved (Hattori, 2004). A two-compartment model analysis increased the accuracy of cerebral blood flow values by separating the vascular component from the blood flow value (Ohta, 1992; Ohta, 1996). The method includes an assumption that the metabolized and recirculating activity of ^{15}O is negligible during scanning time but the $CMRO_2$ values tend to be overestimated (Poulsen, 1997). Recently, an advanced method based on the autoradiographic method was proposed with a shorter scanning time (Kudomi, 2005). In this method, the metabolized and recirculating

activity of ^{15}O is corrected to calculate oxygen consumption by sequential scanning of $H_2{}^{15}O$- and $^{15}O_2$-PET.

Contrarily to ^{17}O NMR, the PET approach is unable to distinguish the signals coming from the $^{15}O_2$ molecules bound to hemoglobin (or freely dissolved in blood and tissue space) from those emitted by the ^{15}O atoms in the metabolically-generated $H_2{}^{15}O$ molecules. Therefore, in practice, PET requires multiple experiments for independent assessments of: (1) the metabolically generated $H_2{}^{15}O$ during an inhalation of $^{15}O_2$ gas; (2) cerebral blood flow, which can be experimentally determined by a bolus injection of $H_2{}^{15}O$; (3) the ^{15}O-labeled content in arteries; and (4) cerebral blood volume, which can be experimentally determined by an inhalation of $C^{15}O$ gas or by making approximation assumptions (Zhu, 2005). Another limitation is that ^{15}O is a positron-emitting isotope with a half-life of only 2 min.

2.5. qBOLD

The quantitative BOLD (qBOLD) technique is MRI-based and provides a regional *in vivo* oxygen extraction fraction (OEF) measurement. One of the important parameters defining oxygen consumption is OEF, the percent of the oxygen removed from the blood by tissue during its passage through the capillary network. Previously, authors used this parameter to characterize the baseline state of the normal human brain (Raichle, 2001). Indeed, the discovery of BOLD contrast in MRI opened up broad opportunities to study hemodynamic properties of the brain (Ogawa, 1990). However, while the dynamic properties of BOLD contrast during functional activation have received much consideration, very little attention has been paid to the nature of BOLD contrast during the resting or baseline state of the brain. Because resting brain is responsible for approximately 20% of total human body oxygen consumption, understanding brain functioning in the baseline state is important for understanding brain performance in health and disease. BOLD approach capitalizes on the fact that deoxygenated blood has different magnetic susceptibility as compared to oxygenated blood, which in turns has magnetic susceptibility similar to the tissue. Due to this effect, the deoxyhemoglobin containing part of the blood vessels network in the brain creates mesoscopic field inhomogeneities (refers to changes in magnetic field over distances that are smaller than the voxel dimensions but much larger than the atomic and molecular scales) in the surrounding tissue leading to more rapid MRI signal decay than from standard T_2 decay

alone. Because these field inhomogeneities are tissue specific, measuring the MRI signal decay rate may provide information on the tissue structure and functioning. Previously, a study developed a theoretical model of BOLD contrast that analytically connects the BOLD signal to hemodynamic parameters such as the deoxyhemoglobin-containing blood volume, deoxyhemoglobin concentration, and OEF (Yablonskiy, 1994). A subsequent publication developed a theoretical background and experimental method that allows the separation of mesoscopic field inhomogeneity effects from both macroscopic and microscopic inhomogeneities (Yablonskiy, 1998). Such separation allows one to take full advantage of the mesoscopic, tissue-specific magnetic field inhomogeneity effects to extract quantitative information about tissue hemodynamic properties. Earlier attempts to directly implement this method *in vivo* have not produced conclusive results (An, 2000; An, 2003). The simplistic model used, describing brain tissue as one compartment structure similar to water in a phantom, is not sufficient to describe real brain tissue. Recently, a study developed a BOLD MR-based method that allows quantitative evaluation of tissue hemodynamic parameters, such as the blood volume, deoxyhemoglobin concentration, and OEF. The proposed method, termed quantitative BOLD, is based on a MR signal model that incorporates prior knowledge about brain tissue composition and considers signal fluid from gray and white matters, cerebrospinal fluid, and blood. The model, based on a multicomponent approach, analytically connects the BOLD effect to hemodynamic parameters, such as the deoxyhemoglobin-containing blood volume, deoxyhemoglobin concentration, and OEF (He, 2007). The OEF measurements provided by the qBOLD approach were validated by a study which compares qBOLD OEF measurements against direct measurements of the blood oxygenation level. The study demonstrated a very good agreement between qBOLD approach and direct measurements (He, 2008).

2.6. Comparative table of methods to measure oxygen consumption *in vivo*

	^{17}O MRI	***qBOLD***	***^{15}O PET***	***NIRS***	***Microelectrodes***
Quantitative measurement	Yes	No	Yes	Yes	Yes
Imaging	Yes	Yes	Yes	No	No
Direct measurement	No	No	No	No	No
	Mathematical model	Mathematical model	Mathematical model	Mathematical model	Mathematical model
Invasive measurement	No	No	No	Yes	Yes
Organ used	Brain	Brain	Brain	Tumors	Tumors
Clinical use	No	Yes	Yes	No	No
Cost	Expensive	Expensive	Expensive	Inexpensive	Inexpensive
Others	Influence of flow	Influence of flow	Influence of flow	Requires animal sacrifice	Electrodes consume oxygen

Most of the methods described here are not applicable to tumors due to the flow influence, do not provide a direct measurement of pO_2 and some of them are invasive. Consequently, one of the thesis projects was to develop new methods to measure the *in vivo* oxygen consumption of tumors non invasively.

V. Arsenic Trioxide

Arsenic was first used by Greek and Chinese healers more than 2000 years ago to treat everything from syphilis to cancer, but was also the favourite poison of the Savellis, the Borgias and Agatha Christie. By the mid-twentieth century, the arrival of antibiotics and chemotherapy led to the abandonment of arsenic-based treatments, which remained in use only for treating trypanosomiasis. In the 1970s, arsenic trioxide (As_2O_3) was found to be able to induce complete remission in patients with acute promyelocytic leukemia (APL) in China. Additional studies confirmed that low doses of As_2O_3 can induce complete remission in 90% of relapsed APL patients (Soignet, 1998). Importantly, it has become evident that apoptotic effects of As_2O_3 are not restricted to APL cells but also can be observed in other malignant cells, such as myeloma cells, chronic myeloid leukemia cells, as well as various solid tumors cells.

1. Clinical effects of As_2O_3 in acute promyelocytic leukemia (APL)

The vast majority of cases of APL are characterized by the t(15;17) translocation. This translocation generates a fusion between the PML (promyelocytic leukemia) gene and the RARα (retinoic acid receptor) gene, which encodes a transcription factor. The resulting PML-RARα fusion protein blocks the expression of genes required for normal myeloid differentiation. Sequence analysis of the PML gene has indicated the presence of a cysteine-rich region that may be a principal candidate for interaction with trivalent arsenic. Expression of the PML-RARα fusion protein in leukemic cells disrupts the nuclear bodies, and the PML protein is dispersed into smaller fragments of these structures (Miller, 2002a; de Thé, 1990).

Clinically, APL is sensitive to antileukemic chemotherapy mainly consisting of an anthracycline and cytosine arabinoside, and to the differentiation therapy with all-trans retinoid acid (ATRA) (Chen, 1997). As_2O_3 has been proposed as an alternative to treatment with ATRA because it can induce complete remission in both RA-sensitive and RA-resistant APL patients (Miller, 2002b). Treatment of APL patients with As_2O_3 is associated with disappearance of the PML-RARα fusion transcript. Exactly how As_2O_3 mediates its efficacy is not fully understood. Two main mechanisms of action of As_2O_3 have been identified from both *in vivo* and *in vitro* studies: promotion of APL cell differentiation (observed at low level of As_2O_3) and induction of apoptosis (observed at high levels of As_2O_3) (Figure 20) (Chen, 1997; Miller 2002a).

Degradation of the fusion protein, PML-RARα, is the most likely mechanism by which As_2O_3 induces cell differentiation in APL cells. Degradation of PML-RARα allows malignant promyelocytes to overcome their maturation (Miller, 2002a). In clinical trials, cell samples taken from APL patients treated with As_2O_3 suggest that partial differentiation of the maturation-arrested leukemia cells contributes to the therapeutic effect (Soignet, 1998). As_2O_3 degrades the fusion protein and induces differentiation in APL cells whether or not they are resistant to retinoic acid. The partial differentiation effects of As_2O_3 appear to be unique to APL because of the direct effect of As_2O_3 on PML-RARα degradation. As_2O_3-induced apoptosis, in contrast, occurs via a variety of mechanisms, which appear to be independent of the presence of PML-RARα (see below).

As_2O_3 can be used as a single agent and induces complete remission with only a minimal myelosupression. Investigators in China introduced As_2O_3, alone and in combination with chemotherapies, as a cancer therapeutic for patients with APL, achieving notable rates of complete remission. In newly diagnosed patients, complete remission rates have ranged from 70% to 90%, and in relapsed patients, rates of 65% to >90% have been reported (Miller, 2002a; Shen, 1997).

Arsenic trioxide was approved for clinical use in relapsed and refractory APL in 2000. Advantages of single-agent arsenic trioxide are the consistently high complete remission rate in many studies and low resistance to the drug and better tolerability because combination with chemotherapy is not required. As_2O_3 with or without ATRA is currently being trialed in patients with newly diagnosed, previously untreated APL. Overall, As_2O_3 is well tolerated by patients and toxicities are manageable and reversible. Generally, most adverse events do not require discontinuation of treatment (Dilda, 2007).

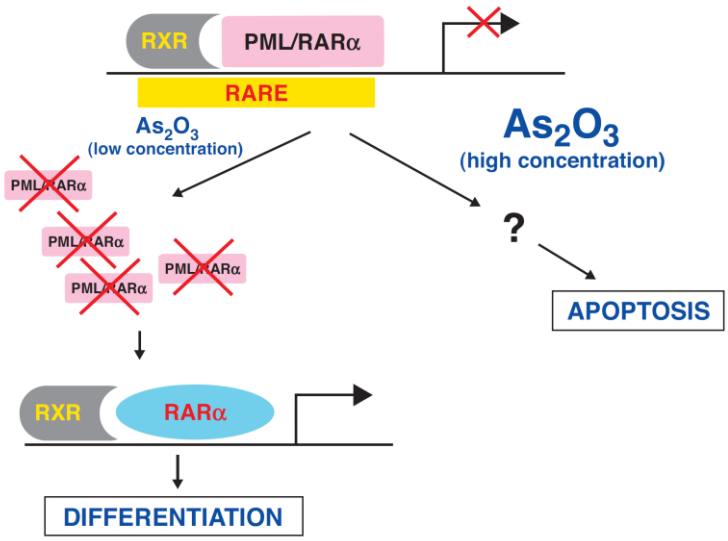

Figure 20: Response of APL cells to As_2O_3 (Miller, 2002a).

2. Effects of As_2O_3

As_2O_3 acts on cells through a variety of mechanisms, influencing numerous signal transduction pathways and resulting in a vast range of cellular effects that include apoptosis induction, growth inhibition and angiogenesis inhibition. We described essentially the oxidative stress which represents the main pathway by which As_2O_3 induces apoptosis. As_2O_3 inhibits many enzymes by reacting with biological ligands that possess available sulfur groups. As mentioned above, the effects of As_2O_3 are not restricted to APL but are also observed in solid tumors and the responses vary depending on cell type and the dose of arsenic.

2.1. Apoptosis

The apoptotic effect of As_2O_3 has been observed in various cell lines but the general mechanisms via which As_2O_3 induces apoptosis are not clear and are subject of intense debate. The induction of apoptosis by As_2O_3 is likely mediated via the production of ROS (reactive oxygen species) that damage mitochondria (Jing, 1999; Chen, 1998; Bahlis, 2002; Sumi, 2010). Mitochondria have been shown to play a major role in programmed cell death. Moreover, these organelles are critical to cellular survival and growth because they are necessary for generation of energy synthesizing ATP. Synthesis of ATP requires consumption of high amounts of oxygen, which routinely leads to the generation of ROS such as hydrogen peroxide, superoxide anion, and organic peroxides.

These ROS can lead to cellular damage if they are not detoxified by antioxidant systems. The GSH (glutathione) redox system represents one of the most important cellular defence systems against oxidative stress, and mitochondria are known to have high levels of GSH. Enhancing production of ROS within mitochondria and inhibiting GSH production may lead to oxidative stress and the induction of apoptosis (Dalton, 2002). Moreover, cancer cells are in general metabolically active, produce high levels of ROS, and are under intrinsic oxidative stress, the malignant cells are more vulnerable to further oxidative stress by exogenous ROS- generating agents (Pelicano, 2003). Accumulation of intracellular ROS leads to disruption of the mitochondrial membrane potential, release of cytochrome c with subsequent activation of the caspase cascade, and ultimately to programmed cell death through apoptosis.

The degree of cell death was correlated with the intracellular levels of ROS. Reactive oxygen species generated in response to arsenic exposure lead to accumulation of intracellular H_2O_2 (Jing, 1999; Woo, 2002) (figure 21). As_2O_3 has been showed to increase H_2O_2 levels in NB4 (APL cell line) cells mainly by inhibiting the activity of GPx (glutathione peroxidase) (figure 21), which is a major H_2O_2 scavenging thiol-enzyme, probably by the binding of As_2O_3 to vicinal thiol group in GPx. Cotreatment with a GPx inhibitor, and, to a lesser extent, with a catalase inhibitor, potentiates the induction of apoptosis by As_2O_3. The high sensitivity of cells to As_2O_3 appears to reside in cell-specific pattern of expression of GPx and catalase (Woo, 2002), as well as GST (glutathione-S-transferase: an enzyme involved in the detoxification of a variety of xenobiotics), which represents the major As_2O_3 detoxifying enzyme. Thus, high levels of GSH, which is a proton donor for the GPx-catalyzed breakdown of H_2O_2 and for the GST-catalyzed detoxification of As_2O_3, ensure rapid rates for these reactions, thus conferring a protective effect (Jing, 1999). Other findings are also consistent with these observations: As_2O_3 induces apoptosis in solid tumors with generation of ROS, H_2O_2-resistant solid tumors cells are less responsive, and catalase-deficient solid tumor cells are hypersensitive to arsenic (Cheng, 2010; Maeda, 2004; Woo, 2002). On the other hand, it is possible that As_2O_3 increases the mitochondrial production of H_2O_2. For instance, 20 μmol/L arsenite led to H_2O_2 accumulation through a mechanism thought to depend on the activation of NADPH oxidase (Chen, 1998). As_2O_3 has also been found to increase superoxide generation in leukemia cells by hindering mitochondrial respiration and this caused an inhibition of respiration (Pelicano, 2003).

Studies showed that the modulation of the redox system, and particularly the GSH content, determines the sensitivity of the cells toward As_2O_3 (Figure 21). GSH is the major antioxidant of the cells and functions to scavenge free radicals and detoxify toxins and chemotherapeutic agents. GSH can bind As_2O_3 from attacking its target by formation of transient $As(GS)_3$ complex. Studies showed that 1 to 2 µmol/L As_2O_3, the therapeutically effective concentrations of As_2O_3 which induce remission in APL with minimal toxicity (Shen, 1997), induced apoptosis within 3 days in lymphoid, myeloid and solid tumor cells (Dai, 1999; Jing, 1999; Grad, 2001; Cheng, 2010; Biswas, 2010). The apoptotic effect of As_2O_3 was inversely correlated with GSH content in malignant cells. NB4 cells, sensitive to As_2O_3, showed a GSH content three times lower compared to cells lines not responding to As_2O_3. Two human breast cancer lines with low GST were also sensitive to low concentrations of As_2O_3 and the sensitivity to As_2O_3 was inversely proportional to GSH levels in both breast carcinoma cell lines (Dai, 1999). The compounds that lower the GSH content potentiate the apoptotic effect of As_2O_3, whereas protecting or increasing the GSH level protects the cells from apoptotic effect of As_2O_3 (Dai, 1999). Multiple myeloma (MM) and solid tumor cells are protected from the apoptotic effect of As_2O_3 if treated with antioxidant NAC (*N*-acetyl-*L*-cysteine), which preserves the GSH content (Dai, 1999; Grad, 2001; Cheng, 2010). On the other hand, BSO (buthionine sulfoxide), which inhibits the synthesis of glutamyl-cysteine, lowers the GSH content of APL and solid tumor cells, and potentiates the apoptotic effect of As_2O_3 (Dai, 1999; Maeda, 2004; Cheng, 2010). In BSO-treated cells, 1 µmol/L As_2O_3 induces apoptosis in 70% of the cells in only 12 hours of treatment, and less sensitive cell lines become as sensitive as NB4 (Dai, 1999). The *in vivo* study also showed that this combination induced tumor (orthotopic model of prostate cancer metastasis) growth inhibition in both primary and metastatic lesions, and that this combination therapy prolonged survival rate compared to As_2O_3 treatment alone, with moderated side effects (Maeda, 2004).

Potential synergy of As_2O_3 and ascorbic acid (AA) has been shown *in vitro* and *in vivo* (Dai, 1999; Grad, 2001; Bahlis, 2002; Biswas, 2010). Indeed, studies showed that AA in combination with As_2O_3 has a potentiating effect on apoptosis in lymphoid, myeloid and hepatocarcinoma cell lines (Dai, 1999; Grad, 2001; Bahlis, 2002; Li, 2006). Although heralded as an antioxidant, AA also has prooxidant activities. Auto-oxidation of AA to dehydroascorbate can result in production of H_2O_2. Dehydroascorbate is then rapidly

reduced back to AA by glutaredoxin in a GSH-dependent manner. This reduction of dehydroascorbate to AA results in a decrease of reduced intracellular GSH (Grad, 2001). This decrease was correlated with an increase in ROS production (Grad, 2001; Li, 2006). This synergic effect manifested also in an epithelial mammary carcinoma line, whereas normal breast or embryo fibroblasts were insensitive to the combined treatment. This selective action of ascorbic acid may be partially due to the low concentration of catalase in some malignant cells (Dai, 1999). Moreover, the apoptosis induced by combined-treatment was abrogated in the presence of NAC. Thus, AA potentiated As_20_3-induced apoptosis through the oxidative pathway by increasing the ROS level (Grad, 2001; Li, 2006). A Phase I clinical trial showed that As_20_3 (0,25mg/Kg/day) combined with AA (1000mg/day) in six relapsed/refractory myeloma patients is well tolerated during the treatment period. Partial response (≥25% decrease in disease markers) has been observed in two patients and stable disease (0%-25% decrease in disease markers) in four patients (Bahlis, 2002).

The apoptotic process induced by ROS due to As_20_3 was accompanied by the loss of mitochondrial membrane potential, the down-regulation of Bcl-2 protein and followed by the activation of caspases (Figure 21). The mitochondrial membrane potential collapse was observed in numerous cell lines and is an important event in As_20_3-induced apoptosis (Zhu, 1999; Cai, 2003; Han, 2008; Woo, 2002). This event causes the release of cytochrome c from mitochondria to the cytosol (Chen, 1998). The down-regulation of Bcl-2 protein which plays an important role in the apoptosis progress was also observed after As_20_3-treatment. An overexpression of Bcl-2 blocked As_20_3-induced apoptosis, demonstrating that Bcl-2 plays a major role in As_20_3-induced apoptosis in tumor cells. However, authors did not observe Bcl-2 degradation (Jing, 1999). It is known that mitochondrial membrane potential collapse results in the activation of caspases, which play a central role in the apoptosis-signaling pathway. Indeed, As_20_3 markedly increases the cleavage of caspase-3 and caspase-9, which are implicated in the apoptosis progress in most cells (Ai, 2006; Park, 2000; Maeda, 2001; Han, 2008; Zhu, 1999; Jing, 1999; Wang, 2009). However, in a study, caspases activation was not required for cell death because caspase inhibitors could not rescue the cells from As_20_3-induced cell death (Kang, 2004).

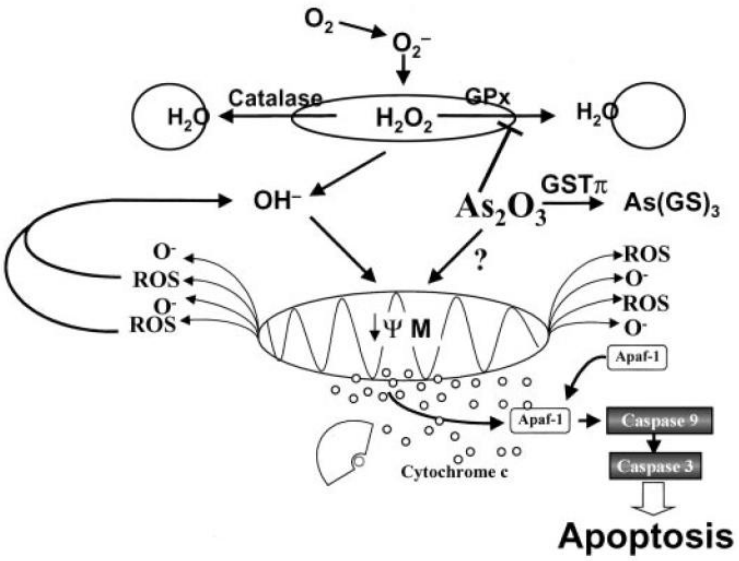

Figure 21: As_2O_3 induces apoptosis via changes in the mitochondrial membrane potential. As_2O_3 treatment of malignant cells results in increased intracellular levels of hydrogen peroxide, which lowers mitochondrial membrane potential and leads to cytochrome c release and subsequent activation of caspase pathway (Miller, 2002b).

2.2. Growth inhibition

As_2O_3 was shown to inhibit the proliferation of multiple myeloma and solid tumor cells by inducing the cell cycle arrest as well as triggering the apoptosis. As_2O_3 exhibits a dose-dependent inhibition of cellular proliferation in these cell lines (Bornstein, 2005; Park, 2000; Shao, 2005; Han, 2008). As_2O_3 was able to prominently induce a G_1 phase and/or a G_2/M phase arrest of multiple myeloma cells (Park, 2000). These results were consistent with those of other investigators who showed that anti-proliferative action of arsenical compound was linked to a G_1 phase arrest in lymphoid neoplasm, bladder carcinoma (Wang, 2009) and a G_2/M phase arrest in NB4 cells, prostate and gastric carcinoma cancer cell lines (Cai, 2003; Maeda, 2001; Shao, 2005) at lower doses. Therefore, it is likely that As_2O_3 may induce the cell cycle arrest of a G_1 phase and/or a G_2/M phase depending on the cell type, suggesting that the molecular mechanisms of cell cycle arrest by As_2O_3 have great variety. As_2O_3-induced cell cycle arrest in multiple myeloma cells seemed to result from the inactivation of CDK6 (cyclin-dependent kinase: regulator of cell cycle in eucaryotes) in a G_1 phase and the inactivation of cdc2 (important role in the S phase and the G_2/M progression of the cell

cycle) in a G_2/M phase through the induction of p21 (inhibitor of CDKs) (Park, 2000, Han, 2008). However, regulation of expression of cell cycle-related proteins differs significantly depending on cell type (Zhu, 1999; Maeda, 2001). As_2O_3 also induces growth inhibition *in vivo* in solid tumors (Maeda, 2001; Shen, 2004) and inhibition of the metastatic potential of retroperitoneal lymph node and mouse hepatoma (Maeda, 2001; Zhao, 2009). Mitotic arrest seems a common mechanism for As_2O_3-induced apoptosis in most cancer cells (Cai, 2003).

2.3. Angiogenesis inhibition

Angiogenesis is recognized as playing a role in the pathophysiology of many human malignancies. It is an important factor in the tumor progression and is closely related to invasion and metastases. The anti-vascular effects of As_20_3 were first observed *in vivo* by Lew at al. The study clearly demonstrated that a single injection of As_20_3 induced a selective vascular shut-down of tumor blood perfusion at 2h and 6h leading to massive central necrosis in murine solid tumors (methylcholanthrene-induced fibrosarcoma) within 4h and steadily progressed until at least 48h (Lew, 1999). Similar results were also obtained in fibrosarcoma and carcinoma (Lew, 2002; Griffin, 2005; Monzen, 2004). The underlying mechanisms of vascular shut-down and central necrosis are not easily explained. However, a probable mechanism could be an increase of the expression of adhesion molecules and cytokines in the tumor. A study showed a clear increase in expression of adhesion molecules ICAM (intercellular adhesion molecule), VCAM (vascular cell adhesion molecule), E-selectin (Griffin, 2000), and cytokines TNF-α (tumor necrosis factor- α) 2 hours after As_20_3 treatment (Griffin, 2000; Lew, 2002; Griffin, 2005). Consequently, the expression of adhesion molecules in the tumor vasculature could slow the circulation and eventually block the passage of blood as white blood cells adhere to the vascular wall (Griffin, 2000). Among the factors contributing to angiogenesis, vascular endothelial growth factor (VEGF) is recognized as one of the most important molecules in the formation of new blood vessels. Over-expression is suggested to participate in the carcinogenic process. As_20_3 can inhibit VEGF expression *in vitro* and *in vivo* and suppress angiogenesis (Xiao, 2006). Finally, As_20_3 was also showed to decrease the formation of new blood vessels in tumor tissues, inhibit proliferation of vascular endothelial cells and induce their apoptosis, which

results in down-regulation of endothelial growth factor receptors expression in tumor tissues in a dose-dependent manner (Xiao, 2007).

2.4. As_2O_3 and radiotherapy

The induction of apoptotic cell death is a significant mechanism of tumor cells under the influence of radio/chemotherapy, and resistance to these treatments has been link to some cancer cell lines with a low propensity for apoptosis. Several studies indicated that combining radiation and As_2O_3 may be a new and more effective mean of cancer treatment (Lew, 2002; Monzen, 2004; Griffin, 2005; Kim, 2003; Ning, 2006; Chun, 2002; Kang, 2008; Ho, 2009). Indeed, Lew at al. demonstrated that As_2O_3 combined to irradiation, both after single and fractionated irradiation, enhances tumor growth delay and local tumor control. The study suggested that the increased production of TNF-α by As_2O_3 (observed in the study) might be responsible for the synergistic effect of radiation and As_2O_3 (Lew, 2002). A widely studied aspect of As_2O_3 exposure is the depletion of the glutathione level in cells, which may lead to oxidative stress and that has been linked to increases in radiosensitivity (Monzen, 2004; Jones, 1990). However, Griffin at al. showed a greatest regrowth delay when combining treatment and radiation every 3 days (5 Gy of radiation were followed immediately by 8 mg/Kg As_2O_3 at 3 days intervals up to a total of 30Gy), at the time of maximal tumor oxygenation (measured by Eppendorf pO_2 histograph) in their model (Griffin, 2005). Therefore, increase in radiation response of the tumors appears to be partially the result of increased tumor oxygenation. Subsequent studies have found that As_2O_3 was highly effective in enhancing radiotherapy of rat gliomas and xenografted human glioblastomas (Kim, 2003; Ning, 2006) but the mechanism was not clearly demonstrated. Recently, the combined treatment, As_2O_3 and irradiation, has been showed to increase apoptotic cell death, which was correlated with the increase in intracellular reactive oxygen species generation, the loss of mitochondria membrane potential, and the activation of caspase-3 (Ho, 2009). Similar results were also demonstrated *in vitro* and *in vivo* in human cervical cancer (Chun, 2002; Kang, 2008). Authors also investigated possible adverse effects of combined treatment with As_2O_3 and radiation. No obvious liver dysfunction was caused by the combined treatment since the levels of aspartate aminotransferase and alanine aminotransferase were unchanged. Moreover, no significant toxic effects

either by observation of activity, weight or pathological morphology, indicating that the combination with As_20_3 and irradiation was well tolerable treatment (Xie, 2007).

2.5. Conclusion

Investigations using many different experimental systems suggest that As_20_3 may offer significant therapeutic benefits to patients. As_20_3 presents numerous known effects on tumor cells, and As_20_3 seems also to act on the mitochondrial respiratory chain but little is known about the mechanisms by which As_20_3 inhibits the mitochondrial respiratory chain, particularly *in vivo*. We therefore made the hypothesis that As_2O_3 could be an important modulator of tumor oxygenation by affecting the oxygen consumption of tumor cells. This will be part of our project in the present thesis. It is important to note that reports have revealed that different cell lines may have distinct, even opposite response to As_20_3. The effects of As_20_3 vary considerably, depending of the cell type and the dose administered. The clinical effects of As_20_3 are being trialed against solid tumors that are mostly refractory to current therapies. As_2O_3 has been trialed in different cancer (liver, pancreatic prostate, gastric...) but the results are not yet available and most clinical studies are underway (Dilda, 2007).

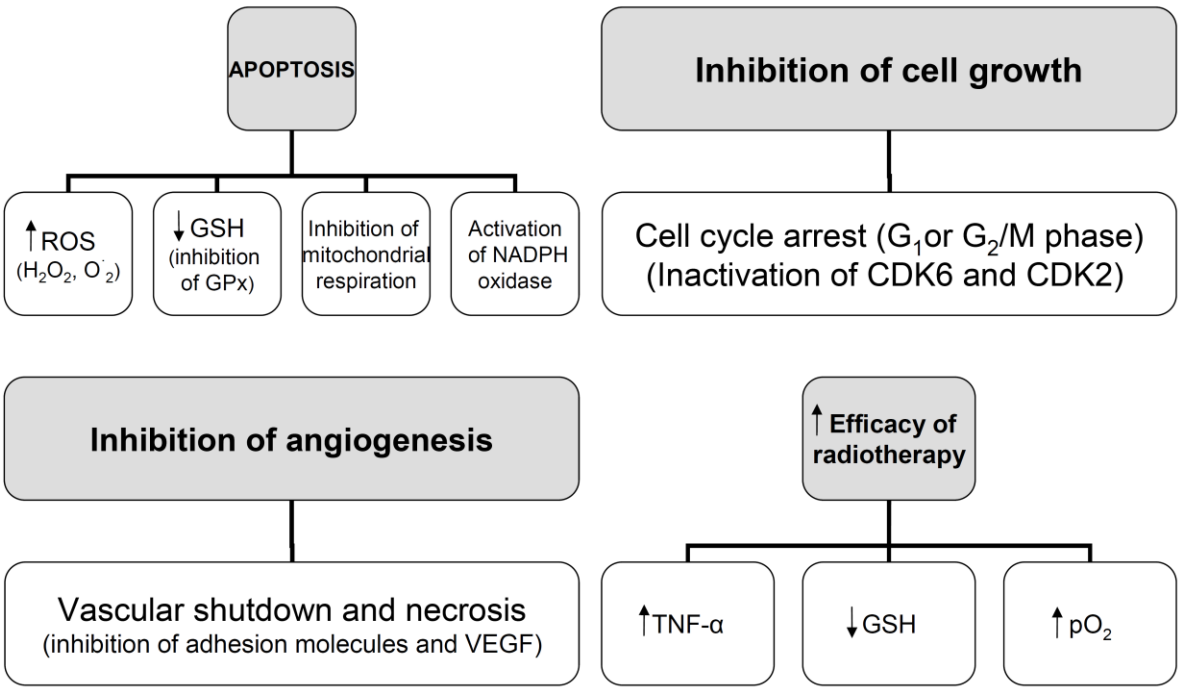

Figure 22: Major effects of As_2O_3. As_2O_3 acts on cells through a variety of mechanisms, influencing numerous signal transduction pathways and resulting in a vast range of cellular effects that include apoptosis induction, growth inhibition, angiogenesis inhibition and enhancement of radiotherapy efficacy.

Chapter 2: Aims of the thesis

The aim of the thesis was to evaluate and validate new techniques to measure oxygen consumption by tumor cells (*in vitro* and *in vivo*), and to identify and characterize a pharmacological drug able to modulate tumor oxygen consumption and evaluate its effects on tumor radiosensitivity (figure 23).

First, we compared three methods able to measure oxygen consumption *in vitro*: EPR oximetry, the Clark electrode, and a fluorescence method. The action of two treatments able to decrease cellular oxygen consumption to different degrees (by acting on the mitochondrial respiratory chain) was evaluated using the three above mentioned techniques. A systematic comparison has been performed in terms of sensitivity and practical aspects.

A second objective of the thesis was to develop new methods to measure oxygen consumption *in vivo*. For that purpose, we used *in vivo* EPR oximetry and ^{19}F MRI relaxometry and we designed a protocol in which pO_2 was monitored in the tissue of interest during a breathing challenge. The challenge included sequential breathing of carbogen (95% O_2 and 5% CO_2) and air. During carbogen breathing, local pO_2 increases progressively and reaches a plateau value, whereas while switching back to air, pO_2 returns to its basal values. Our hypothesis was that the return kinetics could be mainly influenced by the local oxygen consumption. Hyperthyroidism is known to dramatically affect the oxygen consumption rate of muscle and tumor cells and was used to validate our protocol of *in vivo* oxygen consumption measurement. Hyperthyroidism was induced by chronic treatment with L-thyroxine. The same protocol was used with ^{19}F MRI in order to map the oxygen consumption of tumors, and thereby include the heterogeneity aspect in the measurement.

Finally, we evaluated the effect of As_2O_3 on tumor oxygen consumption and response to radiotherapy. For that purpose, we assessed the tumor pO_2, blood perfusion, oxygen consumption and GSH content in two tumor cell lines (TLT and LLC). We also evaluated the cytotoxic effects of As_20_3 by LDH leakage and, finally, studied the impact of As_2O_3 on the sensitivity of the experimental tumors to irradiation.

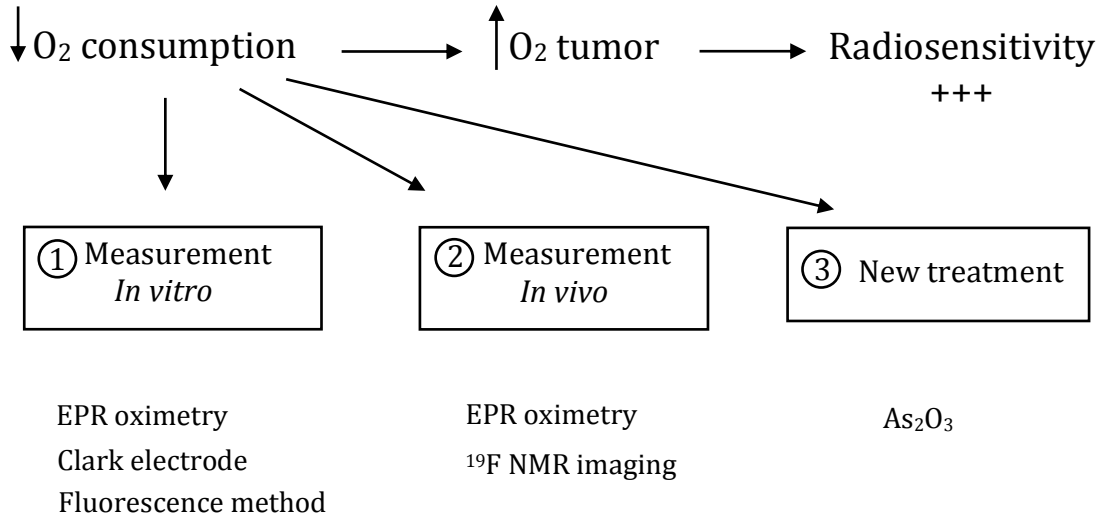

Figure 23: Aims of the thesis: validation of new techniques to measure oxygen consumption by tumor cells (in vitro and in vivo) and, identification and characterization of a pharmacological drug able to modulate tumor oxygen consumption and evaluation of its effects on tumor radiosensitivity.

Chapter 3: Characterization and development of methods to measure oxygen consumption

I. Methods to measure oxygen consumption *in vitro*: comparison of three existing methods

Comparison of methods for measuring oxygen consumption in tumor cells *in vitro*

Caroline Diepart, Julien Verrax, Pedro Buc Calderon , Olivier Feron, Bénédicte F. Jordan , Bernard Gallez

Analytical Biochemistry 396 (2010) 250–256

Analytical Biochemistry 396 (2010) 250–256

Contents lists available at ScienceDirect

Analytical Biochemistry

journal homepage: www.elsevier.com/locate/yabio

Comparison of methods for measuring oxygen consumption in tumor cells in vitro

Caroline Diepart [a], Julien Verrax [b], Pedro Buc Calderon [b], Olivier Feron [c], Bénédicte F. Jordan [a], Bernard Gallez [a,*]

[a] Laboratory of Biomedical Magnetic Resonance, Louvain Drug Research Institute, Université catholique de Louvain, B-1200 Brussels, Belgium
[b] Laboratory of Pharmacokinetics, Metabolism, Nutrition, and Toxicology, Louvain Drug Research Institute, Université catholique de Louvain, B-1200 Brussels, Belgium
[c] Laboratory of Pharmacotherapy, Université catholique de Louvain, B-1200 Brussels, Belgium

ARTICLE INFO

Article history:
Received 6 July 2009
Available online 18 September 2009

Keywords:
EPR
ESR
Oxygen consumption
Oximetry
Clark electrode
Fluorescence method

ABSTRACT

The oxygen consumption rate of tumor cells affects tumor oxygenation and response to therapies. Highly sensitive methods for determining cellular oxygen consumption are, therefore, needed to identify treatments that can modulate this parameter. We compared the performances of three different methods for measuring cellular oxygen consumption: electron paramagnetic resonance (EPR) oximetry, the Clark electrode, and the MitoXpress fluorescent assay. To compare the assays, we used K562 cells in the presence of rotenone and hydrocortisone, compounds that are known to inhibit the mitochondrial electron transport chain to different extents. The EPR method was the only one that could identify both rotenone and hydrocortisone as inhibitors of tumor cell oxygen consumption. The Clark electrode and the fluorescence assay demonstrated a significant decrease in cellular oxygen consumption after administration of the most potent inhibitor (rotenone) but failed to show any significant effect of hydrocortisone. EPR oximetry is, therefore, the most sensitive method for identifying inhibitors of oxygen consumption on cell assays, whereas the Clark electrode offers the unique opportunity to add external compounds during experiments and still shows great sensitivity in studying enzyme and chemical reactions that consume oxygen (non-cell assays). Finally, the MitoXpress fluorescent assay has the advantage of a high-sample throughput and low bulk requirements but at the cost of a lower sensitivity.

The importance of oxygen in cancer biology is now well established. Hypoxia is a cause of tumor resistance to radiation and other cytotoxic treatments. Multiple clinical studies using the Eppendorf pO_2 (partial pressure of oxygen)[1] histograph have demonstrated a direct relationship between tumor hypoxia (low oxygen concentration, $pO_2 < 10$ mmHg) and disease progression in a wide variety of human cancers. Hypoxia is also involved in the development of a more aggressive phenotype and contributes to metastasis [1,2].

Tumor oxygenation depends on the balance between oxygen supply and consumption, and both factors should be considered in developing strategies to reduce tumor hypoxia. A number of strategies have been considered in an effort to improve tumor oxygenation during radiation treatment, with the goal of increasing tumor sensitivity to irradiation. Theoretical simulation of oxygen handling in tumors [3] suggests that decreasing the oxygen consumption rate of tumor tissue could be a particularly effective strategy to reduce the fraction of hypoxic tissue in solid tumors. Indeed, several pharmacological drugs that inhibit cellular oxygen consumption have been characterized in vivo for their potential to increase tumor oxygenation and, thereby, to enhance radiosensitivity. Meta-iodobenzylguanidine [4], insulin [5], anti-inflammatory drugs [6], corticoids [7], inhibitors of vascular endothelial growth factor (VEGF) receptor tyrosine kinase (SU5416) [8], and thyroid hormones [9] all play a major role in the metabolism of tumor cells by modifying the rate of oxygen consumption. Other means of reducing oxygen consumption have also been proposed, including administration of glucose, through the Crabtree effect [10], and decreasing local tumor temperature to less than 25 °C [11].

In view of its clinical importance, several techniques have been developed to measure oxygenation status in tissues and tumors in living animals and humans [12,13], but methods to measure rates of oxygen consumption are more limited [14,15]. Three common methods are currently available to measure oxygen consumption in vitro: electron paramagnetic resonance (EPR) oximetry, the Clark oxygen electrode, and the MitoXpress fluorescent assay. EPR is a powerful technology that permits continuous monitoring of oxygenation in tissues (Fig. 1A). The method is based on the variation of the linewidth of a paramagnetic material in the presence of oxygen-consuming cells in a closed system. The effect of treatments on the tumor cell oxygen consumption rate can be

* Corresponding author. Fax: +32 2 764 73 90.
E-mail address: bernard.gallez@uclouvain.be (B. Gallez).

[1] *Abbreviations used:* pO_2, partial pressure of oxygen; VEGF, vascular endothelial growth factor; EPR, electron paramagnetic resonance; FBS, fetal bovine serum; DMSO, dimethyl sulfoxide; LiPc, lithium phthalocyanine.

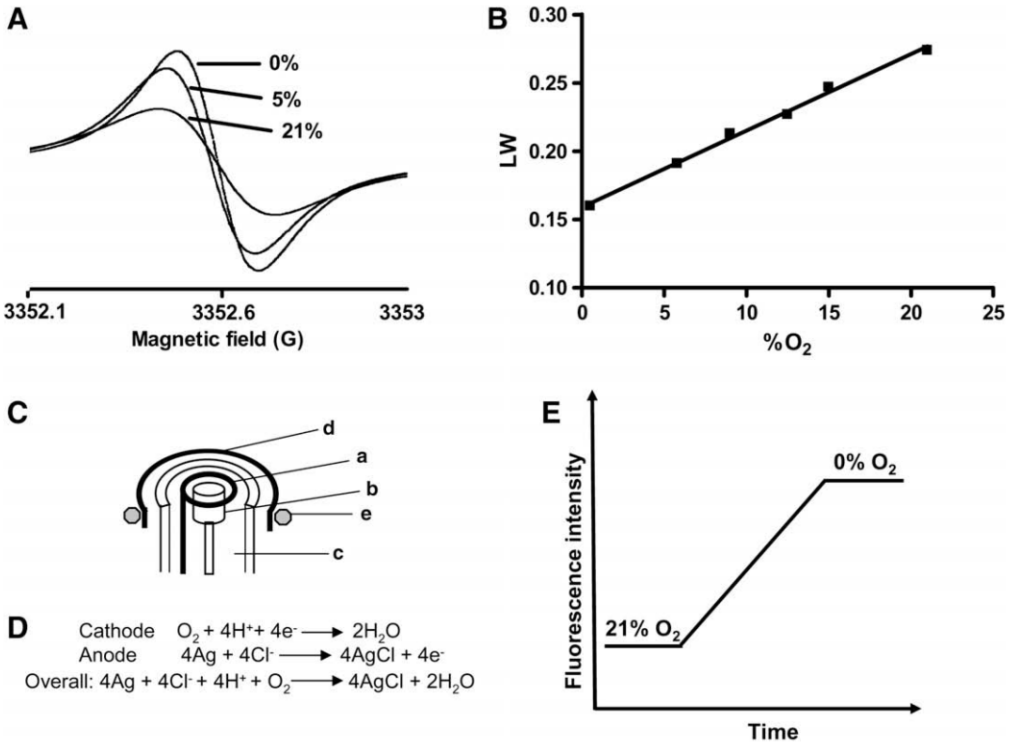

Fig. 1. Principles of the measurement of oxygen using EPR oximetry, the Clark electrode, and the MitoXpress fluorescent assay. (A) EPR spectra recorded in nitrogen or in air. (B) Calibration curve (EPR linewidth [LW] as a function of the pO_2). (C) The Clark-type electrode consists of a platinum electrode (a) and a reference Ag/AgCl electrode (b) covered by a film of half-saturated KCl electrolyte (c) enclosed within a Teflon membrane (d) that is held in place by a rubber ring (e). (D) Current flows from the silver electrode to the platinum electrode as electrons are released into solution from the latter. Removal of electrons from solid silver produces silver ions. The silver ions combine with chloride ions in solution to precipitate silver chloride on the surface of the silver electrode. This leaves potassium ions behind; however, because hydrogen ions are taken out of solution by the consumption of oxygen, the charge remains balanced. (E) Schematic fluorescence intensity profile of MitoXpress during the oxygen consumption assay.

measured because of the relationship between EPR linewidth and pO_2 (Fig. 1B) [16]. The Clark oxygen electrode consists of an anode and a cathode in contact with an electrolyte solution and covered by a semipermeable membrane. Oxygen diffuses through the membrane to the cathode, where it is reduced. The current produced by the electrode is proportional to the oxygen tension in the solution [17] (Fig. 1C and D). Finally, the MitoXpress assay is based on a phosphorescent oxygen-sensitive probe developed by Luxcel. The assay is based on the ability of oxygen to quench the excited state of the MitoXpress probe. Depletion of oxygen in the surrounding solution is perceived as an increase in probe phosphorescence signal. Therefore, changes in oxygen consumption, reflecting changes in mitochondrial activity, are measured as changes in MitoXpress probe signal over time [18] (Fig. 1E).

Oxygen consumption by tumor cells is increasingly recognized as a key parameter for evaluating the efficacy of chemo- and radiotherapy. It is, therefore, timely to compare the sensitivity of the available methods for determining oxygen consumption. In the current study, we compared three methods for measurement of cellular oxygen consumption. We applied the three methods described above to tumor cells exposed to rotenone or hydrocortisone, treatments known to inhibit the mitochondrial electron transport chain to different extents [7,19], so as to provide insight into the advantages and disadvantages of each technique.

Materials and methods

Cell lines

K562 human chronic myelogenous leukemia cells were purchased from the European Collection of Cell Cultures (ECACC, Salisbury, UK). The cells were routinely cultured in RPMI-1640 containing 10% fetal bovine serum (FBS), 1.2% glutamine, and 1% penicillin–streptomycin. The cultures were kept at a density of 1 to 2×10^5 cells/ml. The medium was changed at 48- to 72-h intervals. All cultures were kept at 37 °C in a 95% air/5% CO_2 atmosphere with 100% humidity.

Chemicals

Hydrocortisone was purchased from Pfizer (Solu-Cortef, Pharmacia, Pfizer, Belgium) and diluted in saline. Rotenone was purchased from Sigma–Aldrich (Bornem, Belgium) and diluted in dimethyl sulfoxide (DMSO) to 0.5 mg/ml (Sigma–Aldrich). Cells were treated with hydrocortisone (140 μM for 60 min) or rotenone (20 μM for 30 min) in all of the experiments. Menadione sodium bisulfite (vitamin K_3) and sodium ascorbate (vitamin C) were purchased from Sigma (St. Louis, MO, USA) and diluted in distilled water to 20 μM and 2 mM, respectively.

Measurement of oxygen consumption rate by EPR

EPR spectra were recorded on a Bruker EMX EPR spectrometer operating at 9.5 GHz. Cells were suspended in 10% dextran (to maintain cells in suspension) in complete medium. A neutral nitroxide, ^{15}N 4-oxo-2,2,6,6-tetramethylpiperidine-d_{16}-^{15}N-1-oxyl at 0.2 mM (CDN Isotopes, Pointe-Claire, QC, Canada), was added to 100-μl aliquots of tumor cells (2×10^7 cells/ml and 5×10^6 cells/ml), which were then drawn into glass capillary tubes. The capillary tube was visually checked to avoid air bubbles and was disregarded if it did not conform. The probe (0.2 mM in 20% dextran in complete medium) was calibrated at various pO_2 values between

100% nitrogen and air so that the linewidth measurements could be related to pO_2 at any value. Nitrogen and air were mixed in an Aalborg gas mixer, and the oxygen content was analyzed using a Servomex oxygen analyzer OA540. The sealed tubes were placed into quartz EPR tubes, and samples were kept at 37 °C. The resulting linewidth reports on pO_2, and so oxygen consumption rates were obtained by measuring the pO_2 in the closed tube over time and determining the slope of the resulting linear plot [5].

Fluorescence-based assay of cell respiration

Cultured cells were diluted with prewarmed air-saturated (37 °C) medium (without phenol red) to the desired concentration (2×10^7 cells/ml), and 150 μl/well was dispensed into a 96-well plate (black body, clear bottom). An A65 N-1 oxygen probe (Luxcel Biosciences, Cork, Ireland), supplied as dry powder in a vial, was reconstituted in 1 ml of water [20]. Next, 10 μl of this solution was transferred into each well, and the wells were then covered with 100 μl of prewarmed (37 °C) mineral oil. Time-resolved measurements were carried out at 37 °C on a Victor X4 plate reader (PerkinElmer Life Sciences, Waltham, MA, USA) using standard 340-nm excitation and 642-nm emission filters, reading every minute for 90 min. Oxygen consumption rates were assessed by determining the rate of increase in the probe fluorescent signal for each sample (i.e., $\Delta I/\Delta t$) by linear regression using instrument software. These values were then corrected with respect to blanks (baseline slopes in the absence of cells) and normalized with respect to initial intensity (with 21% of oxygen) (I_{21} at 37 °C) to give normalized intensities [20].

Measurement of oxygen consumption rate by Clark-type electrode

The YSI 5300 Clark-type electrode (Yellow Springs Instrument, Yellow Springs, OH, USA) consists of a platinum cathode and a silver anode, both in contact with an electrolyte solution (50% saturated KCl solution). It is covered at the tip by a semipermeable membrane that is permeable to gases. The electrode was placed and fixed on the top of the measuring chamber. A magnetic stirrer was positioned on the bottom of the measuring chamber. To maintain a stable chamber temperature, an additional surrounding chamber was filled with water and connected with a water circulation system. When a current is applied to the electrodes, the platinum electrode is negatively charged, whereas the silver electrode is positively charged. Oxygen diffuses through the Teflon membrane to the platinum electrode, where it is reduced. The current produced by the electrode is proportional to the oxygen tension in the solution [17]. Air-saturated medium (4 ml) was introduced into the electrode chamber (capacity of 10 ml) and incubated until a steady baseline was obtained on the chart. Cells were suspended in 100 μl (5×10^6 cells/ml) of medium and introduced into the incubation chamber using a Hamilton syringe. The Clark electrode was also used to measure the oxygen uptake from a mixture of ascorbate (2 mM) and menadione (20 μM) dissolved in well-oxygenated phosphate buffer (0.05 M). All of the measurements were carried out at 37 °C.

Statistical analysis

Results are presented as means ± standard errors. Comparisons between groups were analyzed by Student's *t* test or analysis of variance (Dunnett's multiple comparison test) for experiments with more than two groups. *P* values less than 0.05 were considered as statistically significant.

Results

We first compared the oxygen consumption rate using EPR oximetry and the Clark electrode. Using EPR, we measured the decrease in pO_2 over time and observed a significant difference in oxygen consumption between control cells and cells treated with hydrocortisone or rotenone (5×10^6 cells/ml) (Fig. 2). The graphs present the variations in the percentage of oxygen as a function of time. The mean slope was –0.55 ± 0.01 μM/min/5×10^6 cells for control cells ($n = 4$) (Fig. 2A). The slopes were statistically different for rotenone-treated cells (−0.12 ± 0.009 μM/min/5×10^6 cells, $P < 0.001$, $n = 4$) and for hydrocortisone-treated cells (−0.367 ± 0.007 μM/min/5×10^6 cells, $P < 0.001$, $n = 4$). However, using the Clark electrode (Fig. 2B), there was a significant difference between control and rotenone-treated cells ($P < 0.05$, $n = 4$), but cells treated with hydrocortisone had a nonsignificant trend to slower oxygen consumption ($P > 0.05$, $n = 6$). The mean slopes were −0.4 ± 0.07 μM/min/5×10^6 cells for control cells, −0.19 ± 0.008 μmol/L/min/5×10^6 cells for rotenone-treated cells, and −0.32 ± 0.05 μM/min/5×10^6 cells for hydrocortisone-treated cells.

In a second experiment, we measured oxygen uptake in the presence of a cocktail of menadione (vitamin K_3) and ascorbate in a cell-free system using the Clark electrode system. This type of experiment is feasible only with the Clark system, in which extra compounds can be added during the experiment by an access slot in the plunger of the electrode. This type of experiment is not possible with EPR oximetry, which requires a closed and sealed setup. Compared with the rates observed with ascorbate alone, the addition of a solution of menadione was associated with an enhanced

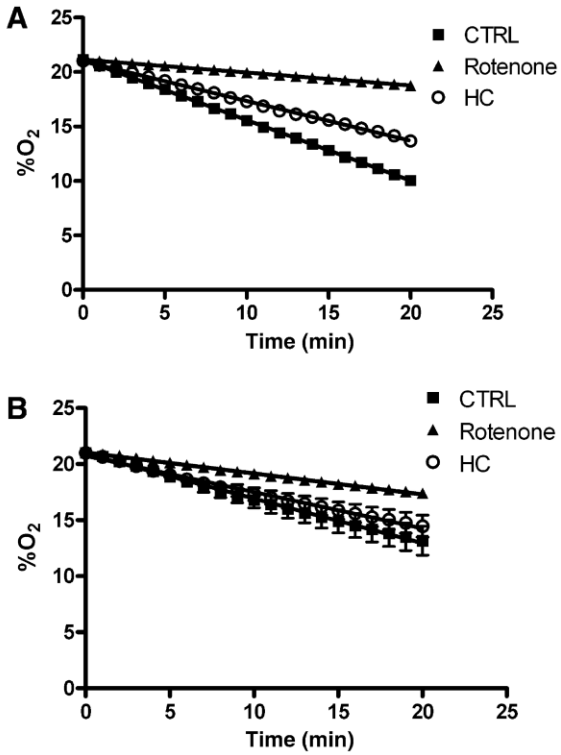

Fig. 2. Oxygen consumption rate measured by EPR oximetry and Clark electrode of K562 cells (5×10^6 cells/ml). (A) When using EPR oximetry, rotenone- and hydrocortisone-treated cells consumed oxygen significantly more slowly than control cells ($P < 0.01$, $n = 4$). (B) When using the Clark electrode, only rotenone induced a significant decrease in oxygen consumption ($P < 0.01$, $n = 4$ for rotenone-treated cells and $n = 6$ for control and hydrocortisone-treated cells). CTRL, control; HC, hydrocortisone.

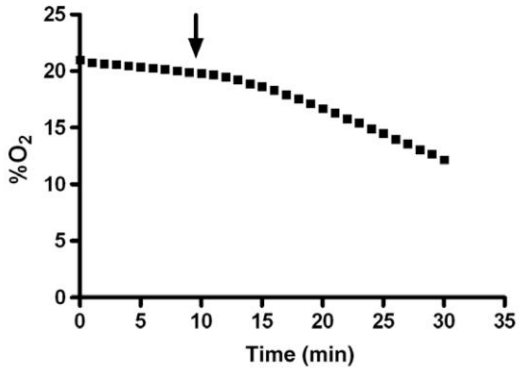

Fig. 3. Effect of 20 μM menadione (vitamin K_3) on oxygen uptake in the presence of 2 mM ascorbate (vitamin C). The arrow corresponds to the injection of menadione. The results are mean values of three separate experiments ± standard errors.

oxygen uptake, as shown in Fig. 3. These results are consistent with those obtained in a previous study [21].

We then compared the ability of the MitoXpress fluorescence assay to detect changes in the oxygen consumption rates of K562 cells treated with rotenone and hydrocortisone. It should be emphasized that no oxygen consumption was visible in the conditions described in the first assay comparing EPR oximetry and the Clark electrode. Indeed, it was necessary to use a concentration of 20×10^6 K562 cells/ml to observe significant oxygen consumption with the MitoXpress assay. It is impossible to inject this quantity of cells using a Hamilton syringe, so the results could be compared only with the EPR method and not with the Clark electrode (see above). Fig. 4A shows the results of the evolution of the normalized fluorescence intensity over the time period. The initial portion of the profile, reflecting temperature equilibration, was disregarded. The graph with the initial portion of the profile show that the starting intensities are the same for the various procedures. The slopes were calculated from the 20th minutes. Initially, the probe emission is quenched by dissolved oxygen present at air-saturated concentrations. When the level of oxygen consumption due to cellular respiration exceeds the rate of back diffusion, a depletion in dissolved oxygen is observed. This is achieved by using a sufficient concentration of cells and adding a layer of mineral oil to impede back diffusion of oxygen. Oxygen depletion reduces the quenching effect, resulting in an increase in probe emission intensity. To make it easier to compare the kinetics, the relative evolution of the fluorescence intensity compared with the initial value is shown in Fig. 4B. There was a marked decrease in respiratory activity of K562 cells treated with rotenone ($P < 0.01$) (Fig. 4B and C), although the small decrease observed in the presence of hydrocortisone was not significant. We used EPR oximetry to measure oxygen consumption using the same concentration of tumor cells

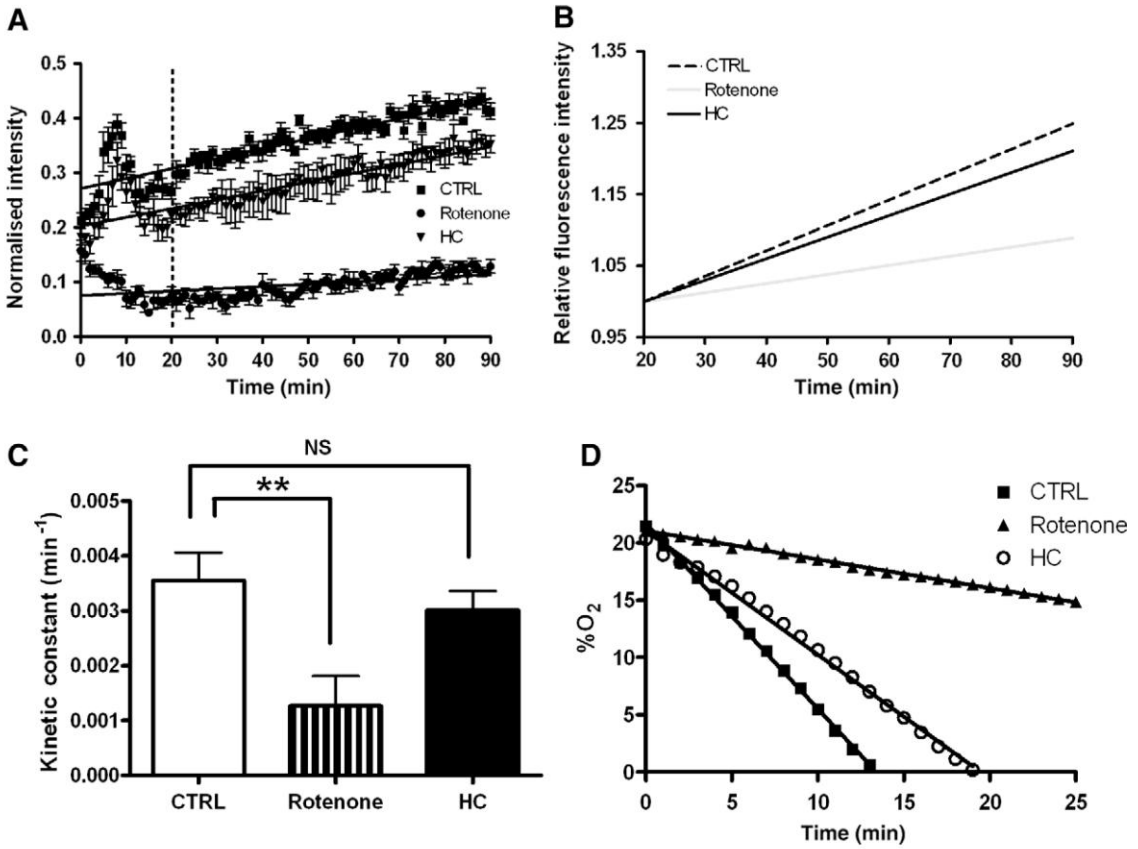

Fig. 4. Oxygen consumption rate of K562 cells (20×10^6 cells/ml) measured by EPR oximetry and MitoXpress fluorescence. (A) Normalized intensity of the assay. By MitoXpress, only rotenone induced a significant decrease in oxygen consumption ($P < 0.01$, $n = 6$). (B) Relative fluorescence intensity of control and treated cells. (C) Kinetic constants measured in control and treated cells. The kinetic constants measured in control cells were higher than those in rotenone-treated cells but not higher than those in hydrocortisone-treated cells ($^{**}P < 0.01$). (D) When using EPR, rotenone- and hydrocortisone-treated cells consumed oxygen significantly more slowly than control cells ($P < 0.01$, $n = 4$). CTRL, control; HC, hydrocortisone; NS, nonsignificant.

(20×10^6 cells/ml) (Fig. 4D). Hydrocortisone induced a significant reduction in oxygen consumption (-1.1 ± 0.02 μM/min/20×10^6 cells, $P < 0.001$), as did rotenone (-0.25 ± 0.007 μM/min/20×10^6 cells, $P < 0.001$), compared with control cells (-1.62 ± 0.01 μM/min/20×10^6 cells).

Discussion

The current study is the first to compare three methods for measuring cellular oxygen consumption. This comparison provides insight into which is the best method for demonstrating the effects of a given treatment on the mitochondrial respiratory chain and may, therefore, be helpful for optimizing existing therapies such as chemotherapy and radiotherapy. Indeed, it has been predicted theoretically that modification of oxygen consumption influences oxygen transport much more effectively than modification of oxygen delivery [3]. Our group further validated this approach as an effective way of radiosensitizing experimental tumors in vivo [5–9]. In the current study, the action of two different treatments acting on the mitochondrial respiratory chain to decrease cellular oxygen consumption to different degrees was evaluated using three techniques: EPR, Clark electrode, and MitoXpress fluorescence. EPR showed a significant decrease in oxygen consumption by K562 cells treated with rotenone and hydrocortisone. The Clark electrode and MitoXpress systems demonstrated a significant decrease in cellular oxygen consumption after administration of rotenone, but there were no significant effects on cells treated with hydrocortisone.

The known advantages of the EPR method include the fact that the cells and oxygen sensors are distributed homogeneously throughout the samples and that the spin probe does not consume oxygen, allowing low concentrations of oxygen in solutions to be measured [19]. It is known that the reduction of nitroxides and the oxidation of hydroxylamines by cells are strongly dependent on the concentration of oxygen. However, the kinetic constants are altered only at very low oxygen concentrations [22,23]. So, the oxygen consumption by the system itself does not play a role above 3% of oxygen, as we used in our study. This method has been shown to be a useful tool for accurate repeated measurements of local concentrations of oxygenation and respiration in cell suspensions [5–9,24,25]. In the current study, EPR oximetry was the most sensitive method for demonstrating subtle differences in oxygen consumption rates. Moreover, EPR measurements were not limited by the numbers of cells, in contrast to the other two techniques, although for different reasons. Indeed, with the Clark electrode the number of cells is limited by the volume added to the incubation chamber, whereas with the MitoXpress method a minimal sensitivity threshold needs to be reached to provide reproducible measurements (i.e., 20×10^6 cells/ml). However, a key limitation of the EPR method is that it is not technically possible to add additional compounds during the experiment. In this study, for instance, we could not measure the oxygen consumption of the mixture of ascorbate and menadione. Moreover, ascorbate interferes with the nitroxide used as the oxygen probe by reducing the free radical into the diamagnetic hydroxylamine that is EPR silent [26]. A possible solution to this problem would be to use a particulate probe such as lithium phthalocyanine (LiPc) to measure the oxygen consumption of the mixture [24], but the EPR system still does not have the facility to enable extra compounds to be added during the experiment. Finally, the cost of the equipment required for EPR oximetry may represent a barrier to choosing EPR for the measurement of cellular oxygen consumption.

The Clark-type oxygen electrode has long been the main technique for measuring pO_2 and oxygen consumption, and it is still widely used on a laboratory scale. Although this measurement approach has proved to be very useful, the methodology is associated with a number of inherent limitations. These include the oxygen consumption by the electrode, the sensitivity to mass exchange (stirring requirements) that may damage the cells during a long experiment, and the need for a large assay volume compared with other techniques. Here we used a standard system with a sample chamber size of 2 to 10 ml. A micro system with a sample chamber size of 600 μl is also available, but the volume is still larger than in the other two methods (100 μl for EPR and <100 μl for fluorescence). Nevertheless, the method offers the unique advantage of being able to add other compounds during the experiment, and this is particularly important in the measurement of mitochondrial oxygen consumption. Indeed, classical mitochondrial assessments entail analysis of oxygen consumption after the addition of substrates (e.g., glutamate, succinate) (state 2), consumption rate on the addition of ADP (state 3), and final return to the basal state after all ADP has been phosphorylated (state 4). For the EPR and fluorescence methods, sequential additions are difficult, so that state 2 is substituted for state 4, yielding a nontraditional ratiomet-

Table 1
Comparison of main characteristics of the three methods for measuring oxygen consumption.

	EPR	Clark electrode	MitoXpress fluorescence
Equipment	EPR spectrometer, probe (nitroxide)	Clark electrode and chamber	Standard microtiter plate, standard fluorescent reader, and oxygen-sensitive probe
Assay volume	100 μl	2–10 ml/600 μl	<100 μl
Cell concentration	Any	Maximum 10×10^6 cells/ml	Minimum 20×10^6 cells/ml
Stirring requirements	No	Yes	No
System sealed	Yes	Yes	Partially
Probe	Yes	No	Yes
Usability	Easy but some knowledge needed	Easy	Easy
Sampling	1 at a time	1 at a time	>96 at a time
Compound addition	Not possible	Possible (syringe)	Not possible
Reproducibility	High	Poor for cells; high for enzyme and chemical reactions	Poor
Sensitivity	High	Poor for cells; high for enzyme and chemical reactions	Poor
Price of equipment	Expensive	Inexpensive	Medium
Price of consumables	Inexpensive	Inexpensive	Inexpensive
Value of pO_2	Quantitative	Semiquantitative	Qualitative

Table 2
Comparison of sensitivity of methods for evaluating the effects of treatments that inhibit oxygen consumption by tumor cells.

	MitoXpress fluorescence	EPR	EPR	Clark electrode
Rotenone	36% ± 18 ($P < 0.01$)	15% ± 0.64 ($P < 0.001$)	22% ± 2.3 ($P < 0.001$)	47.5% ± 11.3 ($P < 0.05$)
Hydrocortisone	83% ± 17.2 ($P > 0.05$)	68% ± 0.7 ($P < 0.001$)	67% ± 1.1 ($P < 0.001$)	80% ± 21.1 ($P > 0.05$)

Note. Each value is expressed as a percentage of the kinetic constant obtained using untreated tumor cells.

ric index [18,27]. The Clark electrode seems to be an easy, reproducible, and sensitive technique for studying enzyme and chemical reactions that consume oxygen, as shown in the assay using the mixture of menadione and ascorbate [21,28].

The advantages of the fluorescence method are the simplicity of the measurement procedure, the high-sample throughput (up to 384 wells), and the low bulk requirements (standard multiwall plates, standard fluorescent reader, and oxygen-sensitive probe). However, to achieve the convenience of measurement in a standard microplate, a level of sensitivity is sacrificed. Due to the incomplete sample sealing in the microplate formats and the associated back diffusion of atmospheric oxygen, the rate of change of dissolved oxygen measured using this approach is lower than the consumption rates measured using a sealed system [18,20]. The concentration of K562 cells should be at least 20×10^6 cells/ml to be able to measure oxygen consumption in this system. The MitoXpress method, using partially sealed systems, produces the same general trends as the Clark electrode system, with fully sealed systems, but does not provide a real value of the pO_2, so it is not possible to measure the absolute quantity of oxygen consumed. The fluorescence assay detected only the effect of a treatment with a strong action on the mitochondrial respiratory chain. In addition, as with EPR, it is not possible to add other compounds during the experiment. A comparison of the main characteristics of the three techniques is given in Table 1, and a quantitative comparison is provided in Table 2.

In conclusion, EPR oximetry appears to be the most sensitive method for measuring the oxygen consumption rate of cells; in the current study, it was the only method able to identify hydrocortisone as an effective inhibitor of oxygen consumption by tumor cells. However, the Clark electrode remains the most appropriate system if the addition of compounds during the course of the experiment is required and shows a very good sensitivity for non-cell assays. The MitoXpress fluorescent method is a cheap, simple, and direct way of measuring cellular oxygen consumption with a sensitivity that is comparable to that of the Clark electrode for cell assays; however, it does not provide the opportunity of adding additional compounds during the experiment.

Acknowledgments

This work was supported by grants from the Belgian National Fund for Scientific Research (FNRS), the Televie, the Fonds Joseph Maisin, the Fondation Belge contre le Cancer, the Saint-Luc Foundation, the "Actions de Recherches Concertées–Communauté Française de Belgique–ARC 04/09-317," the "Pôle d'attraction Interuniversitaire PAI VI (P6/38," and a grant (Nathypox) from the Region Bruxelloise.

References

[1] S.J. Lunt, N. Chaudary, R.P. Hill, The tumor microenvironment and metastatic disease, Clin. Exp. Metastasis 26 (2009) 19–34.
[2] P. Vaupel, L. Harrison, Tumor hypoxia: causative factors, compensatory mechanisms, and cellular response, Oncologist 9 (Suppl. 5) (2004) 4–9.
[3] T.W. Secomb, R. Hsu, E.T. Ong, J.F. Gross, M.W. Dewhirst, Analysis of the effects of oxygen supply and demand on hypoxic fraction in tumors, Acta Oncol. 34 (1995) 313–316.
[4] J.E. Biaglow, Y. Manevich, D. Leeper, B. Chance, M.W. Dewhirst, W.T. Jenkins, S.W. Tuttle, K. Wroblewski, J.D. Glickson, C. Stevens, S.M. Evans, MIBG inhibits respiration: potential for radio- and hyperthermic sensitization, Int. J. Radiat. Oncol. Biol. Phys. 42 (1998) 871–876.
[5] B.F. Jordan, V. Gregoire, R.J. Demeure, P. Sonveaux, O. Feron, J. O'Hara, V.P. Vanhulle, N. Delzenne, B. Gallez, Insulin increases the sensitivity of tumors to irradiation: involvement of an increase in tumor oxygenation mediated by a nitric oxide-dependent decrease of the tumor cells oxygen consumption, Cancer Res. 62 (2002) 3555–3561.
[6] N. Crokart, K. Radermacher, B.F. Jordan, C. Baudelet, G.O. Cron, V. Gregoire, N. Beghein, C. Bouzin, O. Feron, B. Gallez, Tumor radiosensitization by antiinflammatory drugs: evidence for a new mechanism involving the oxygen effect, Cancer Res. 65 (2005) 7911–7916.
[7] N. Crokart, B.F. Jordan, C. Baudelet, G.O. Cron, J. Hotton, K. Radermacher, V. Gregoire, N. Beghein, P. Martinive, C. Bouzin, O. Feron, B. Gallez, Glucocorticoids modulate tumor radiation response through a decrease in tumor oxygen consumption, Clin. Cancer Res. 13 (2007) 630–635.
[8] R. Ansiaux, C. Baudelet, B.F. Jordan, N. Crokart, P. Martinive, J. Dewever, V. Gregoire, O. Feron, B. Gallez, Mechanism of reoxygenation after antiangiogenic therapy using SU5416 and its importance for guiding combined antitumor therapy, Cancer Res. 66 (2006) 9698–9704.
[9] B.F. Jordan, N. Christian, N. Crokart, V. Gregoire, O. Feron, B. Gallez, Thyroid status is a key modulator of tumor oxygenation: implication for radiation therapy, Radiat. Res. 168 (2007) 428–432.
[10] S.A. Snyder, J.L. Lanzen, R.D. Braun, G. Rosner, T.W. Secomb, J. Biaglow, D.M. Brizel, M.W. Dewhirst, Simultaneous administration of glucose and hyperoxic gas achieves greater improvement in tumor oxygenation than hyperoxic gas alone, Int. J. Radiat. Oncol. Biol. Phys. 51 (2001) 494–506.
[11] D.K. Kelleher, C. Nauth, O. Thews, W. Krueger, P. Vaupel, Localized hypothermia: impact on oxygenation, microregional perfusion, metabolic and bioenergetic status of subcutaneous rat tumours, Br. J. Cancer 78 (1998) 56–61.
[12] J.L. Tatum, G.J. Kelloff, R.J. Gillies, J.M. Arbeit, J.M. Brown, K.S. Chao, J.D. Chapman, W.C. Eckelman, A.W. Fyles, A.J. Giaccia, R.P. Hill, C.J. Koch, M.C. Krishna, K.A. Krohn, J.S. Lewis, R.P. Mason, G. Melillo, A.R. Padhani, G. Powis, J.G. Rajendran, R. Reba, S.P. Robinson, G.L. Semenza, H.M. Swartz, P. Vaupel, D. Yang, B. Croft, J. Hoffman, G. Liu, H. Stone, D. Sullivan, Hypoxia: importance in tumor biology, noninvasive measurement by imaging, and value of its measurement in the management of cancer therapy, Int. J. Radiat. Biol. 82 (2006) 699–757.
[13] B. Gallez, C. Baudelet, B.F. Jordan, Assessment of tumor oxygenation by electron paramagnetic resonance: principles and applications, NMR Biomed. 17 (2004) 240–262.
[14] C. Diepart, B.F. Jordan, B. Gallez, A new EPR oximetry protocol to estimate the tissue oxygen consumption in vivo, Radiat. Res. 172 (2009) 220–225.
[15] Y. Song, J.G. Kim, R.P. Mason, H. Liu, Investigation of rat breast tumor oxygen consumption by near-infrared spectroscopy, J. Phys. D 38 (2005) 2682–2690.
[16] P.E. James, S.K. Jackson, O.Y. Grinberg, H.M. Swartz, The effects of endotoxin on oxygen consumption of various cell types in vitro: an EPR oximetry study, Free Radic. Biol. Med. 18 (1995) 641–647.
[17] D. von Heimburg, K. Hemmrich, S. Zachariah, H. Staiger, N. Pallua, Oxygen consumption in undifferentiated versus differentiated adipogenic mesenchymal precursor cells, Respir. Physiol. Neurobiol. 146 (2005) 107–116.
[18] J. Hynes, L.D. Marroquin, V.I. Ogurtsov, K.N. Christiansen, G.J. Stevens, D.B. Papkovsky, Y. Will, Investigation of drug-induced mitochondrial toxicity using fluorescence-based oxygen-sensitive probes, Toxicol. Sci. 92 (2006) 186–200.
[19] T. Presley, P. Kuppusamy, J.L. Zweier, G. Ilangovan, Electron paramagnetic resonance oximetry as a quantitative method to measure cellular respiration: a consideration of oxygen diffusion interference, Biophys. J. 91 (2006) 4623–4631.
[20] J. Hynes, R. Hill, D.B. Papkovsky, The use of a fluorescence-based oxygen uptake assay in the analysis of cytotoxicity, Toxicol. In Vitro 20 (2006) 785–792.
[21] J. Verrax, M. Delvaux, N. Beghein, H. Taper, B. Gallez, C.P. Buc, Enhancement of quinone redox cycling by ascorbate induces a caspase-3 independent cell death in human leukaemia cells: an in vitro comparative study, Free Radic. Res. 39 (2005) 649–657.
[22] K. Chen, J.F. Glockner, P.D. Morse, H.M. Swartz, Effects of oxygen on the metabolism of nitroxide spin labels in cells, Biochemistry 28 (1989) 2496–2501.
[23] M.A. Pals, H.M. Swartz, Oxygen-dependent metabolism of potential magnetic resonance contrast agents, Invest. Radiol. 22 (1987) 497–501.
[24] G. Ilangovan, J.L. Zweier, P. Kuppusamy, Microximetry: simultaneous determination of oxygen consumption and free radical production using electron paramagnetic resonance spectroscopy, Methods Enzymol. 381 (2004) 747–762.

[25] G. Ilangovan, S. Osinbowale, A. Bratasz, M. Bonar, A.J. Cardounel, J.L. Zweier, P. Kuppusamy, Heat shock regulates the respiration of cardiac H9c2 cells through upregulation of nitric oxide synthase, Am. J. Physiol. Cell Physiol. 287 (2004) C1472–C1481.
[26] B. Gallez, C. De Meester, R. Debuyst, F. Dejehet, P. Dumont, Mutagenicity of nitroxyl compounds: structure–activity relationships, Toxicol. Lett. 63 (1992) 35–45.
[27] H. Bugger, J.M. Chemnitius, T. Doenst, Differential changes in respiratory capacity and ischemia tolerance of isolated mitochondria from atrophied and hypertrophied hearts, Metabolism 55 (2006) 1097–1106.
[28] L. Escobar, C. Salvador, M. Contreras, J.E. Escamilla, On the application of the Clark oxygen electrode to the study of enzyme kinetics in apolar solvents: the catalase reaction, Anal. Biochem. 184 (1990) 139–144.

II. Methods to measure oxygen consumption of tumor cells *in vivo*

1. EPR oximetry

A New EPR Oximetry Protocol to Estimate the Tissue Oxygen Consumption *In Vivo*

Caroline Diepart, Bénédicte F. Jordan and Bernard Gallez

Radiation Research 172 (2009) 220–225

RADIATION RESEARCH **172**, 220–225 (2009)
0033-7587/09 $15.00

DOI: 10.1667/RR1448.1

A New EPR Oximetry Protocol to Estimate the Tissue Oxygen Consumption *In Vivo*

Caroline Diepart, Bénédicte F. Jordan and Bernard Gallez[1]

Laboratory of Biomedical Magnetic Resonance, Université catholique de Louvain, B-1200 Brussels, Belgium

Diepart, C., Jordan, B. F. and Gallez, B. A New EPR Oximetry Protocol to Estimate the Tissue Oxygen Consumption *In Vivo*. *Radiat. Res.* 172, 220–225 (2009).

The oxygen consumption rate in tumors affects tumor oxygenation and response to therapies. A new EPR method was developed to measure tissue oxygen consumption non-invasively. The protocol was based on the measurement of pO_2 during a carbogen challenge. The following sequence was used: (1) basal value during air breathing; (2) saturation of tissue with oxygen by carbogen breathing; (3) switch back to air breathing. The assumption was that the kinetics of the return to the basal value after oxygen saturation would be governed mainly by tissue oxygen consumption. This challenge was applied in hyperthyroid mice (generated by chronic treatment with L-thyroxine) and control mice because hyperthyroidism is known to dramatically affect the oxygen consumption rate of tumor and muscle cells. Muscle and tumor cells from the hyperthyroid mice consumed oxygen faster than muscle and tumor cells from the control mice, which is consistent with the results of *in vitro* studies. Tumor perfusion was not affected by the treatment with L-thyroxine. This method gives an index that may reasonably be ascribed to the local oxygen consumption and has the unique advantage of being adaptable to *in vivo* studies. © 2009 by Radiation Research Society

INTRODUCTION

The partial pressure of oxygen (pO_2) is a crucial factor that affects the response of tumors to radiation and other cytotoxic treatments. Over the past decade, clinical studies using oxygen microelectrodes have demonstrated the potential value of measuring pO_2 in tumors to determine the probability of response to conventional radiation therapy. Several studies have shown improved outcomes for cancer patients whose tumors have smaller hypoxic fractions. Tumor hypoxia also promotes metastasis, selects cells with malignant phenotypes, and promotes angiogenesis (*1*).

[1] Address for correspondence: CMFA/REMA, Avenue Mounier 73.40, B-1200 Brussels, Belgium; e-mail: bernard.gallez@uclouvain.be.

Tumor oxygenation depends on a balance between oxygen supply and consumption, and both should be considered in developing strategies to reduce tumor hypoxia. A number of strategies have been considered in an effort to improve tumor oxygenation during radiation treatment, with the goal of increasing tumor sensitivity to radiation. Theoretical simulation of oxygen transport to tumors (*2*) suggests that decreasing the oxygen consumption rate of tumor tissue could be a particularly effective strategy to reduce the fraction of hypoxic tissue in solid tumors. Several drugs that inhibit cellular oxygen consumption have been characterized for their potential to increase tumor oxygenation and thereby enhance radiosensitivity. Meta-iodobenzylguanidine (*3*), insulin (*4*), anti-inflammatory drugs (*5*), corticoids (*6*), some antagonists of vascular endothelial growth factor (VEGF, SU5416) (*7*), and anti-thyroid hormones (*8*) all modify the rate of oxygen consumption by tumor cells. Other means to reduce oxygen consumption have also been proposed, including using the Crabtree effect through administration of glucose (*9*) and decreasing local tumor temperature to less than 25°C (*10*).

There are a number of useful methods for measuring pO_2 or $[O_2]$ *in vivo* (*11, 12*), but methods to measure the tissue oxygen consumption rate are limited. Electron paramagnetic resonance (EPR) can measure oxygen consumption *in vitro* and *ex vivo*. The method is based on the variation of the line width of a paramagnetic material in the presence of consuming cells in a closed system. Because there is a relationship between the line width and the pO_2, the effects of treatments on the tumor cell oxygen consumption rate can be measured (*4*). Positron emission tomography (PET) allows *in vivo* measurements and quantification of physiological processes using short-lived positron-emitting radiopharmaceuticals. The PET technique enables measurement of cerebral oxygen consumption using a short inhalation of $[^{15}O]$-O_2 (*13*); however, this method cannot be applied in tissues with disorganized vascular architecture, such as tumors. Only one method can measure the oxygen consumption rate of tumor cells *in vivo* (*14*). Dewhirst *et al.* reported determinations of the oxygen consumption

rate in microscopic tumor regions bound by microvessels. Profiles of tissue pO_2 were measured along lines crossing the regions using oxygen microelectrodes. Theoretical simulations of the oxygen diffusion in the regions were made, and consumption rates were estimated for the best fit between measured and simulated values (*14*). However, such electrodes are difficult to use, involve a significant degree of invasiveness, and cannot be used for repeated measurements.

In vivo EPR oximetry presents some advantages that make the technique a tool of choice to monitor tissue oxygenation: non-invasiveness, repeatability, sensitivity at low pO_2, localized measurements, little or no toxicity, and ability to make several measurements simultaneously (*15*). Here we developed a new *in vivo* EPR method that can estimate tissue oxygen consumption non-invasively. For this purpose, we designed a protocol where pO_2 was monitored in the tissue of interest during a breathing challenge. During carbogen breathing, local pO_2 increases progressively. When breathing is switched back to air, pO_2 returns to its basal values. Our hypothesis was that the return kinetics could be influenced by the local oxygen consumption. As proof of concept, we applied this protocol in muscle and tumor tissues in hyperthyroid mice and control mice. Hyperthyroidism was induced by chronic treatment with L-thyroxine; this treatment is known to dramatically affect the oxygen consumption rate of muscle and tumor cells (*8, 16*).

MATERIALS AND METHODS

Tumor Model

A transplantable mouse liver tumor (TLT) model was implanted in the legs of NMRI mice. The measurements were performed when the tumor reached 8.0 ± 1.0 mm. All animal experiments were conducted in accordance with national animal care regulations.

Treatments

Mice were treated with L-thyroxine (0.003%) in drinking water for 3 weeks. Animals were anesthetized by inhalation of isoflurane mixed with 21% oxygen in a continuous flow, delivered by a nose cone. Induction of anesthesia was performed using 3% isoflurane; isoflurane was then stabilized at 1.8% for a minimum of 15 min before any measurement.

In Vivo Evaluation of Tissue Oxygenation and Oxygen Consumption

EPR oximetry using charcoal (CX 0670-1; EM Sciences, Gibbstown, NJ) as the oxygen-sensitive probe was used to evaluate changes in tumor oxygenation, using a protocol described previously (*17*). EPR spectra were recorded using an EPR spectrometer (Magnettech, Berlin, Germany) with a low-frequency microwave bridge operating at 1.2 GHz and an extended loop resonator. A suspension of charcoal was injected in the center of the tumor and in the muscle (100 mg/ml; 70 µl injected, particle size of 1–25 µm). Charcoal particles were used because of their metabolic stability and their high sensitivity to subtle changes in tissue oxygenation. The localized EPR measurements correspond to an average of the pO_2 values in a volume of ~10 mm^3 (*17*). The protocol to measure oxygen consumption was performed as follows: When three similar measurements had been obtained under air-breathing conditions, the breathing gas was switched to carbogen. Carbogen breathing was maintained until the local pO_2 reached a maximum (plateau of at least three similar measurements). The gas was then switched back to air and measurements were made until the pO_2 returned to its basal values. Measurements were performed at 5-min intervals during the first part of the experiment (before switching back to air) and at 2- to 4-min intervals during the second part of the experiment. The return kinetics (Δ pO_2 as a function of time, after switching back to air breathing) wass measured by a monoexponential fitting. We also performed an additional experiment in which blood flow to the hind limb was stopped by ligation of the leg after carbogen breathing. The ligation was performed when we obtained the maximal pO_2 after carbogen breathing. Immediately after the ligation, the pO_2 was measured over time. A blue hind limb indicated the success of the clamping. The technique of clamping has been used and validated in experiments with radiation in our laboratory (*8*). In the present experiment, the mean pO_2 measured in tumors before carbogen breathing was 2.9 ± 0.2 mmHg, and the pO_2 measured after clamping was 0.5 ± 0.1 mmHg.

Patent Blue Staining

Patent Blue (Sigma-Aldrich) was used to obtain a rough estimate of the TLT tumor perfusion after treatment with L-thyroxine. This technique involves the injection of 200 µl of Patent Blue solution (1.25%) into the tail vein of the mice. After 1 min, a uniform distribution of the staining through the body was obtained, and mice were killed humanely. Tumors were carefully excised and cut in two size-matched halves. Pictures of each tumor cross section were taken with a digital camera. To compare the stained and unstained areas, an in-house program running on IDL (Interactive Data Language, RSI, Boulder, CO) was used. For each tumor, a region of interest (stained area) was defined on the two pictures, and the percentage of stained area in the whole cross section was determined. The mean of the percentage of the two pictures was then calculated and used as an indicator of tumor perfusion.

RESULTS

Thyroid status influences the oxygen consumption rate of tumor cells (*8*). Tumor cells extracted from control mice consumed oxygen more slowly than tumor cells extracted from hyperthyroid mice. The mean slopes were -1.41 ± 0.11 µ*M*/min ($n = 11$) and -1.91 ± 0.15 µ*M*/min ($n = 9$), respectively (*8*), and were significantly different from each other (Student's t test, $P < 0.05$). Measurements in isolated muscle cells using this protocol were not possible due to difficulties in dissociating the muscle structure rapidly.

Typical evolutions of pO_2 during the breathing challenge are shown in Fig. 1. The first arrow corresponds to the start of the carbogen challenge. The second arrow corresponds to the time when carbogen was switched back to air. Measurements of the evolution of pO_2 in the tumors are shown in the top panels (Fig. 1A and B, for control and hyperthyroid mice, respectively), while experiments in muscles are shown in the bottom panels (Fig. 1C and D, for control and hyperthyroid mice, respectively). In this figure, it can be seen that (1) the kinetics of the return to basal values was faster in hyperthyroid mice than in control mice and (2) the kinetics of the return to basal values was faster in

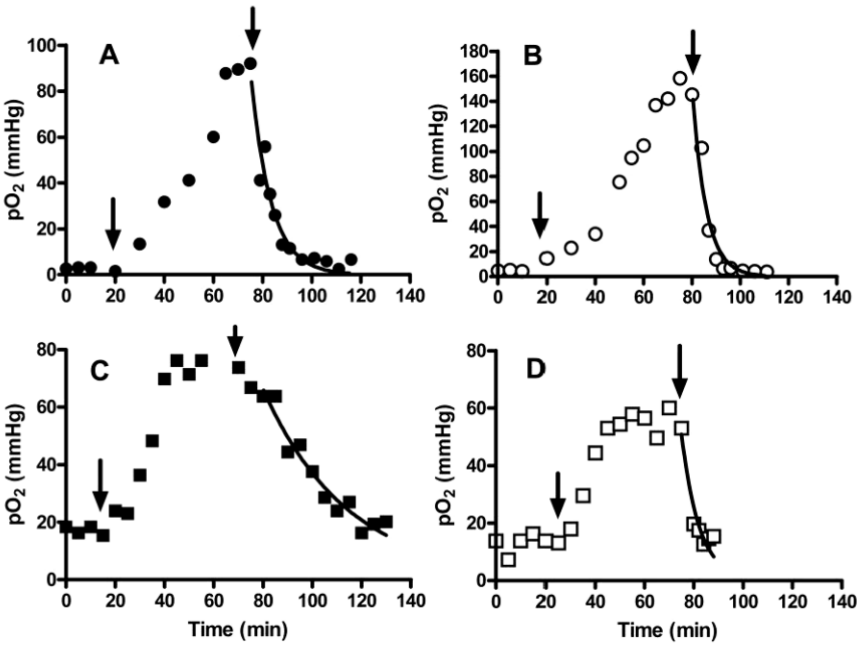

FIG. 1. Evolution of the pO_2 during breathing challenge in tumor and muscle of hyperthyroid and control mice. The measurements were carried out using an EPR spectrometer operating at 1.2 GHz, using charcoal particles as oxygen sensors. First arrow: air switched to carbogen; Second arrow: carbogen switched to air. Upper panels: Typical evolution of pO_2 during the breathing challenge in tumors of a control (panel A) and a hyperthyroid (panel B) mouse. Bottom panels: Typical evolution of pO_2 during the breathing challenge in muscle of a control (panel C) and a hyperthyroid (panel D) mouse. The measurements were done using charcoal in mice at L-band.

tumors than in muscle. Only a few data points were measurable when the return kinetics was rapid, as observed in hyperthyroid mice (Fig. 1B and D). The maximal pO_2 reached after carbogen breathing was lower in hyperthyroid mice than in the control group (84 ± 48.6 mmHg and 123 ± 38 mmHg, respectively). This is consistent with the rapid oxygen consumption by the tissues in hyperthyroid mice. It should be noted that the extent of increase in pO_2 was variable from one mouse to another, especially in tumors. However, the return kinetics was reproducible within groups when the results were expressed as a percentage of the maximal pO_2 reached after carbogen breathing. This is illustrated in Fig. 2 for tumor experiments carried out in hyperthyroid and control mice. The difference between return kinetics observed for tumors in control mice and in hyperthyroid mice is illustrated in Fig. 2A and B (log plot), and individual evolutions of pO_2 are presented in Fig. 2C (control mice) and D (hyperthyroid mice). These graphs illustrate that the measurements were reasonably reproducible within a group and that the return kinetics was systematically faster for hyperthyroid mice (most data points are below 25% of the maximal pO_2 value after 10 min, in contrast to control mice; Fig. 2C and D). The return kinetics measured in muscles of control and hyperthyroid mice is presented in Fig. 3A (normal plot) and B (log plot).

Quantitative estimation of the return kinetics was carried out using a monoexponential curve, because this estimation fitted the experimental data well. The constants of the kinetics (k expressed as min^{-1}) are presented in Fig. 4. Thyroid status significantly modified the constants of the kinetics. The constants for hyperthyroid mice were higher than those for control mice for both tumors and muscles. The k values in tumors were 0.13 ± 0.01 min^{-1} (mean ± standard error, $n = 7$) and 0.18 ± 0.01 min^{-1} (mean ± standard error, $n = 8$) in control and hyperthyroid mice, respectively; this difference was significant (Student's t test, $P < 0.05$). The k values in muscles were 0.09 ± 0.01 min^{-1} (mean ± standard error, $n = 11$) and 0.18 ± 0.02 min^{-1} (mean ± standard error, $n = 13$) in control and hyperthyroid mice, respectively; this difference was highly significant ($P < 0.001$). The constants of the kinetics were greater ($P < 0.05$) in tumors from euthyroid mice than in muscles. However, there were no statistically significant differences between the constants of the kinetics for tumors and muscles in the hyperthyroid mice. To measure oxygen consumption without the potential confounding factors of variability in perfusion and vascular pO_2, we performed an additional experiment consisting of clamping the blood flow to the hind limb after carbogen breathing. The constants after clamping were not significantly different from those in the

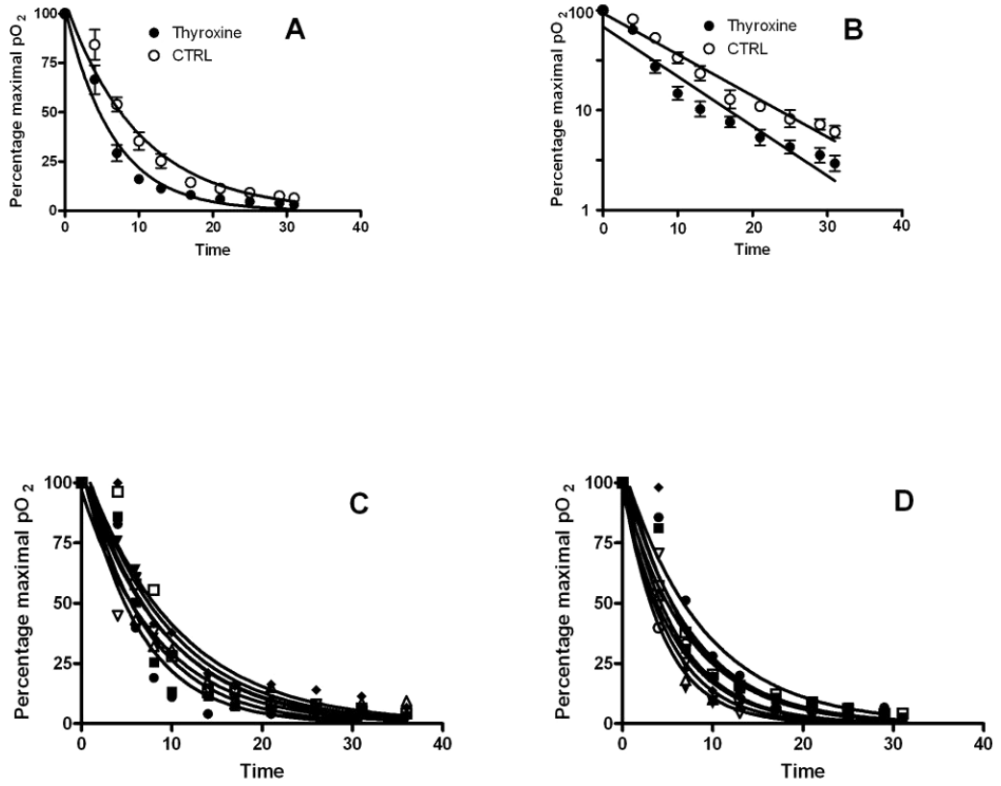

FIG. 2. Return kinetics after carbogen breathing measured in tumors of control (CTRL) and hyperthyroid mice. The results are expressed as a percentage of the maximal pO_2 reached after carbogen breathing (mean ± standard error). Panel A: Normal plot; panel B: log plot; panel C: individual measurements obtained in tumors from control mice; panel D: individual measurements obtained in tumors from hyperthyroid mice.

previous experiment (without clamping). The k values were 0.14 ± 0.02 min^{-1} (mean ± standard error, $n = 5$) and 0.22 ± 0.02 min^{-1} (mean ± standard error, $n = 8$) in control and hyperthyroid mice, respectively.

The effect of L-thyroxine treatment on the tumor blood perfusion was estimated using the colored area observed in tumors 1 min after i.v. injection of Patent Blue (Fig. 5). This method has been validated previously by our group and compared with DCE-MRI data (*6, 7, 20*). No difference was observed between control mice and hyperthyroid mice [71.5 ± 2.7% ($n = 10$) and 70.0 ± 3.5% ($n = 12$), respectively, Student's t test].

DISCUSSION

Tissue oxygen consumption is a key factor in physiology and physiopathology. Modulating tissue oxygen consumption (for example, by hibernation) is an essential part of therapeutic strategy in intensive care medicine and in organ transplantation. In oncology, it has been predicted (*3*) and verified experimentally (*5, 6, 8*) that modification of oxygen consumption is more efficient at correcting tumor hypoxia than modification of oxygen delivery. Although oxygen consumption is thus very important, limited non-invasive methods are available to measure it. In this study, we attempted to develop a new method that can highlight differences in oxygen consumption by different tissues. The use of normal and hyperthyroid mice provided ideal models of tissues with different oxygen consumption rates. First it was confirmed *ex vivo* that treatment with L-thyroxine did change tumor oxygen consumption. The oxygen consumption rate was shown to be significantly enhanced in hyperthyroid mice compared to control mice (*8*). Remarkably, this difference in the oxygen consumption rate was correlated with higher constants of the kinetics, reflecting the rapidity of the return of oxygenation to basal values after presaturation with oxygen (Fig. 4). It is also important to note that the perfusion of the tissues was not affected by the L-thyroxin treatment (Fig. 5). It has also been shown that perfusion of tumors remains unchanged during carbogen breathing (*18, 19*). Thus the perfusion is not responsible for the change in return kinetics, and local oxygen consumption is likely the main factor responsible for this return to initial oxygenation levels. The clamping experiment definitely confirms that our technique is measuring the oxygen consumption of tumor cells without any major influence of confounding factors such as perfusion and vascular pO_2. Interestingly, the constants of kinetics for euthyroid mice were higher in tumors than in muscles (Fig. 4). It is well

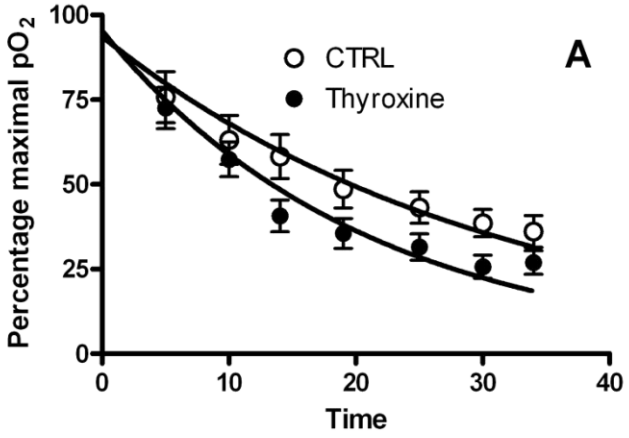

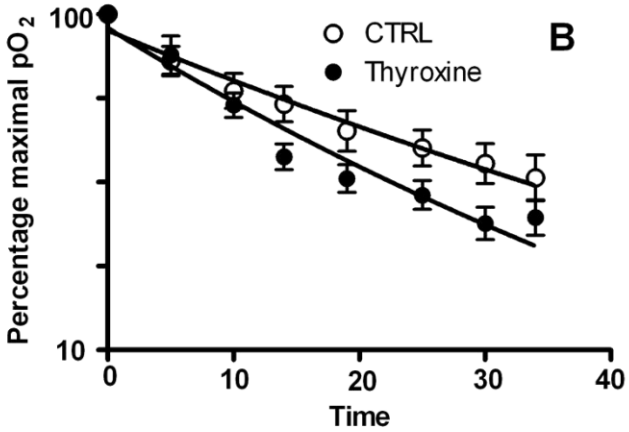

FIG. 3. Return kinetics after carbogen breathing measured in muscles of control (CTRL) and hyperthyroid mice. The results are expressed as a percentage of the maximal pO_2 reached after carbogen breathing (mean ± SEM). Panel A: Normal plot; panel B: log plot.

known that the high rate of tumor cell proliferation and metabolism present in tumors increases oxygen consumption by tumor tissues. However, careful interpretation of the results is important in this case since we are comparing two different tissues with different perfusion rates (i.e., oxygen will be refreshed faster in muscle than in tumor). Perfusion can be a confounding factor when comparing results from poorly and highly perfused tissues. This problem is not present when we study the effect of a treatment on a single tissue. Also, we showed by our clamping experiments that measurements on tumors are not influenced by such a factor, probably because tumors already have very low perfusion rates. Although the experiments were carried out in two tissues that are physiologically and morphologically very

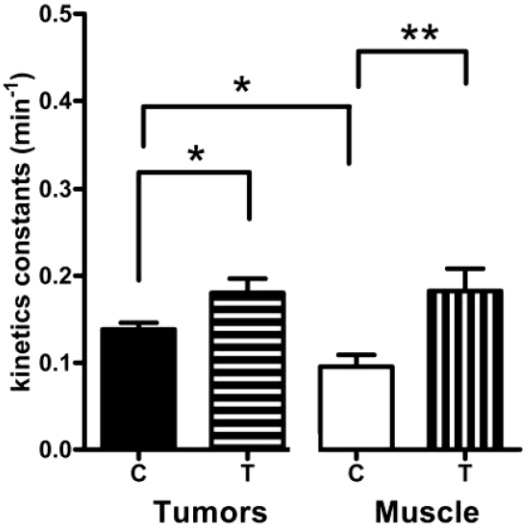

FIG. 4. Constants of kinetics measured in tumor and muscle *in vivo*. $*P < 0.05$; $**P < 0.01$. C: Control, T: thyroxine. The constants measured in tumors and muscles from hyperthyroid mice were higher than in control mice. In euthyroid mice, the constants were higher in tumors than in muscles. In hyperthyroid mice, there was no significant difference between the constants for tumors and muscles.

different, the results obtained are in agreement with the known oxygen consumption rates for hyper- and euthyroid mice. The variability of response after carbogen breathing can be explained by the fact that EPR oximetry is measuring a single point (mean value of ~10 mm^3) in the tumor. Some highly responding regions (such as in the periphery of the tumor) can dramatically influence the mean value. This could be addressed by developing a method to obtain parametric maps of oxygen consumption to be able to probe the heterogeneity of response (see below).

It should be emphasized that our method does not provide a quantitative absolute value of oxygen con-

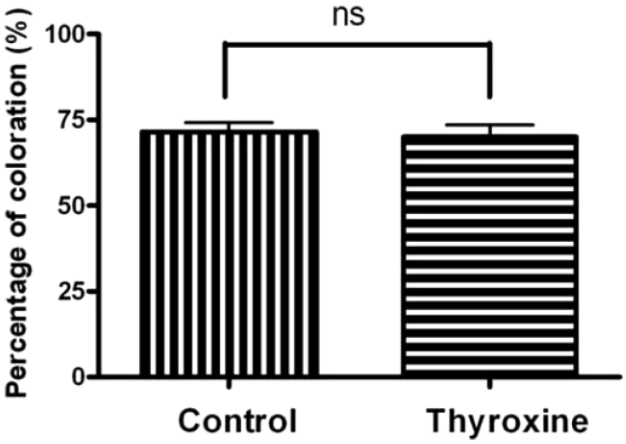

FIG. 5. Perfusion assessed in TLT tumors by the Patent Blue staining technique. No significant difference was observed between control and hyperthyroid mice.

sumption (for example, in terms of μmol of oxygen consumed by millions of cells and per unit of time). Rather, it gives an index that may reasonably be ascribed to the local oxygen consumption. Such a qualitative parameter is also used in *in vivo* EPR to estimate the redox status of a tissue by measuring the kinetics of reduction of nitroxide in tissues (*21, 22*). There are several potential applications of the present work. First, this method should be considered for evaluating *in vivo* the efficacy of different modifiers of oxygen consumption or inhibitors of respiration. Second, the protocol could be transferred to other imaging modalities that are able to visualize oxygen in tissues, such as EPR imaging and ^{19}F NMR imaging, to provide parametric maps reflecting oxygen consumption. Finally, the possibility that EPR may be used in humans in the near future is another reason to pay more attention to this technique (*23*). It should be noted that the carbogen challenge is already being used in the first clinical EPR studies, and our technique to measure oxygen consumption *in vivo* could be an important tool for use in human subjects.

ACKNOWLEDGMENTS

This work is supported by grants from the Belgian National Fund for Scientific Research (FNRS), the Televie, the Fonds Joseph Maisin, the Fondation Belge contre le Cancer, the Saint-Luc Foundation, the "Actions de Recherches Concertées-Communauté Française de Belgique-ARC 04/09-317", and the "Pôle d'attraction Interuniversitaire PAI VI (P6/38)". BJ is a research associate of the FNRS.

Received: April 28, 2008; accepted: April 30, 2009

REFERENCES

1. P. Vaupel and L. Harrison, Tumor hypoxia: causative factors, compensatory mechanisms, and cellular response. *Oncologist* **9** (Suppl. 5), 4–9 (2004).
2. T. W. Secomb, R. Hsu, E. T. Ong, J. F. Gross and M. W. Dewhirst, Analysis of the effects of oxygen supply and demand on hypoxic fraction in tumors. *Acta Oncol.* **34**, 313–316 (1995).
3. J. E. Biaglow, Y. Manevich, D. Leeper, B. Chance, M. W. Dewhirst, W. T. Jenkins, S. W. Tuttle, K. Wroblewski, J. D. Glickson and S. M. Evans, MIBG inhibits respiration: potential for radio- and hyperthermic sensitization. *Int. J. Radiat. Oncol. Biol. Phys.* **42**, 871–876 (1998).
4. B. F. Jordan, V. Gregoire, R. J. Demeure, P. Sonveaux, O. Feron, J. O'Hara, V. P. Vanhulle, N. Delzenne and B. Gallez, Insulin increases the sensitivity of tumors to irradiation: involvement of an increase in tumor oxygenation mediated by a nitric oxide-dependent decrease of the tumor cells oxygen consumption. *Cancer Res.* **62**, 3555–3561 (2002).
5. N. Crokart, K. Radermacher, B. F. Jordan, C. Baudelet, G. O. Cron, V. Gregoire, N. Beghein, C. Bouzin, O. Feron and B. Gallez, Tumor radiosensitization by antiinflammatory drugs: evidence for a new mechanism involving the oxygen effect. *Cancer Res.* **65**, 7911–7916 (2005).
6. N. Crokart, B. F. Jordan, C. Baudelet, G. O. Cron, J. Hotton, K. Radermacher, V. Gregoire, N. Beghein, P. Martinive and B. Gallez, Glucocorticoids modulate tumor radiation response through a decrease in tumor oxygen consumption. *Clin. Cancer Res.* **13**, 630–635 (2007).
7. R. Ansiaux, C. Baudelet, B. F. Jordan, N. Crokart, P. Martinive, J. Dewever, V. Gregoire, O. Feron and B. Gallez, Mechanism of reoxygenation after antiangiogenic therapy using su5416 and its importance for guiding combined antitumor therapy. *Cancer Res.* **66**, 9698–9704 (2006).
8. B. F. Jordan, N. Christian, V. Gregoire, O. Feron and B. Gallez, Thyroid status is a key modulator of tumor oxygenation: Implication for radiation therapy. *Radiat. Res.* **168**, 428–432 (2007).
9. S. A. Snyder, J. L. Lanzen, R. D. Braun, G. Rosner, T. W. Secomb, J. Biaglow, D. M. Brizel and M. W. Dewhirst, Simultaneous administration of glucose and hyperoxic gas achieves greater improvement in tumor oxygenation than hyperoxic gas alone. *Int. J. Radiat. Oncol. Biol. Phys.* **51**, 494–506 (2001).
10. D. K. Kelleher, C. Nauth, O. Thews, W. Krueger and P. Vaupel, Localized hypothermia: impact on oxygenation, microregional perfusion, metabolic and bioenergetic status of subcutaneous rat tumours. *Br. J. Cancer* **78**, 56–61 (1998).
11. B. Gallez, C. Baudelet and B. F. Jordan, Assessment of tumor oxygenation by electron paramagnetic resonance: principles and applications. *NMR Biomed.* **17**, 240–262 (2004).
12. D. S. Vikram, J. L. Zweier and P. Kuppusamy, Methods for noninvasive imaging of tissue hypoxia. *Antioxid. Redox Signal.* **9**, 1745–1756 (2007).
13. P. H. Poulsen, D. F. Smith, L. Ostergaard, E. H. Danielsen, A. Gee, S. B. Hansen, J. Astrup and A. Gjedde, *In vivo* estimation of cerebral blood flow, oxygen consumption and glucose metabolism in the pig by [^{15}O]water injection, [^{15}O]oxygen inhalation and dual injections of [^{18}F]fluorodeoxyglucose. *J. Neurosci. Methods* **77**, 199–209 (1997).
14. M. W. Dewhirst, T. W. Secomb, E. T. Ong, R. Hsu and J. F. Gross, Determination of local oxygen consumption rates in tumors. *Cancer Res.* **54**, 3333–3336 (1994).
15. H. M. Swartz, Using EPR to measure a critical but often unmeasured component of oxidative damage: oxygen. *Antioxid. Redox Signal.* **6**, 677–686 (2004).
16. R. Gredilla, T. M. Lopez, M. Portero-Otin, R. Pamplona and G. Barja, Influence of hyper- and hypothyroidism on lipid peroxidation, unsaturation of phospholipids, glutathione system and oxidative damage to nuclear and mitochondrial DNA in mice skeletal muscle. *Mol. Cell. Biochem.* **221**, 41–48 (2001).
17. B. Gallez, B. F. Jordan, C. Baudelet and P. D. Misson, Pharmacological modifications of the partial pressure of oxygen in murine tumors: evaluation using *in vivo* EPR oximetry. *Magn. Reson. Med.* **42**, 627–630 (1999).
18. M. W. Dewhirst, E. T. Ong, G. L. Rosner, S. W. Rehmus, S. Shan, R. D. Braun, D. M. Brizel and T. W. Secomb, Arteriolar oxygenation in tumour and subcutaneous arterioles: effects of inspired air oxygen content. *Br. J. Cancer Suppl.* **27**, S241–S246 (1996).
19. M. E. Powell, S. A. Hill, M. I. Saunders, P. J. Hoskin and D. J. Chaplin, Effect of carbogen breathing on tumour microregional blood flow in humans. *Radiother. Oncol.* **41**, 225–231 (1996).
20. R. Ansiaux, C. Baudelet, B. F. Jordan, N. Beghein, P. Sonveaux, W. J. De, P. Martinive, V. Gregoire, O. Feron and B. Gallez, Thalidomide radiosensitizes tumors through early changes in the tumor microenvironment. *Clin. Cancer Res.* **11**, 743–750 (2005).
21. P. Kuppusamy, H. Li, G. Ilangovan, A. J. Cardounel, J. L. Zweier, K. Yamada, M. C. Krishna and J. B. Mitchell, Noninvasive imaging of tumor redox status and its modification by tissue glutathione levels. *Cancer Res.* **62**, 307–312 (2002).
22. G. Ilangovan, H. Li, J. L. Zweier, M. C. Krishna, J. B. Mitchell and P. Kuppusamy, *In vivo* measurement of regional oxygenation and imaging of redox status in RIF-1 murine tumor: effect of carbogen-breathing. *Magn. Reson. Med.* **48**, 723–730 (2002).
23. N. Khan, B. B. Williams, H. Hou, H. Li and H. M. Swartz, Repetitive tissue pO_2 measurements by electron paramagnetic resonance oximetry: current status and future potential for experimental and clinical studies. *Antioxid. Redox Signal.* **9**, 1169–1182 (2007).

2. ^{19}FMRI

In vivo mapping of tumor oxygen consumption using ^{19}F-MRI relaxometry

Caroline Diepart, Julie Magat, Bénédicte F.Jordan, and Bernard Gallez

NMR in biomedicine, 2010. In press

In vivo mapping of tumor oxygen consumption using ^{19}F-MRI relaxometry

Caroline Diepart[1], Julie Magat[1], Bénédicte F.Jordan[1*], and Bernard Gallez[1*]

1: Biomedical Magnetic Resonance Group, Louvain Drug Research Institute, Université catholique de Louvain, Avenue Mounier 73, B-1200 Brussels, Belgium

* : BF Jordan and B. Gallez are co-senior authors

Corresponding author:

Prof. Bernard Gallez, PhD
REMA
Avenue Mounier 73.40
B-1200 Brussels
Belgium
bernard.gallez@uclouvain.be
phone: 32 2 7647391
fax: 32 2 764.73.90

Manuscript submitted as Full length paper to *NMR in Biomedicine*

Short title: *In vivo* mapping of tumor oxygen consumption with 19F-MRI

Key words: tumor oxygenation; oxygen consumption; 19F-MRI; tumor micro-environment

Sponsors:
This work is supported by grants from the Belgian National Fund for Scientific Research (FNRS), the Televie, the Fonds Joseph Maisin, the Saint-Luc Foundation, the "Actions de Recherches Concertées-Communauté Française de Belgique-ARC 09/14-020", and the « Pôle d'attraction Interuniversitaire PAI VI (P6/38) ». BJ is a research associate of the FNRS.

List of abbreviations:
PET: positron emission tomography; BOLD: blood oxygenation level dependent; OEF: oxygen extraction fraction; NIRS: near-infrared spectroscopy; HFB: hexafluorobenzene; TLT: transplantable mouse liver tumor; SNAP-IR: snapshot inversion recovery; S/N: signal to noise ratio

Abstract

We recently developed a new EPR protocol in order to estimate tissue oxygen consumption *in vivo*. Because it is crucial to probe heterogeneitiy of response in tumors, the aim of the present study was to apply our protocol along with ^{19}F-MRI relaxometry for *mapping* the oxygen consumption in tumors. The protocol includes the continuous measurement of tumor pO_2 during the following respiratory challenge: 1) basal values during air breathing; 2) increasing pO_2 values during carbogen breathing until saturation of tissue with oxygen; 3) switching back to air breathing. We previously demonstrated using EPR oximetry that the kinetics of the return to the basal value after oxygen saturation are mainly governed by tissue oxygen consumption. This challenge was applied in hyperthyroid mice (generated by chronic treatment with L-thyroxine) and control mice, as hyperthyroidism is known to dramatically affect the oxygen consumption rate of tumor cells. Our recently developed snapshot inversion recovery MRI fluorocarbon oximetry technique allowed to measure the pO_2 return kinetics with a high temporal resolution. Kinetic constants (i.e. oxygen consumption rates) were higher for tumor from hyperthyroid mice than from control mice, data that are consistent with our previous EPR study. The corresponding histograms of the ^{19}F MRI data showed that the kinetics constants display a shift to the right for the hyperthyroid group, indicating a higher oxygen consumption in these tumors. The color maps show a large heterogeneity in terms of oxygen consumption rate within a tumor. In conclusion, ^{19}F-MRI relaxometry allows the non invasive mapping of the oxygen consumption in tumors. The ability of assessing heterogeneity of tumor response is critical in order to identify potential tumor regions that might be resistant to treatment and lead to a lack of success of the therapy.

Introduction

Hypoxia plays a crucial role in the resistance of tumor to chemo and radiotherapy. Several studies have shown improved outcomes for cancer patients whose tumors have lower hypoxic fractions (1). Tumor hypoxia depends on the balance between oxygen supply and consumption, and both factors should be considered in developing strategies to reduce tumor hypoxia. A number of strategies have been considered in an effort to improve tumor oxygenation during radiation treatment, with the goal of increasing tumor sensitivity to irradiation. Theoretical simulation of oxygen handling in tumors (2) suggests that decreasing the oxygen consumption rate of tumor tissue could be a particularly effective strategy to reduce the fraction of hypoxic tissue in solid tumors. Indeed, several pharmacological drugs that inhibit cellular oxygen consumption have been characterized *in vivo* for their potential to increase tumor oxygenation and thereby to enhance radiosensitivity. Meta-iodobenzylguanidine (3), insulin (4, 5, 6), anti-inflammatory drugs (7), corticoids (8), inhibitors of vascular endothelial growth factor (VEGF) receptor tyrosine kinase (SU5416 and ZD6474) (9, 10), and thyroid hormones (11), all play a major role in the metabolism of tumor cells by modifying the rate of oxygen consumption. Other means of reducing oxygen consumption have also been proposed, including administration of glucose, through the Crabtree effect (12), and decreasing local tumor temperature to less than 25° C (13).

Given the importance of oxygen, many techniques for measuring pO_2 in living animals and humans have been developed (14), but methods to measure rates of oxygen consumption *in vivo* are more limited. Among these methods, positron emission tomography (PET) allows *in vivo* measurements and quantification of physiological processes using short-lived positron emitting radiopharmaceuticals. The PET technique enables measurement of cerebral oxygen consumption using a short inhalation of [^{15}O]-O_2 (15, 16). However, this method cannot be applied in tissues with disorganized vascular architecture, such as tumors. The quantitative BOLD (blood oxygenation level dependent) is MRI-based and provides a regional *in vivo* OEF (oxygen extraction fraction measurement) of brain, defining oxygen consumption (17, 18). However, this technique provides only an indirect measurement of oxygen consumption as the method is based on a theoretical model and the deoxyhemoglobin content can be affected by both the local blood flow and volume. ^{17}O Magnetic resonance imaging has also been used to measure cerebral blood flow and oxygen consumption in the cat brain. The technique

has the potential to image cerebral blood flow and oxygen consumption in humans but does not provide a direct measurement of the oxygen consumption (19, 20). Moreover, this technique requires flow measurements. Dewhirst et al. reported determinations of the oxygen consumption rate in microscopic tumor regions bound by microvessels using oxygen microelectrodes. Theoretical simulations of the oxygen diffusion in the regions were made, and consumption rates were estimated for the best fit between measured and simulated values (21). However, such electrodes are difficult to use, involve a significant degree of invasiveness, and cannot be used for repeated measurements. The NIRS (Near-Infrared Spectroscopy) can provide an approach to quantify tumor oxygen consumption rate, but the method requires animal sacrifice. The model describes changes in tumor oxyhemoglobin concentration, as a function of time, before and after potassium chloride induced cardiac arrest (22).

Recently, we developed a new *in vivo* EPR oximetry protocol that can estimate tissue oxygen consumption non-invasively (23). For this purpose, we designed a protocol where pO_2 was monitored in the tissue of interest during a breathing challenge: 1) basal values during air breathing; 2) increasing pO_2 values during carbogen breathing until saturation of tissue with oxygen; 3) rapidly decreasing pO_2 values while switching back to air breathing. We thereby showed that the kinetics of the return to the basal value after oxygen saturation were mainly governed by tissue oxygen consumption. To validate our approach, we applied this protocol in muscle and in tumor tissues in hyperthyroid mice and control mice. Hyperthyroidism is known to dramatically affect the oxygen consumption rate of muscle and tumor cells (11, 24). It was induced by chronic treatment with L-thyroxine. Muscle and tumor cells from the hyperthyroid mice consumed oxygen faster than muscle and tumor cells from the control mice, data that were consistent with *in vitro* studies (11). Tumor perfusion was not affected by the treatment with L-thyroxine. We qualified this method as being able to give an index of the local oxygen consumption. Even though the measure is indirect, it provides the unique advantage of being adapted to *in vivo* studies (23).

In the present study, we applied breathing challenge protocol to map the oxygen consumption of tumors using ^{19}F MR relaxometry after intratumoral injection of HFB (hexafluorobenzene). This spatial information is critical to probe the heterogeneity aspect of the oxygen consumption in tumors. ^{19}F MRI has been developed by the group of Mason to image pO_2 as well as to follow dynamic changes in tumors (25). Our group

recently adapted this method using snapshot inversion recovery (SNAP-IR) in order to increase the time resolution with a similar spatial resolution (26). The technique was applied to monitor acute changes in pO_2 in an experimental tumor model. Here, we demonstrated the feasibility of monitoring *in vivo* tumor oxygen consumption using a SNAP-IR ^{19}F MRI protocol.

Materials and Methods

Tumor model

A transplantable mouse liver tumor (TLT) model was implanted in the gastrocnemius muscle of NMRI mice. The measurements were performed when the tumor reached 8.0 ± 1.0 mm (1 week after tumor cells injection). Tumors were implanted in hyperthyroid and control mice (n=6 for each group). Hyperthyroid mice were obtained by treating the mice with L-thyroxine (0.003%) in drinking water for 3 weeks prior to tumor transplantation. All animal experiments were conducted in accordance with national animal care regulations.

Animal preparation

Before MRI measurements, animals were anesthetized by inhalation of isoflurane mixed with 21 % oxygen in a continuous flow, delivered by a nose cone. Induction of anesthesia was performed using 3 % of isoflurane; and then isoflurane was stabilized at 1.8 % for a minimum of 15 minutes before any measurement. Isoflurane was chosen as it does not compromise the tumor hemodynamics (31).

Hexafluorobenzene (HFB) was deoxygenated by bubbling nitrogen for 5 min before use and was injected into the tumor and deposited along three tracks (3×30µl) encompassing both central and peripheral regions. Warm air was used during MRI acquisition to maintain mouse body temperature.

^{19}F MRI measurements

MRI was performed with a 4.7T (200MHz, ^{1}H), 40cm inner diameter bore system (Bruker Biospec, Ettlingen, Germany). A tunable $^{1}H/^{19}F$ surface coil was used for RF transmission and reception. MRI scout images were obtained for both ^{1}H (200.1MHz) and ^{19}F (188.3 MHz). HFB parametric images of the spin-lattice relaxation time (T_1) were estimated using a snapshot inversion recovery (SNAP-IR) pulse sequence (30). The pulse sequence consisted of a nonselective hyperbolic, secant inversion pulse, followed by acquisition of a series of 512 rapid gradient echo images (repetition time =10.9ms,

echo time = 4.2ms, flip angle = 1°, matrix = 32×16, field of view = 60×30mm, bandwidth = 12.5kHz, total acquisition = 1.5min). Raw (k-space) data were zero-filled to a matrix size of 64×64, resulting in interpolated 64×64 images.

The measurement of oxygen consumption was performed using a protocol described previously (23): When 3 identical measurements had been obtained under air breathing conditions, the breathing gas was switched to carbogen. Carbogen breathing was maintained until the local pO_2 reached a maximum (45min according to EPR) (23). The gas was then switched back to air and measurements were made until the pO_2 returned to its basal values. Measurements were performed at 10 min intervals during the first part of the experiment (before switching back to air), and at 3 min intervals during the second part of the experiment.

Data processing

Data were processed using home made routines in Matlab.

^{19}F MRI images analysis

For each ^{19}F MRI image, a polygonal region of interest encompassing the tumor (ROI) was defined. For each voxel, the signal to noise ratio (S/N) was estimated and voxels with S/N<5 were removed. A non linear fit was used to determine the T_1 relaxation in each pixel of the ROI (a three parameter fit was performed on the signal intensity during inversion time using the standard inversion-recovery equation), having ratio T_1 error/T_1 <50%. A time T_1 map was created with 0<T_1<10ms due to eq. (1).

The calibration curve between the relaxation rate R_1 ($R_1 = \frac{1}{T_1}$) and the pO_2 was estimated in a previous work on *in vitro* samples (30).

$$pO_2(mmHg) = \frac{R_1(s^{-1}) - 0.1048}{0.002} \quad (eq.1)$$

The correlation between T_1 (s) and pO_2 (mmHg) was used to obtain a map of the partial oxygen pressure for each voxel. We estimated that pO_2 values had to be less than 500 mmHg. Even though the evolution of pO_2 was observed during the entire breathing protocol, only the pO_2 values after switching back to air breathing were considered for further analysis, since the return kinetics have been shown to be related to oxygen consumption (see introduction and ref.23). The return kinetics were estimated by a monoexponential fitting (a.exp(-k.x)+b), where the k value represents the kinetic of oxygen consumption in min^{-1}. Fitting conditions were the following: relative difference

between two consecutive pO_2 values less than 5% and each voxel with a k value between 0 and 1.

K map analysis

A cartography of pO_2 return kinetics in each voxel was performed, showing both experimental and fitted data. Data were normalized and voxels with a mean of relative errors between experimental and fitted data superior to 30% were not considered. Finally, aberrant voxels corresponding to fitting with less than 5 points were removed.

Results and discussion

Typical changes in tumor pO_2 assessed with ^{19}F MR relaxometry during the breathing challenge is shown in Fig. 1. The first arrow corresponds to the start of the carbogen challenge. The second arrow corresponds to the time when carbogen was switched back to air. The sampling time of our SNAP-IR technique allowed to probe the return kinetics with a sufficient temporal resolution. Quantitative estimation of the return kinetics was carried out using a monoexponential curve, as this estimation fitted well with the experimental data (Fig.1) (23).

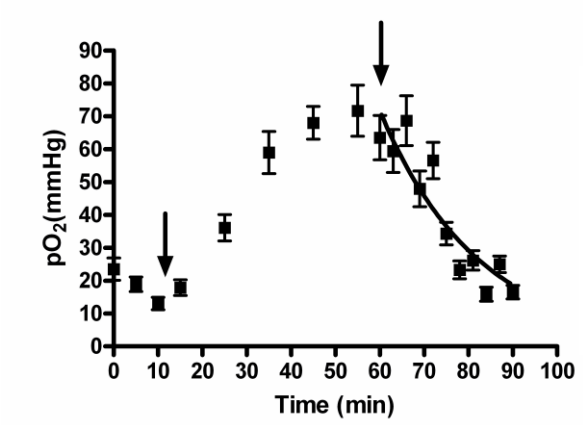

Fig.1
Typical changes of pO_2 (mmHg) over time (min) during the breathing challenge in one control tumor. 1st arrow: air switched to carbogen; 2nd arrow: carbogen switched to air.

As shown previously with EPR oximetry, the thyroid status significantly modified the kinetics constants. Kinetics constants of tumors from hyperthyroid mice were higher than in control tumors (Fig.2A). The k values were 0.076 ± 0.01 min^{-1} (mean ± standard error, n=6) and 0.125 ± 0.015 min^{-1} (mean ± standard error, n=6) in control and treated tumors, respectively; each k value was assessed from a ROI encompassing the whole tumor and k values were then averaged between groups and compared statistically (Student's t test, $P<0.05$). The corresponding histogram (reflecting averaged k values

from both groups) was also generated, showing a shift of the kinetics constants to the right (lower k values) for the treated tumors (i.e. from hyperthyroid mice) (Fig.2B).

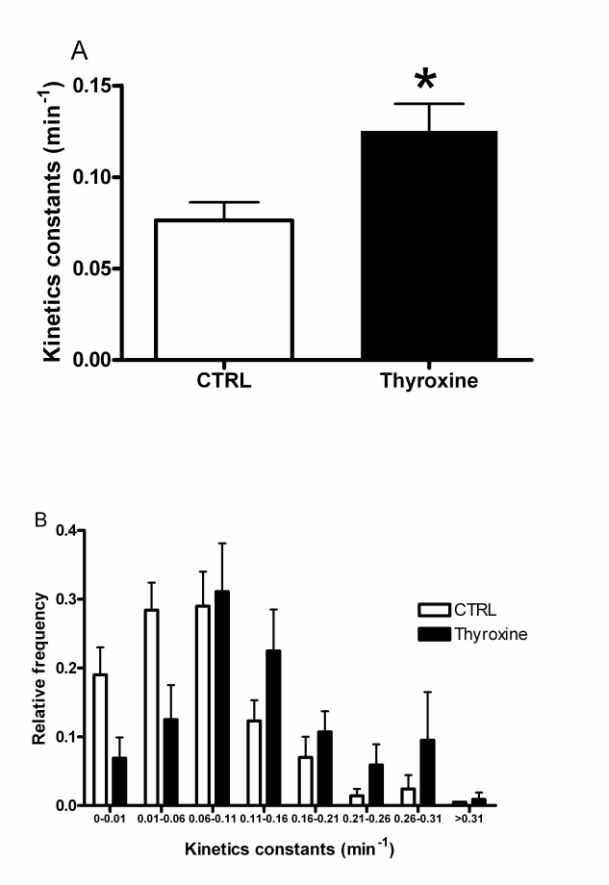

Fig.2
A. *Mean of kinetics constants (min^{-1}) measured in tumors for control and thyroxine treatment. The kinetics constants measured in tumors from hyperthyroid mice were higher than in control mice. *, P<0.05.*
B. *Corresponding cumulative histogram normalized of different k values obtained with ^{19}F MRI data for all mice, generated by defining regions of interest encompassing the whole tumor.*

The results obtained by ^{19}F MRI were similar to our previous EPR study: a significant difference between control and tumors from hyperthyroid mice was observed and the typical changes in the pO_2 matched also well with the EPR technique (similar patterns were observed in response to carbogen breathing with both techniques). However, the range of absolute k values did not match between the two techniques. This further emphasizes the fact that our method does not provide a quantitative absolute value of oxygen consumption, but rather an index that may reasonably be ascribed to the local oxygen consumption. This difference in terms of k values can be explained by the intrinsic differences of the two techniques to probe oxygenation: EPR spectroscopy provides local measurements (mean sampling volume of 10 mm^3) that can be highly influenced by highly hypoxic regions (32), while ^{19}F MR relaxometry provides parametric oxygen values (quantitative mapping of oxygenation) that are usually higher to what is found using other techniques (including invasive fiber optic probes) as observed by our group and others (25, 30, 33), probably because of the

lipophilic property of the sensor (HFB) in which oxygen is more soluble. Even though some earlier reports argued that HFB localized to chronically hypoxic regions and showed values in good agreement with electrode-derived pO_2 (34), we do believe that we interrogate both poorly perfused (chronically hypoxic) regions and well-perfused regions according to the distribution of the basal pO_2 values as well as the large response observed during carbogen breathing, as further discussed in our first HFB study (30). Nevertheless, the k (consumption rates) values can be qualified as qualitative parameters that can be compared between treatments using a single technique, but not be compared from one technique to another.

We previously showed that the perfusion was not responsible for the change in return kinetics, and that local oxygen consumption was the main factor responsible for this return to initial oxygenation levels. Indeed, a clamping experiment confirmed that our technique was measuring the oxygen consumption of tumor cells without any major influence of confounding factors such as perfusion and vascular pO_2 (23). However, in the future, it should be interesting to measure the perfusion by a DCE-MRI study, to completely rule out the influence of perfusion on the kinetics constants, or to develop a combined method with proper analysis in order to exclude any perfusion confounding factors. Also, no correlation was found between tumor pO_2 at saturation (maximal pO_2 during the carbogen challenge) or between baseline pO_2 values and the kinetics constants, those factors are therefore not influencing the estimation of oxygen consumption rate (data not show). Moreover, constants were determined on normalized graphs (see below, Fig. 3B).

For each tumor, we generated color kinetics constants maps derived from the ^{19}F MRI data in each pixel of the tumor, reflecting the heterogeneity in the k values, due to differences in oxygen consumption. Figure 3A shows typical oxygen consumption maps for a control tumor and for a tumor implanted in a hyperthyroid mouse. We can observe a difference in the kinetics constants between the control and the treated tumors, marked by a global increase of the red color (corresponding to high kinetics constants) (Fig.3A). The pO_2 evolution of each pixel in an arbitrary region of interest is illustrated in figure 3B (initial pO_2 in normalized to 1 in each pixel). We can see that the return at the baseline for a control mouse is much longer than for a treated mouse. A typical histogram of the corresponding typical tumors representing all k values from all the pixels within the tumor was also generated (Fig.3C). It shows a clear shift to the right of

the tumor's kinetics constants in the treated tumor (i.e. tumor from hyperthyroid mice). This analysis therefore includes the spatial intra-tumoral heterogeneity information (Fig.3), contrarily to the analysis showing averaged histograms generated from ROIs encompassing the whole tumor (Fig.2).

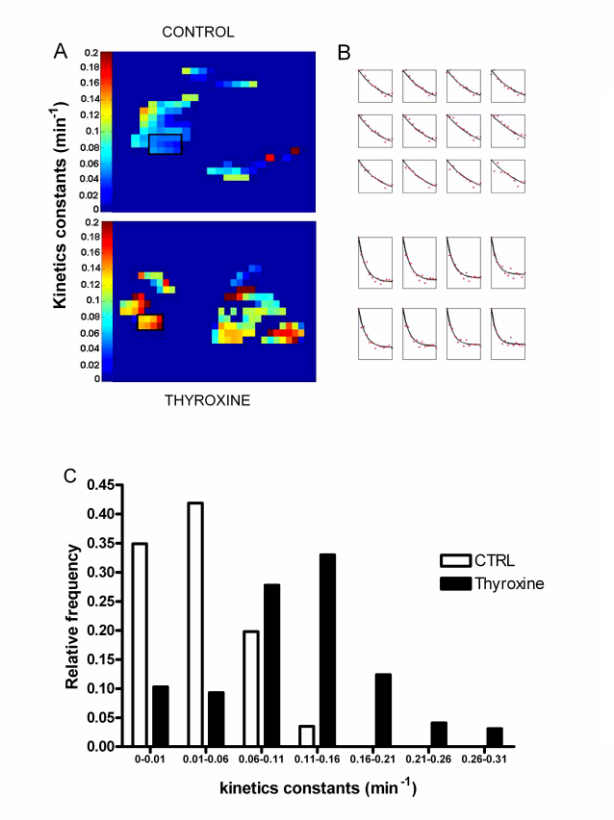

Fig.3
A. *Typical oxygen consumption map in min^{-1} of one control and one hyperthyroid tumor after the carbogen challenge.*
B. *Evolution of kinetics constants for the selected pixels: in dark line the fitting data, and in red dots the experimental data.*
C. *Typical cumulative histogram normalized of k values of the corresponding control and hyperthyroid tumors (generated pixel by pixel from a single tumor).*

In conclusion, ^{19}F MR relaxometry was successfully used to provide maps of an index of oxygen consumption in experimental tumors (constants extracted from the return kinetics after an hyperoxic challenge, an index that may be reasonably ascribed to the local oxygen consumption). We found considerable intra-tumoral heterogeneity in the distribution of the kinetic constants. Indeed, in spite of a difference in oxygen consumption between control and hyperthyroid mice, both showed a large variability in terms of k values. Oxygen consumption by tumor cells might therefore be responsible for intra-tumoral pO_2 heterogeneity, along with the chaotic architecture of the vascular network. This technique offers the unique advantage of being able to probe oxygen consumption *in vivo* in a non invasive way along with the spatial information that is required to probe heterogeneity. The ability to assess heterogeneity of tumor response is critical in order to identify potential tumor regions that might be resistant to

treatment and lead to a lack of success of a therapy. Currently, no clinical application of PFC oximetry has been carried out due to the invasiveness and biocompatibility issues of intra-tumoral implantation of PFC (33).

References

1. Vaupel P, Harrison L. Tumor hypoxia: causative factors, compensatory mechanisms, and cellular response. *Oncologist* 2004; **9 Suppl 5:** 4-9.

2. Secomb TW, Hsu R, Ong ET, Gross JF, Dewhirst MW. Analysis of the effects of oxygen supply and demand on hypoxic fraction in tumors. *Acta. Oncol.* 1995; **34:** 313-316.

3. Biaglow JE, Manevich Y, Leeper D, Chance B, Dewhirst MW, Jenkins WT, Tuttle SW, Wroblewski K, Glickson JD, Stevens C, Evans SM. MIBG inhibits respiration: potential for radio- and hyperthermic sensitization. *Int. J. Radiat. Oncol. Biol. Phys.* 1998; **42:** 871-876.

4. Jordan BF, Gregoire V, Demeure RJ, Sonveaux P, Feron O, O'Hara J, Vanhulle VP, Delzenne N, Gallez B. Insulin increases the sensitivity of tumors to irradiation: involvement of an increase in tumor oxygenation mediated by a nitric oxide-dependent decrease of the tumor cells oxygen consumption. *Cancer Res.* 2002; **62:** 3555-3561.

5. Jordan BF, Sonveaux P, Feron O, Gregoire V, Beghein N, Dessy C, Gallez B. Nitric oxide as a radiosensitizer: evidence for an intrinsic role in addition to its effect on oxygen delivery and consumption. *Int. J. Cancer* 2004; **109:** 768-773.

6. Jordan BF, Beghein N, Crokart N, Baudelet C, Gregoire V, Gallez B. Preclinical safety and antitumor efficacy of insulin combined with irradiation. *Radiother. Oncol*. 2006; **81:** 112-117.

7. Crokart N, Radermacher K, Jordan BF, Baudelet C, Cron GO, Gregoire V, Beghein N, Bouzin C, Feron O, Gallez B. Tumor radiosensitization by antiinflammatory drugs: evidence for a new mechanism involving the oxygen effect. *Cancer Res.* 2005; **65:** 7911-7916.

8. Crokart N, Jordan BF, Baudelet C, Cron GO, Hotton J, Radermacher K, Gregoire V, Beghein N, Martinive P, Bouzin C, Feron O, Gallez B. Glucocorticoids modulate tumor radiation response through a decrease in tumor oxygen consumption. *Clin. Cancer. Res.* 2007; **13:** 630-635.

9. Ansiaux R, Baudelet C, Jordan BF, Crokart N, Martinive P, Dewever J, Gregoire V, Feron O, Gallez B. Mechanism of Reoxygenation after Antiangiogenic Therapy Using SU5416 and Its Importance for Guiding Combined Antitumor Therapy. *Cancer Res.* 2006; **66:** 9698-9704.

10. Ansiaux R, Dewever J, Gregoire V, Feron O, Jordan BF, Gallez B. Decrease in tumor cell oxygen consumption after treatment with vandetanib (ZACTIMA; ZD6474) and its effect on response to radiotherapy. *Radiat. Res.* 2009; **172:** 584-591.

11. Jordan BF, Christian N, Crokart N, Gregoire V, Feron O, Gallez B. Thyroid status is a key modulator of tumor oxygenation: implication for radiation therapy. *Radiat. Res.* 2007; **168:** 428-432.

12. Snyder SA, Lanzen JL, Braun RD, Rosner G, Secomb TW, Biaglow J, Brizel DM, Dewhirst MW. Simultaneous administration of glucose and hyperoxic gas achieves greater improvement in tumor oxygenation than hyperoxic gas alone. *Int. J. Radiat. Oncol. Biol. Phys.* 2001; **51:** 494-506.

13. Kelleher DK, Nauth C, Thews O, Krueger W, Vaupel P. Localized hypothermia: impact on oxygenation, microregional perfusion, metabolic and bioenergetic status of subcutaneous rat tumours. *Br. J. Cancer* 1998; **78:** 56-61.

14. Tatum JL, Kelloff GJ, Gillies RJ, Arbeit JM, Brown JM, Chao KS, Chapman JD, Eckelman WC, Fyles AW, Giaccia AJ, Hill RP, Koch CJ, Krishna MC, Krohn KA, Lewis JS, Mason RP, Melillo G, Padhani AR, Powis G, Rajendran JG, Reba R, Robinson SP, Semenza GL, Swartz HM, Vaupel P, Yang D, Croft B, Hoffman J, Liu G, Stone H, Sullivan D. Hypoxia: importance in tumor biology, noninvasive measurement by imaging, and value of its measurement in the management of cancer therapy. *Int. J. Radiat. Biol.* 2006; **82:** 699-757.

15. Mintun MA, Raichle ME, Martin WR, Herscovitch P. Brain oxygen utilization measured with O-15 radiotracers and positron emission tomography. *J. Nucl. Med.* 1984; **25:** 177-187.

16. Okazawa H, Kudo T. Clinical impact of hemodynamic parameter measurement for cerebrovascular disease using positron emission tomography and (15)O-labeled tracers. *Ann. Nucl. Med.* 2009; **23:** 217-227.

17. He X, Yablonskiy DA. Quantitative BOLD: mapping of human cerebral deoxygenated blood volume and oxygen extraction fraction: default state. *Magn. Reson. Med.* 2007; **57:** 115-126.

18. He X, Zhu M, Yablonskiy DA. Validation of oxygen extraction fraction measurement by qBOLD technique. *Magn. Reson. Med.* 2008; **60:** 882-888.

19. Pekar J, Ligeti L, Ruttner Z, Lyon RC, Sinnwell TM, van GP, Fiat D, Moonen CT, McLaughlin AC. In vivo measurement of cerebral oxygen consumption and blood flow using ^{17}O magnetic resonance imaging. *Magn. Reson. Med.* 1991; **21:** 313-319.

20. Zhu XH, Zhang N, Zhang Y, Zhang X, Ugurbil K, Chen W. In vivo 17O NMR approaches for brain study at high field. *NMR Biomed.* 2005; **18:** 83-103.

21. Dewhirst MW, Secomb TW, Ong ET, Hsu R, Gross JF. Determination of local oxygen consumption rates in tumors. *Cancer Res.* 1994; **54:** 3333-3336.

22. Song Y, Kim JG, Mason RP, Liu H. Investigation of rat breast tumor oxygen consumption by near-infrared spectroscopy. *J. Phys. D: Appl. Phys.* 2005; **38:** 2682-2690.

23. Diepart C, Jordan BF, Gallez B. A New EPR Oximetry Protocol to Estimate the Tissue Oxygen Consumption In Vivo. *Radiat. Res.* 2009; **172:** 220-225.

24. Gredilla R, Lopez TM, Portero-Otin M, Pamplona R, Barja G. Influence of hyper- and hypothyroidism on lipid peroxidation, unsaturation of phospholipids, glutathione

system and oxidative damage to nuclear and mitochondrial DNA in mice skeletal muscle. *Mol. Cell. Biochem.* 2001; **221:** 41-48.

25. Hunjan S, Zhao D, Constantinescu A, Hahn EW, Antich PP, Mason RP. Tumor oximetry: demonstration of an enhanced dynamic mapping procedure using fluorine-19 echo planar magnetic resonance imaging in the Dunning prostate R3327-AT1 rat tumor. *Int. J. Radiat. Oncol. Biol. Phys.* 2001; **49:** 1097-1108.

26. Jordan BF, Cron GO, Gallez B. Rapid monitoring of oxygenation by ^{19}F magnetic resonance imaging: Simultaneous comparison with fluorescence quenching. *Magn. Reson. Med.* 2009; **61:** 634-638.

27. Baudelet C, Gallez B. Effect of anesthesia on the signal intensity in tumors using BOLD-MRI: comparison with flow measurements by Laser Doppler flowmetry and oxygen measurements by luminescence-based probes. *Magn. Reson. Imaging* 2004; **22:** 905-912.

28. Gallez B, Baudelet C, Jordan BF. Assessment of tumor oxygenation by electron paramagnetic resonance: principles and applications. *NMR Biomed.* 2004; **17:** 240-262.

Chapter 4: Effect of arsenic trioxide on the tumor microenvironment

Arsenic trioxide treatment decreases the oxygen consumption rate by tumors cells and radiosensitizes solid tumors

Caroline Diepart, Oussama Karroum, Julie Magat, Olivier Feron, Julien Verrax, Pedro Buc Calderon, Vincent Grégoire, Bénédicte F. Jordan and Bernard Gallez

Cancer Research, in revision.

Arsenic trioxide treatment decreases the oxygen consumption rate by tumors cells and radiosensitizes solid tumors

Caroline Diepart[1], Oussama Karroum[1], Julie Magat[1], Olivier Feron[2], Julien Verrax[3], Pedro Buc Calderon[3], Vincent Grégoire [4], Bénédicte F.Jordan[1]and Bernard Gallez[1]

1: Louvain Drug Research Institute, Biomedical Magnetic Resonance Group, Université catholique de Louvain, Avenue Mounier 73, B-1200 Brussels, Belgium
2: Laboratory of Pharmacotherapy, Université catholique de Louvain, Avenue Mounier 52, B-1200 Brussels, Belgium
3: Louvain Drug Research Institute, Laboratory of Pharmacokinetics, Metabolism, Nutrition and Toxicology, Université catholique de Louvain, Avenue Mounier 73, B-1200 Brussels, Belgium
4: Center for Molecular Imaging and Experimental Radiotherapy, Avenue Hippocrate, 10, B-1200 Brussels, Belgium

Corresponding author:

Prof. Bernard Gallez, PhD
REMA
Avenue Mounier 73.40
B-1200 Brussels
Belgium
bernard.gallez@uclouvain.be
phone: 32 2 7647391
fax: 32 2 764.73.90

Manuscript submitted to Cancer Research.

Running Title: Arsenic trioxide radiosensitizes solid tumors

Acknowledgments:
This work is supported by grants from the Belgian National Fund for Scientific Research (FNRS), the Televie, the Fonds Joseph Maisin, the Saint-Luc Foundation, the "Actions de Recherches Concertées-Communauté Française de Belgique-ARC 09/14-020", and the « Pôle d'attraction Interuniversitaire PAI VI (P6/38) ». BJ is a research associate of the FNRS.

Abstract

Arsenic trioxide (As_2O_3) has been demonstrated to be a potent agent against acute promyelocytic leukemia (APL) and more recently against solid tumors. As_2O_3 is also known to inhibit mitochondrial respiration in leukemia cells. We hypothesized that As_2O_3 might enhance the radiosensitivity of solid tumors by increasing tumor oxygenation (pO_2), via a decrease in oxygen consumption. The effect of As_2O_3 was studied in two murine radioresistant hypoxic tumor models (TLT and LLC tumors). pO_2 was measured *in vivo* by electron paramagnetic resonance (EPR) oximetry and ^{19}F-MRI relaxometry. Tumor perfusion was assessed by Patent blue staining, and the oxygen consumption rate of tumor cells was measured using high-frequency EPR. As_2O_3 (5 mg/kg, i.p.) caused a rapid increase in pO_2 in both tumor models. The increase in tumor oxygenation was not correlated with an increase in tumor perfusion but was explained by an inhibition of mitochondrial respiration. The decrease in oxygen consumption could be explained to some extent by the observed decrease in GSH content in As_2O_3-treated cells as this may increase intracellular reactive oxygen species (ROS) and lead to disruption of the mitochondrial membrane potential. When TLT tumors were irradiated with X-Rays (10 Gy) during the time-window of reoxygenation induced by the administration of As_2O_3, a significant increase in tumor radiosensitivity was observed. The radiation response was increased 2.2-fold for As_2O_3-treated mice compared to control mice, an effect that was abolished when temporally clamped tumors were irradiated, confirming the involvement of an oxygen effect in the radiosensitizing properties of As_2O_3. These results provide a new rationale for the association of As_2O_3 with irradiation protocols to treat solid tumors.

Introduction

The partial pressure of oxygen (pO_2) is a crucial factor in the response of tumors to irradiation and other cytotoxic treatments. Several studies have shown improved outcomes for cancer patients whose tumors had lower hypoxic fractions (1). Tumor hypoxia results from an imbalance between oxygen delivery and oxygen consumption, either of which may potentially be targeted by therapeutic interventions in order to transiently alleviate tumor hypoxia and potentiate cytotoxic treatments. It has been suggested that modifying oxygen consumption is more efficient at alleviating hypoxia than modifying oxygen delivery (2). Several pharmacological drugs that inhibit cellular oxygen consumption have been characterized for their potential to increase tumor oxygenation and thereby enhance radiosensitivity. Meta-iodobenzylguanidine (3), insulin (4), anti-inflammatory drugs (5), corticoids (6), some antagonists of vascular endothelial (VEGF) receptor tyrosine kinase (SU5416 and ZD6474) (7, 8), and thyroid hormones (9), all play a major role in the metabolism of tumor cells by modifying the rate of oxygen consumption.

Arsenic has been recognized as a medical treatment since the early 1900s and has been used to treat various diseases, from syphilis to cancer. In the 1970s, arsenic trioxide (As_2O_3) was reported to induce complete remission in patients with acute promyelocytic leukemia (APL) in China. Additional studies confirmed that low doses of As_2O_3 could induce complete remission in 90% of relapsed APL patients (10). Importantly, it has become evident that the apoptotic effects of As_2O_3 are not restricted to APL cells but have also been observed in other malignant cells in pre-clinical studies, including myeloma cells, chronic myeloid leukemia cells, and various solid tumors cells, such as esophageal, prostate and ovarian carcinomas (11-13).

Arsenic acts on cells through a variety of mechanisms, influencing numerous signal transduction pathways and resulting in a vast range of cellular effects that include apoptosis induction, growth inhibition, promotion or inhibition of differentiation and inhibition of angiogenesis (11, 14-16). As_2O_3 also seems to inhibit mitochondrial respiratory function in human leukemia cells (17). We therefore hypothesized that As_2O_3 could be an important modulator of tumor oxygenation in solid tumors by affecting the oxygen consumption of tumor cells. The first step of the study was to use electron paramagnetic resonance (EPR) oximetry to monitor pO_2 in experimental tumors after administration of As_2O_3 in order to determine the window of increased tumor

oxygenation. These results were confirmed by ^{19}F-MRI oxygen mapping, a technique that can probe the spatial heterogeneity of response. Patent blue staining (blood flow) and *in vitro* oxygen consumption experiments were performed to investigate the origin of the observed increase in pO_2. The intracellular GSH content was also evaluated to explain a possible mechanism by which As_2O_3 could decrease the oxygen consumption. Finally, the window of reoxygenation was exploited to enhance the response of the tumors to radiation therapy. Our study is the first report of the acute effect of As_2O_3 on oxygen consumption in solid tumors and provides a new rationale for combining As_2O_3 with radiation therapy.

Materials and Methods

Tumor model

Two tumor models were implanted in the gastrocnemius muscle in the rear leg of male mice: the transplantable mouse liver tumor (TLT) model in NMRI mice and the Lewis lung carcinoma (LLC) in C57Black6N mice. Measurements were performed when the tumor size reached 8.0 ± 1.0 mm. All animal experiments were conducted in accordance with national animal care regulations.

Treatments

As_2O_3 was purchased from Sigma-Aldrich (Bornem, Belgium). For the treated group, As_2O_3 was dissolved in PBS (Invitrogen) and given i.p at a dose of 5 mg/kg body weight via a 100 µl injection. Control animals were treated with PBS only. Animals were anesthetized by inhalation of isoflurane mixed with 21% oxygen in a continuous flow, delivered by a nose cone. Anesthesia was induced using 3% isoflurane; isoflurane was then stabilized at 1.8% for a minimum of 15 minutes before any measurement.

Tumor oxygenation

EPR oximetry

EPR oximetry, using charcoal (CX 0670-1; EM Sciences, Gibbstown, NJ) as the oxygen sensitive probe, was used to evaluate changes in tumor oxygenation after treatment with As_2O_3, using a protocol described previously (18). EPR spectra were recorded using an EPR spectrometer (Magnettech, Berlin, Germany) with a low frequency microwave bridge operating at 1.2 GHz and an extended loop resonator. A suspension of charcoal was injected into the center of the tumor 1 day before measurement (100 mg/mL; 70 µL injected, particle size of 1-25 µm). The localized EPR measurements correspond to an

average of the pO_2 values in a volume of ~10 mm^3 (18). The acute effect of As_2O_3 was measured by following the tumor pO_2 status for 2 hours after the single injection. Three measurements were acquired as a baseline before injection.

^{19}F MRI measurements

MRI was performed with a 4.7T (200 MHz, ^{1}H), 40 cm inner diameter bore system (Bruker Biospec, Ettlingen, Germany). A tunable 1H/19F surface coil was used for RF transmission and reception. Parametric images of the spin-lattice relaxation time (T_1) were estimated using a snapshot inversion recovery (SNAP-IR) pulse sequence (19). The pulse sequence consisted of a nonselective hyperbolic, secant inversion pulse, followed by acquisition of a series of 512 rapid gradient echo images. Raw (k-space) data were zero-filled to a matrix size of 64×64, resulting in interpolated 64×64 images. For each image pixel, T_1 was estimated by fitting the standard 3-parameter monoexponential recovery equation describing the signal as a function of inversion time. We denote this computed T_1 as T_1' because the recovery curve is somewhat perturbed by the RF pulses. We then computed $R_1'=1/T_1'$. Calibration of hexafluorobenzene (HFB) was performed as described previously (19). HFB was injected into the tumor and deposited along three tracks (3×30 µl) encompassing central and peripheral regions in a coronal plane. HFB was deoxygenated by bubbling nitrogen for 5 min before use. As_2O_3 was administered by a catheter and the tumor pO_2 was monitored for 2 h.

Patent Blue staining

Patent Blue (Sigma-Aldrich) was use to obtain a rough estimate of the TLT tumor perfusion 1h30 after administration of As_2O_3 or PBS. This technique involved the injection of 200 µl of Patent Blue solution (1.25%) into the tail vein of the mice. After 1 min, a uniform distribution of the stain was obtained throughout the body and the mice were sacrificed. Tumors were carefully excised and cut into two size-matched halves. Pictures of each tumor cross section were taken with a digital camera. To compare the stained versus unstained area, an in-house program running on IDL (Interactive Data Language, RSI, Boulder, CO) was developed. For each tumor, a region of interest (stained area) was defined on each of the two pictures and the percentage stained area of the whole cross section was determined. The mean of the percentages from the two pictures was then calculated and used as an indicator of tumor perfusion.

In-Vitro Evaluation of Oxygen Consumption Rate

TLT cells were routinely cultured in DMEM containing 10% FBS, 4.5 mg/L glucose and 1% penicillin-streptomycin. Confluent cells were suspended in medium without serum 2h before treatment with As_2O_3 (25µM) or PBS. EPR spectra were recorded on a Bruker EMX EPR spectrometer operating at 9 GHz. Tumor cells (2 X 10^7/ml) were suspended in 10% dextran in complete medium. A neutral nitroxide, ^{15}N 4-oxo-2,2,6,6-tetramethylpiperidine-d_{16}-^{15}N-1-oxyl, at 0.2 mM (CDN Isotopes, Pointe-Claire, Quebec, Canada), was added to 100 µl aliquots of tumor cells that were then drawn into glass capillary tubes. The probe (0.2 mM in 20% dextran in complete medium) was calibrated at various pO_2 between 100% nitrogen and air so that the line width measurements could be related to pO_2 at any value. Nitrogen and air were mixed in an Aalborg gas mixer, and the oxygen content was analyzed using a Servomex oxygen analyzer OA540. The sealed tubes were placed into quartz EPR tubes, and samples were maintained at 37°C. As the resulting line width reports on pO_2, oxygen consumption rates were obtained by measuring the pO_2 in the closed tube over time and finding the slope of the resulting linear plot (9).

Cell survival assay

Cellular viability was estimated by measuring the activity of lactate dehydrogenase (LDH) both in the culture medium and in the cell pellet obtained after centrifugation, according to the procedure of Wroblesky and Ladue (20). The results are expressed as the ratio of released activity to total activity.

Tumor regrowth delay assay

The TLT tumor-bearing leg was irradiated locally with 10Gy of 250 kV X-rays (RT 250; Philips Medical Systems; 1.2Gy/min). The tumor was centered in a circular irradiation field measuring 3 cm in diameter. A single dose irradiation of 10 Gy was given 90 min after injection of As_2O_3 or PBS. After radiotherapy, tumor growth was determined daily using a caliper until the diameter reached 16 mm, at which time the mice were sacrificed. A linear fit was performed between 8 and 16 mm, which allowed determination of the time to reach a particular size for each mouse.

Measurement of intracellular GSH

The glutathione content was determined using the Tietze enzyme recycling assay (21), with slight modifications (22). TLT and LLC cells were cultured in DMEM containing 10 FBS, 4.5 mg/L glucose and 1% penicillin-streptomycin. Tumor cells were treated with

As_2O_3 (25 µM) or PBS during 90 minutes for TLT cells and 45 minutes for LLC cells (time of maximal reoxygenation after treatment exposure). Cells were then washed twice with ice-cold phosphate buffered saline and then lysed with a solution of 5-sulfosalicylic acid (5%). After two freeze-thaw cycles, samples were centrifuged at 10 000 g for 10 minutes and the resulting supernatants were kept at -80°C until used. Ten microliters of the samples were then placed in a reaction mixture containing 0.2 U/ml of glutathione reductase, 50 µg/ml 5,5′-Dithio-bis(2-nitrobenzoic acid) and 1 mM ethylenediaminetetraacetaticacid (EDTA) at pH 7. The reaction was initiated by the addition of 50 µM NADPH and changes in absorbance were recorded at 412 nm. Reduced (GSH) and oxidized (GSSG) glutathione were distinguished by the addition of methyl-2-vinylpyridine and their respective concentrations were determined from appropriate standard curves. Results were normalized to the protein content using the method of Lowry (23).

Statistical analysis

Means ± SEs were compared using the unpaired Student's *t* test or ANOVA (multiple comparisons post tests for 3 groups or more). *P* values < 0.05 were considered statistically significant.

Results

As_2O_3 rapidly increases tumor oxygenation

Initial pO_2 values were measured for 15 min before treatment to establish a baseline. The administration of As_2O_3 induced an acute increase in pO_2 in TLT and LLC tumors, an effect that was not observed for the control group (vehicle treated) (Fig. 1). After injection of As_2O_3, the maximal pO_2 was reached at 90 min for TLT and 45 min for LLC tumors, after which pO_2 decreased, enabling a window of reoxygenation after treatment with As_2O_3 to be determined. For TLT tumors, the mean tumor pO_2 after 90 min was 38.58 ± 7.16 mmHg for treated mice (n=6) and 4.26 ± 0.54 mmHg for controls (n=6) (P< 0.01, *t*-test). For LLC tumors, the mean pO_2 after 45 min was 10.46 ±1.3 mmHg for treated mice (n=5) and 4.28 ± 0.27 mmHg for control mice (n=5) (P<0.01, *t*-test).

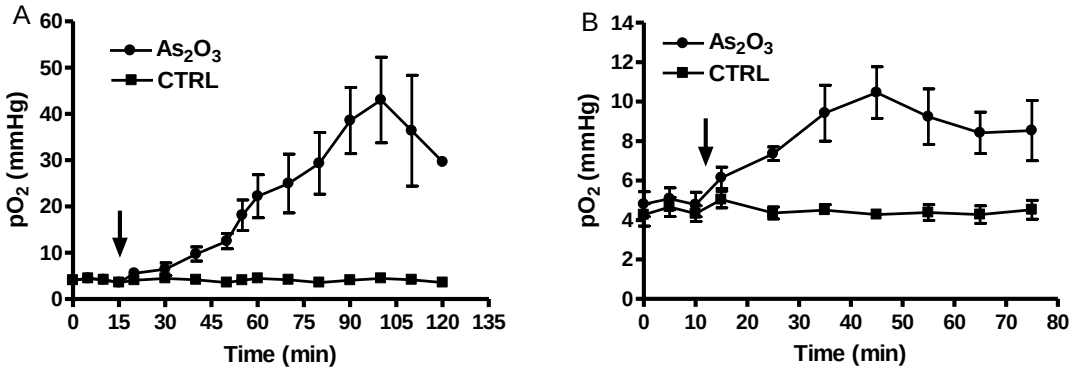

Fig.1
Tumor pO_2 measured by EPR oximetry in TLT (A) and LLC (B) tumors as a function of time. Arrows, injection time of the drug.

The effect of As_2O_3 on pO_2 was further confirmed by ^{19}F MRI relaxometry in TLT tumors, which provides an estimation of the temporal and spatial heterogeneity of response. The mean tumor pO_2 was 15.87 ± 2.17 mmHg before the injection of the drug and 30.74 ± 5.54 mmHg 60 min after As_2O_3-injection (time of maximal pO_2) ($P<0.05$, *t*-test, n=5) (Fig.2A). The evolution of pO_2 over time, as measured by ^{19}F MRI relaxometry, is shown in Fig.2B.

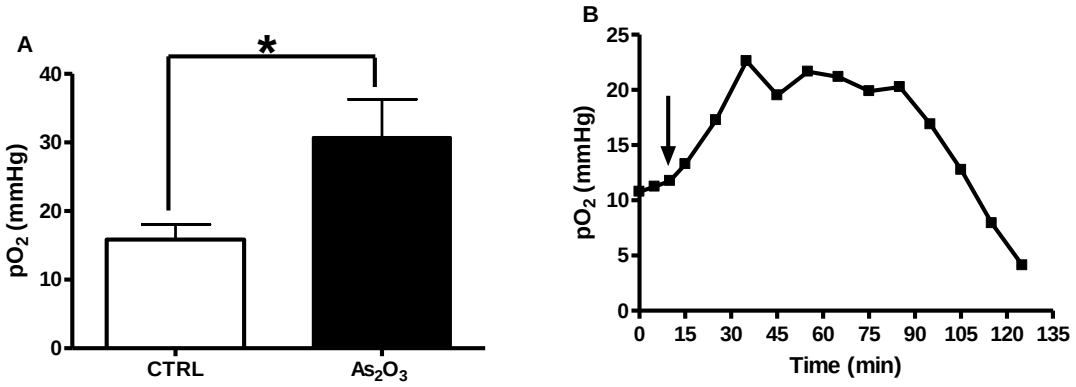

Fig.2
***A:** Tumor pO_2 measured by ^{19}F MRI in TLT tumors. The pO_2 was higher 1h after the injection of As_2O_3 compared to the basal value ($P<0.05$). **B:** Typical graph of tumor pO_2 measured by ^{19}F MRI in TLT tumor of one mouse as a function of time. The arrow corresponds to the time of drug injection.*

To probe the spatial heterogeneity of response, color pO_2 maps and their corresponding histograms were also generated (Fig.3). The color maps show an increase in pO_2 after treatment with As_2O_3, marked by a global increase in the red color (corresponding to pO_2 higher than 10 mmHg). In histogram analysis of these data, the spatial information is

lost but the distribution of values is retained for quantitative analysis. The results show a clear shift of the pO_2 values to the right after As_2O_3 treatment (Fig.3).

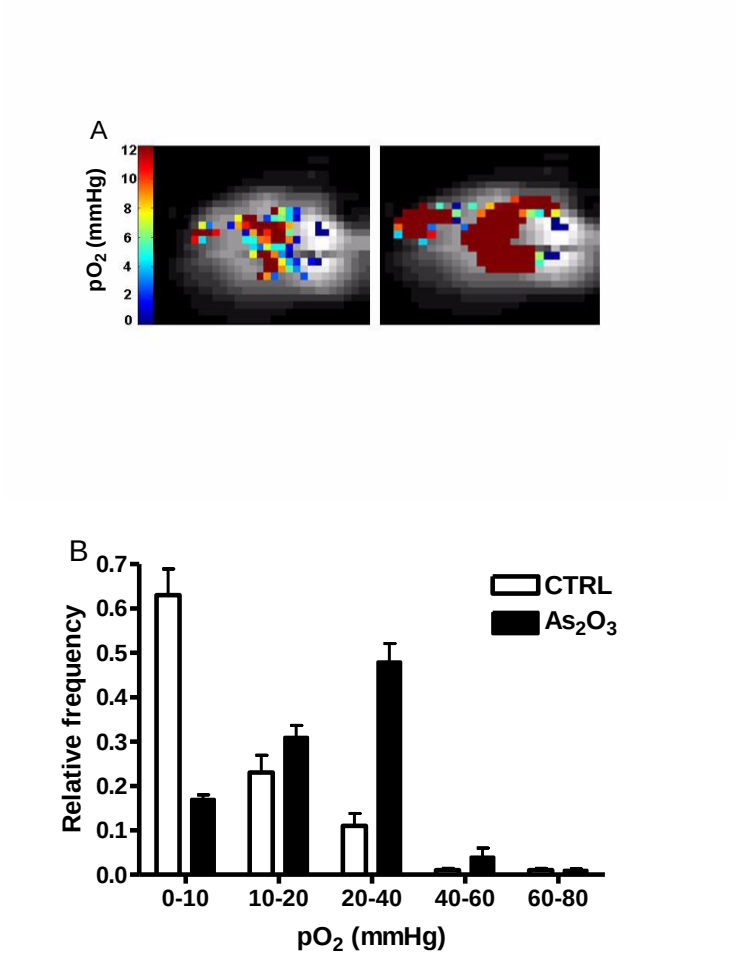

Fig.3
Typical oxygen maps of one TLT tumor before and after As_2O_3 treatment (A) and the corresponding histogram (B).

Note that the basal pO_2 values in TLT tumors measured using EPR and ^{19}F-MRI relaxometry techniques were not exactly the same. This is probably due to the sampling size of the probes as well as to the differences in sensitivity between the two methods and has been discussed in a previously published paper (19). However, the timing of response to As_2O_3, which is the key factor for scheduling radiation therapy, was similar with the two techniques. The reoxygenation window determined the setup for all further experiments (flow estimation, consumption measurement, and therapeutic relevance), which were conducted 90 min after injection for TLT and after 45 min for LLC models.

The reoxygenation induced by As_2O_3 is mediated by an effect on oxygen consumption

To explain the increase in pO_2 induced by As_2O_3, blood perfusion in TLT tumors was investigated using the Patent blue staining assay 90 min after As_2O_3 injection (Fig.4). This method has previously been validated by our group and compared with DCE-MRI data (6, 7). The colored area observed in tumors 1 min after injection of the dye (Patent blue) was decreased in As_2O_3-treated mice (n=8) compared to control mice (n=7) (38.8 ± 4.6% versus 61.2 ± 4.9%, P< 0.01), indicating that blood perfusion was decreased in treated mice compared to control mice.

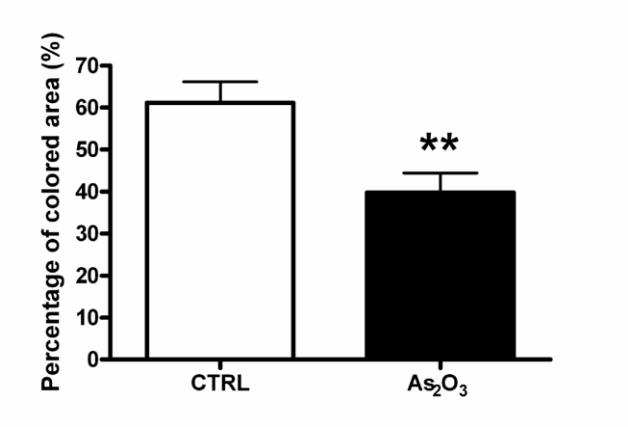

Fig.4
*Effect of As_2O_3 on blood perfusion measured by Patent blue staining. Percentage of coloration and perfusion decrease in treated mice (n= 8) compared to control mice (n=7). **, P<0.01.*

The oxygen consumption of TLT tumor cells was investigated 90 min after treatment, using *in vitro* EPR oximetry. Administration of As_2O_3 significantly decreased the rate of oxygen consumption (Fig.5), with mean slopes of -1.68 ± 0.07 µM/min (n=6) and -3.5 ± 0.1 µM/min (n=7) (P<0.001) for treated and control cells, respectively. As_2O_3-treated cells thus consumed oxygen 2 times slower than control cells.

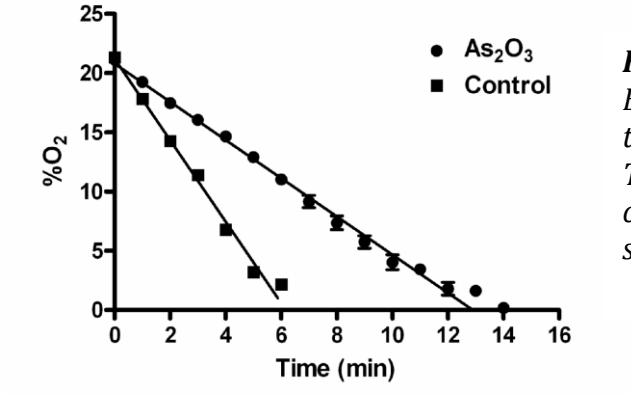

Fig.5
Effect of As_2O_3 administration on tumor oxygen consumption rate in TLT tumor cells. As_2O_3-pretreated cells consumed oxygen significantly more slowly than control cells.

To exclude a possible direct cytotoxic effect of As_2O_3, we also measured the activity of LDH in TLT cells 90 min and 4 h after the administration of As_2O_3. Treatment induced LDH leakage of 23.4 ± 2.5% (90 min after treatment) and 27 ± 2.1% (4h after treatment) compared to 34.1 ± 2.1% (90 min after treatment) and 34.2 ± 2.3% (4h after treatment) in control mice. These results indicate that As_2O_3 did not influence the viability of TLT cells (one-way ANOVA). The results were further confirmed by trypan blue assay (data not shown).

To determine whether the lowering of intracellular GSH content was a possible mechanism by which As_2O_3 could decrease the oxygen consumption of tumor cells, we measured the intracellular content of GSH. GSH contents were 18.3 nmol/mg protein and 42.6 nmol/mg protein for TLT treated and control cells, respectively, and 91.7 nmol/mg protein and 148.7 nmol/mg protein for LLC treated and control cells, respectively (Fig.6).

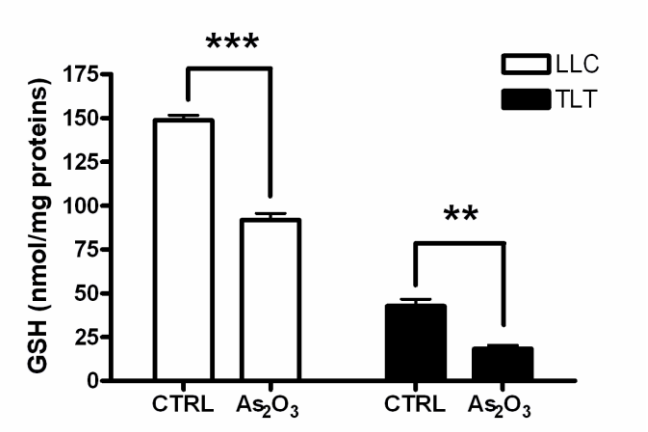

Fig.6
*Intracellular GSH levels in TLT (black box) and LLC (white box) tumor cells. GSH levels were expressed as nmol/mg protein. GSH values are the mean of triplicate measurements. **, P<0.01; ***, P<0.001.*

As_2O_3 radiosensitizes tumors by an oxygen effect

To evaluate the effect of As_2O_3 on tumor regrowth after irradiation, tumor-bearing mice were irradiated with a single dose of 10Gy of X-rays. Figure 7A shows the tumor growth of TLT tumors treated or not with As_2O_3, with or without irradiation. In the non-irradiated groups, there was no significant difference between tumors treated with PBS and those treated with As_2O_3 ($P>0.05$). All irradiated groups showed a significant regrowth delay compared to their respective control group ($P<0.01$). When irradiation was combined with the administration of As_2O_3 at the time of maximal reoxygenation, the regrowth delay (33.2 ± 2 days to reach 12 mm) was significantly increased compared with irradiation alone (14.8 ± 2.4 days) ($P<0.001$, one-way ANOVA,

Tukey's multiple comparison test), resulting in a 2.2-fold increase in radiation response. Importantly, tumors were individually monitored with EPR oximetry after administration of As_2O_3 to make sure that the pO_2 was increased at the time of irradiation. To discriminate between an oxygen effect and a direct radiosensitizing effect, we also irradiated a group of As_2O_3-treated mice whose legs had been temporarily ligated to induce complete hypoxia at the time of irradiation. The regrowth delays were similar for control (16 ± 2.3 days) and As_2O_3+hypoxia-irradiated groups (15.1 ± 3.1 days) but significantly increased for the As_2O_3-irradiated group (33.2 ± 2 days, $P<0.001$) (Fig.7A). As_2O_3 therefore induces an additional regrowth delay due to an oxygen effect. In Fig.7B, we used Kaplan-Meier curves to compare survival times (times for the tumor to reach 16 mm) in the different groups. The median survival time was 42 days for mice who received As_2O_3 combined with irradiation compared to 19.5 days for the irradiated-control group and 10 days for the non-irradiated groups. As_2O_3 administration combined with radiation extended the median survival of mice by more than 20 days compared to control.

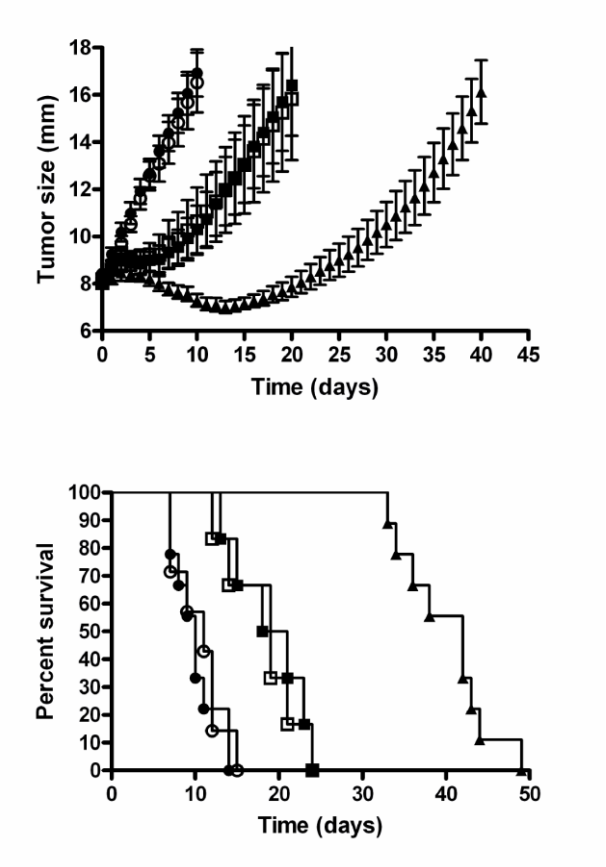

Fig.7

A: Effect of As_2O_3 on TLT tumor regrowth. Mice were treated with PBS (●, n=9), As_2O_3 (○, n=7), 10Gy of radiotherapy after 1h30 of PBS (■, n=6), 10Gy of radiotherapy after 1h30 of As_2O_3 (▲, n=9) or 10Gy of radiotherapy after 1h30 of As_2O_3 plus tumor ligation at the time of irradiation (□, n=6). Each point represents the mean tumor size ± SE. B: Kaplan-Meier analysis of survival. Mice survival curve (time for the tumor to reach 16mm) for each group. As_2O_3 administration combined to radiation extended the median survival of mice by more than 20 days compared to control.

Discussion

The major findings of the present study are: 1) As_2O_3 significantly reduced the tumor hypoxic fraction early after administration of a single dose; 2) the reoxygenation effect was linked to a decrease in the tumor cell oxygen consumption rate; 3) As_2O_3 significantly increased the effectiveness of tumor radiotherapy when irradiation was given at the time of maximal reoxygenation.

In this study, we report that As_2O_3 can induce an acute and transient increase in tumor oxygenation in experimental tumors, with a maximal effect observed 90 min after administration for TLT tumors, and 45 min after administration for LLC tumors (Fig.1-2). A previous study reported an increase in pO_2, measured with an Eppendorf pO_2 histograph, after chronic administration of As_2O_3 in FSA II tumors (24); the maximal reoxygenation was observed at day 3 (24). As tumor reoxygenation may result from an increase in oxygenation delivery and/or a decrease in oxygen consumption, we investigated both aspects to determine the origin of the observed effect. The Patent blue staining assay showed a decrease in tumor perfusion after administration of As_2O_3 (Fig.4), which excludes this parameter as a possible cause of tumor reoxygenation. This observation is in accordance with other studies that demonstrated that a single dose of As_2O_3 induced a decrease in perfusion in tumors (24, 25). The oxygen consumption component was then considered. Tumor cell oxygen consumption was reduced significantly after treatment with As_2O_3. Interestingly, a mathematical model predicted that modification of oxygen consumption would be much more efficient at alleviating hypoxia than modification of oxygen delivery (2), a theoretical hypothesis that has been extensively demonstrated experimentally by our group (4-9).

How does As_2O_3 decrease tumor cell oxygen consumption? The effects of As_2O_3 on oxygen consumption have already been observed *in vitro* by others and the suggested mechanism was the inhibition of respiration upstream of complex IV in the mitochondrial respiratory chain (17). Another mechanism could involve the redox status of the tumor. The GSH (glutathione) redox system is known to modulate the effects of As_2O_3. Previous findings showed that sensitivity to As_2O_3-induced apoptosis was inversely related to the intracellular GSH content and that pharmacological modulation of intracellular GSH content altered sensitivity to As_2O_3 (26). In our study, we observed a decrease in GSH content in As_2O_3-treated cells compared to control cells. This decrease in GSH levels could explain the inhibitory effect of As_2O_3 on oxygen

consumption. Indeed, the GSH redox system represents one of the most important cellular defense systems against oxidative stress. Inhibiting GSH production may lead to oxidative stress by enhancing intracellular ROS, and accumulation of intracellular ROS leads to disruption of the mitochondrial membrane potential (27). Consequently, As_2O_3 could act on the mitochondrial respiratory chain by enhancing intracellular ROS production mediated by decreased GSH levels. Interestingly, the magnitude of reoxygenation (Fig.1) was more pronounced in the TLT tumor model, which has the lowest GSH content, compared to the LLC model, which has the highest GSH content. This observation supports the fact that the reoxygenation may be due in some extent to the effect of As_2O_3 on the redox status of tumor cells. However, further experiments are needed to determine the exact mechanism by which As_2O_3 acts on the mitochondrial respiratory chain.

As the level of oxygenation reached after treatment with As_2O_3 was above the theoretical threshold of radiosensitivity and similar to the level reached by other potential co-treatments identified by our group, we conducted radiosensitizing experiments to test the therapeutic value of the use of As_2O_3 in combination with radiation therapy (9). There was a significant increase in the response of tumors to radiotherapy (by a factor of 2.2) when X-ray irradiation was applied during the reoxygenation window (i.e., at the time of maximal pO_2 induced by As_2O_3). The median length of survival of mice was also extended by more than 20 days compared to controls. As_2O_3 has previously been shown to induce tumor growth delay and to improve fractionated radiotherapy response in other studies that considered different mechanisms and timings of administration (24, 25, 28, 29). Lew at al. showed an important regrowth delay after a single dose or fractionated schedule of radiation when As_2O_3 was administered 60 min after radiation, explained by the increased production of tumor necrosis factor (TNF)-α, known to enhance the antitumor effects of radiation (25). In other tumor cell lines, it appeared that As_2O_3 was also able to directly sensitize tumor cells to the effects of ionizing radiation, contrary to our findings in TLT cells (29). One area related to As_2O_3 exposure that has been widely studied is the depletion of the glutathione level in cells, which may lead to oxidative stress and has been linked to increases in radiosensitivity (29, 30). Griffin at al. reported the greatest regrowth delay when combining treatment and radiation every 3 days, at the time of maximal tumor oxygenation in their model, suggesting that the oxygen level is a factor that is important

in terms of radiosensitization by As_2O_3 (24). In the present study, we observed acute reoxygenation after administration of a single dose of As_2O_3. Furthermore, tumors that were clamped during the irradiation were not radiosensitized, which identifies the 'oxygen effect' as the major factor responsible for the radiosensitization of TLT tumors by As_2O_3, rather than an intrinsic direct radiosensitizing effect of the drug.

In conclusion, we report for the first time that a single dose of As_2O_3 can decrease oxygen consumption by tumor cells in experimental tumors, resulting in a transient reoxygenation of the tumors. This reoxygenation window could be exploited to significantly enhance tumor radiation response, after individual monitoring of the tumor pO_2 before radiation therapy. The oxygen effect was identified as the major factor involved in the sensitization process induced by As_2O_3. Although additional fractionated radiation studies and TCD50 experiments should be conducted for further pre-clinical validation, our study suggests that As_2O_3 could be used as a potential co-treatment for radiation therapy when this is applied at the time of maximum reoxygenation induced by the drug.

References

1. Vaupel P, Harrison L. Tumor hypoxia: causative factors, compensatory mechanisms, and cellular response. Oncologist 2004;9 Suppl 5:4-9.

2. Secomb TW, Hsu R, Ong ET, Gross JF, Dewhirst MW. Analysis of the effects of oxygen supply and demand on hypoxic fraction in tumors. Acta Oncol 1995;34:313-6.

3. Biaglow JE, Manevich Y, Leeper D et al. MIBG inhibits respiration: potential for radio- and hyperthermic sensitization. Int J Radiat Oncol Biol Phys 1998;42:871-6.

4. Jordan BF, Gregoire V, Demeure RJ et al. Insulin increases the sensitivity of tumors to irradiation: involvement of an increase in tumor oxygenation mediated by a nitric oxide-dependent decrease of the tumor cells oxygen consumption. Cancer Res 2002;62:3555-61.

5. Crokart N, Radermacher K, Jordan BF et al. Tumor radiosensitization by antiinflammatory drugs: evidence for a new mechanism involving the oxygen effect. Cancer Res 2005;65:7911-6.

6. Crokart N, Jordan BF, Baudelet C et al. Glucocorticoids modulate tumor radiation response through a decrease in tumor oxygen consumption. Clin Cancer Res 2007;13:630-5.

7. Ansiaux R, Baudelet C, Jordan BF et al. Mechanism of Reoxygenation after Antiangiogenic Therapy Using SU5416 and Its Importance for Guiding Combined Antitumor Therapy. Cancer Res 2006;66:9698-704.

8. Ansiaux R, Dewever J, Gregoire V, Feron O, Jordan BF, Gallez B. Decrease in tumor cell oxygen consumption after treatment with vandetanib (ZACTIMA; ZD6474) and its effect on response to radiotherapy. Radiat Res 2009;172:584-91.

9. Jordan BF, Christian N, Crokart N, Gregoire V, Feron O, Gallez B. Thyroid status is a key modulator of tumor oxygenation: implication for radiation therapy. Radiat Res 2007;168:428-32.

10. Shen ZX, Chen GQ, Ni JH et al. Use of arsenic trioxide (As2O3) in the treatment of acute promyelocytic leukemia (APL): II. Clinical efficacy and pharmacokinetics in relapsed patients. Blood 1997;89:3354-60.

11. Maeda H, Hori S, Nishitoh H et al. Tumor growth inhibition by arsenic trioxide (As2O3) in the orthotopic metastasis model of androgen-independent prostate cancer. Cancer Res 2001;61:5432-40.

12. Shen ZY, Zhang Y, Chen JY et al. Intratumoral injection of arsenic to enhance antitumor efficacy in human esophageal carcinoma cell xenografts. Oncol Rep 2004;11:155-9.

13. Bornstein J, Sagi S, Haj A, Harroch J, Fares F. Arsenic Trioxide inhibits the growth of human ovarian carcinoma cell line. Gynecol Oncol 2005;99:726-9.

14. Woo SH, Park IC, Park MJ et al. Arsenic trioxide induces apoptosis through a reactive oxygen species-dependent pathway and loss of mitochondrial membrane potential in HeLa cells. Int J Oncol 2002;21:57-63.

15. Miller WH, Jr., Schipper HM, Lee JS, Singer J, Waxman S. Mechanisms of action of arsenic trioxide. Cancer Res 2002;62:3893-903.

16. Xiao YF, Liu SX, Wu DD, Chen X, Ren LF. Inhibitory effect of arsenic trioxide on angiogenesis and expression of vascular endothelial growth factor in gastric cancer. World J Gastroenterol 2006;12:5780-6.

17. Pelicano H, Feng L, Zhou Y et al. Inhibition of mitochondrial respiration: a novel strategy to enhance drug-induced apoptosis in human leukemia cells by a reactive oxygen species-mediated mechanism. J Biol Chem 2003;278:37832-9.

18. Gallez B, Jordan BF, Baudelet C, Misson PD. Pharmacological modifications of the partial pressure of oxygen in murine tumors: evaluation using in vivo EPR oximetry. Magn Reson Med 1999;42:627-30.

19. Jordan BF, Cron GO, Gallez B. Rapid monitoring of oxygenation by 19F magnetic resonance imaging: Simultaneous comparison with fluorescence quenching. Magn Reson Med 2009;61:634-8.

20. WROBLEWSKI F, LADUE JS. Lactic dehydrogenase activity in blood. Proc Soc Exp Biol Med 1955;90:210-3.

21. Tietze F. Enzymic method for quantitative determination of nanogram amounts of total and oxidized glutathione: applications to mammalian blood and other tissues. Anal Biochem 1969;27:502-22.

22. Griffith OW. Determination of glutathione and glutathione disulfide using glutathione reductase and 2-vinylpyridine. Anal Biochem 1980;106:207-12.

23. LOWRY OH, ROSEBROUGH NJ, FARR AL, RANDALL RJ. Protein measurement with the Folin phenol reagent. J Biol Chem 1951;193:265-75.

24. Griffin RJ, Williams BW, Park HJ, Song CW. Preferential action of arsenic trioxide in solid-tumor microenvironment enhances radiation therapy. Int J Radiat Oncol Biol Phys 2005;61:1516-22.

25. Lew YS, Kolozsvary A, Brown SL, Kim JH. Synergistic interaction with arsenic trioxide and fractionated radiation in locally advanced murine tumor. Cancer Res 2002;62:4202-5.

26. Dai J, Weinberg RS, Waxman S, Jing Y. Malignant cells can be sensitized to undergo growth inhibition and apoptosis by arsenic trioxide through modulation of the glutathione redox system. Blood 1999;93:268-77.

27. Dalton WS. Targeting the mitochondria: an exciting new approach to myeloma therapy. Commentary re: N. J. Bahlis et al., Feasibility and correlates of arsenic trioxide combined with ascorbic acid-mediated depletion of intracellular

glutathione for the treatment of relapsed/refractory multiple myeloma. Clin. Cancer Res., 8: 3658-3668, 2002. Clin Cancer Res 2002;8:3643-5.

28. Kim JH, Lew YS, Kolozsvary A, Ryu S, Brown SL. Arsenic trioxide enhances radiation response of 9L glioma in the rat brain. Radiat Res 2003;160:662-6.

29. Monzen H, Griffin RJ, Williams BW, Amano M, Ando S, Hasegawa T. Study of arsenic trioxide-induced vascular shutdown and enhancement with radiation in solid tumor. Radiat Med 2004;22:205-11.

30. Jones EL, Douple EB. The effect of in vivo GSH depletion on thermosensitivity, radiosensitivity and thermal radiosensitization. Int J Hyperthermia 1990;6:951-5.

Chapter 5: Discussion

I. Principal findings of the study

We first compared three different methods (EPR, Clark electrode, fluorescence method) capable of measuring the oxygen consumption of cells *in vitro* (see chapter 3I). The action of two different treatments acting on the mitochondrial respiratory chain to decrease cellular oxygen consumption to different degrees was evaluated using these three techniques. EPR showed a significant decrease in oxygen consumption by K562 cells treated with rotenone and hydrocortisone. The Clark electrode and MitoXpress systems demonstrated a significant decrease in cellular oxygen consumption after administration of rotenone, but there were no significant effects for cells treated with hydrocortisone. We showed that EPR oximetry appears to be the most sensitive method for measuring the oxygen consumption rate of tumor cells.

We also attempted to develop a new method that can highlight differences in oxygen consumption by different tissues *in vivo*. For this purpose, we designed a protocol where pO_2 was monitored in the tissue of interest during a breathing challenge (see chapter 3.II). Hyperthyroidism was induced by chronic treatment with L-thyroxine; this treatment is known to dramatically affect the oxygen consumption rate of muscle and tumor cells. We observed an oxygen consumption rate significantly enhanced for hyperthyroid mice compared to control mice. Remarkably, this difference in the oxygen consumption rate was correlated with higher kinetics constants, reflecting the rapidity of the return of oxygenation to basal values after pre-saturation with oxygen. It is also important to note that the perfusion of the tissues was not affected by the L-thyroxin treatment. The clamping experiment definitely confirms that our technique is measuring the oxygen consumption of tumor cells without any major influence of confounding factors such as perfusion and vascular pO_2. This method gives an index that may reasonably be ascribed to the local oxygen consumption, and has the unique advantage of being adapted to *in vivo* studies. The results were confirmed by ^{19}F MRI by mapping the oxygen consumption of tumors. We showed that this technique offers the unique advantage of being able to probe oxygen consumption *in vivo* in a non invasive way along with the spatial information that is required to probe heterogeneity.

Finally, we considered the effect of As_2O_3 on tumor oxygen consumption and radiation response. This was performed by intraperitoneal administration of As_2O_3 to TLT and LLC tumor bearing mice. Tumor oxygenation was progressively increased for both tumor models. This improved tumor pO_2 was demonstrated to be the result of a decrease in tumor oxygen consumption as described in chapter 4. We further showed that this effect was combined with a decrease in tumor blood flow. The decrease in oxygen consumption was explained to some extend by the decrease in GSH content in As_2O_3-treated cells. Finally, the administration of As_2O_3 was also correlated with a significant improvement in tumor radiosensitivity and as the result of an oxygen effect.

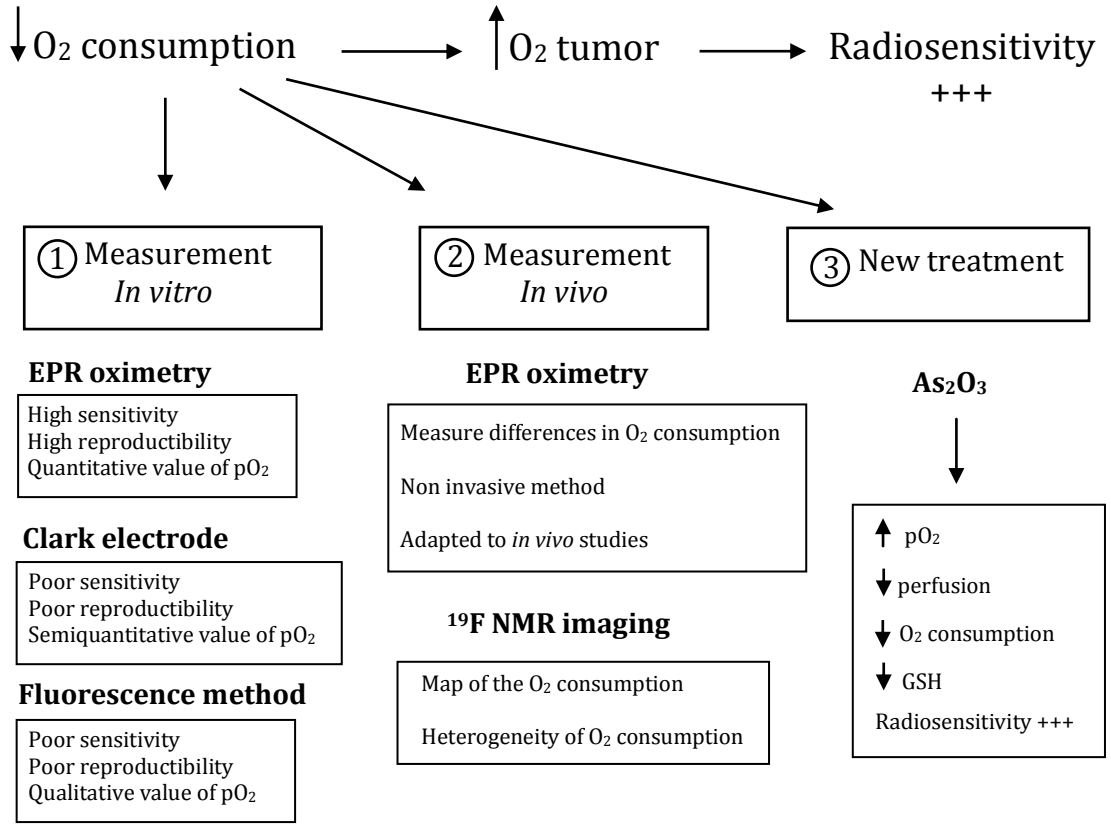

Figure 24: Principal findings obtained by evaluating and developing different methods to measure oxygen consumption by tumor cells (in vitro and in vivo), and by characterizing the effects of As_2O_3 on tumor oxygen consumption and on tumor radiosensitivity.

II. Discussion and Perspectives

1. *In vivo* measurements of oxygen consumption (EPR and ^{19}F MRI)

1.1 EPR oximetry protocol to estimate the tissue oxygen consumption *in vivo*: limitations and perspectives.

As the methods to measure oxygen consumption *in vivo* are very limited, we developed a protocol that can estimate the tissue oxygen consumption *in vivo* by EPR oximetry. The method that we developed is minimally invasive and provides a good index that may be reasonably ascribed to the local oxygen consumption. However our method presents some limitations. The first question is, what are the parameters really measured by the method? Indeed, we cannot exclude a possible influence of hemodynamic parameters on the oxygen consumption measurements. Although the clamping experiments do show that, experimentally, there is no difference in measuring oxygen consumption in clamped or unclamped tumors after carbogen challenge, a contribution of fresh blood arriving at higher rate in the muscle compared to the tumor cannot be excluded. Thus, the blood flow could be a potential confounding factor while measuring oxygen consumption in well perfused tissues. However, in our study, the influence of blood flow is probably low. Indeed, in poor perfused tissues like tumors, the blood flow is extremely limited and the effects of changes in consumption are known to be more important than changes in blood flow (Secomb, 1995). So, our method will be more limited to measure oxygen consumption in well perfused tissues. Due to a likely influence of some hemodynamic parameters, the method does not provide a quantitative parameter but rather an index that may be ascribed to the local oxygen consumption as showed by the study. In the future it should be interesting to improve the protocol by including a simultaneous measurement of the blood flow. Other methods are currently being developed to measure *in vivo* oxygen consumption, such as ^{17}O NMR that is applied to measure *in vivo* cerebral oxygen consumption. *In vivo* ^{17}O NMR has two major applications for studying brain function and cerebral bioenergetics. The first application is to measure the cerebral blood flow through monitoring the washout of inert $H_2{}^{17}O$ tracer in the brain tissue following an intravascular bolus injection of the ^{17}O-labeled water. The second application is to determine the cerebral metabolic rate of oxygen utilization through monitoring the dynamic changes of metabolically generated $H_2{}^{17}O$ from inhaled ^{17}O-labeled oxygen gas in the brain tissue. The method has also been used

in tumors to measure blood flow but not the oxygen consumption. The ^{17}O NMR technique has the potential to image cerebral blood flow and oxygen consumption in humans. Consequently, the protocol could be applied in tumors without blood flow like confounding effect. Moreover, the approach has been applied to image $CMRO_2$ non invasively in humans (Fiat, 1993; Zhu, 2003). Our perspective of this work would be to adapt the ^{17}O method to tumors.

A second question is, what about the use of the method with treatments inducing acute changes? Indeed, an "acute" treatment like As_2O_3 could induce a confounding effect with the carbogen challenge. Indeed, the initial pO_2 of treated mice will differ from that of control mice and the pO_2 will return to its basal value which will differ from one group to another. Moreover, the combination of carbogen with a treatment which induces an increase of the pO_2, could induce a major increase of the pO_2 compared to the non-treated group and induces wrong kinetics constants values. It will be thus difficult to compare control and treated mice. Consequently, as it is now, the method cannot be used to measure the oxygen consumption after administration of an "acute" treatment.

Compared to the other methods described in the introduction of the thesis, our EPR method is the first one to measure the oxygen consumption of tumors non invasively and to provide a direct measurement of oxygen consumption.

1.2. EPR oximetry, oxygen consumption and clinical applications

It is critical to consider a possible clinical application for our oxygen consumption measurement method. EPR oximetry is currently being translated in the clinic with the first clinical studies in diabetic feet and peripheric tumors (see below). There are indeed several reasons for considering the use of *in vivo* EPR in the clinic setting, including its ability to provide clinically useful information (i.e. direct quantitative oxygen measurement) in a manner that has significant advantages over other approaches. The advantages may be in the uniqueness of the information, or the accuracy of the information, or the ease of obtaining the information. Such capabilities have been demonstrated in animals, and these continue to expand and increase. There are three major challenges for moving this technology into clinic: assuring the biocompatibility of the oxygen sensor in humans; modifying the instruments so that they can be used for humans instead of small animals; and increasing the sensitivity and depth at which measurements can be made. Initial clinical studies have already begun using India ink,

which has been used in humans without toxicity for several centuries. The first clinical trial, which was approved and begun at Dartmouth Medical School, will use India ink as oxygen sensor (Williams, 2010). Another possibility for particulate materials is to encapsulate them in oxygen-permeable biocompatible polymers that are already approved for human use (Swartz, 2004).

The human studies have been done at Dartmouth with EPR spectroscopy at 1200MHz using surface resonator and include (Swartz, 2004; Khan, 2007):

- Studies in human subjects with pre-existing tattoos, utilizing the carbon black in the tattoos;
- Measurements of percutaneous oxygen using oxygen-sensitive paramagnetic materials placed on the surface of the skin;
- Measurements of oxygen in the foot of volunteers into which India ink has been injected at the site of interest, as the initial steps in a project to utilize EPR oximetry to follow the status of tissues in diabetic patients with peripheral vascular disease (Figure 25);
- Measurements of oxygen in suitably located tumors (at depths of ≤1cm from the surface). Such measurements provide the level of oxygen in the tumor and how it varies over time, especially during the course of treatment.

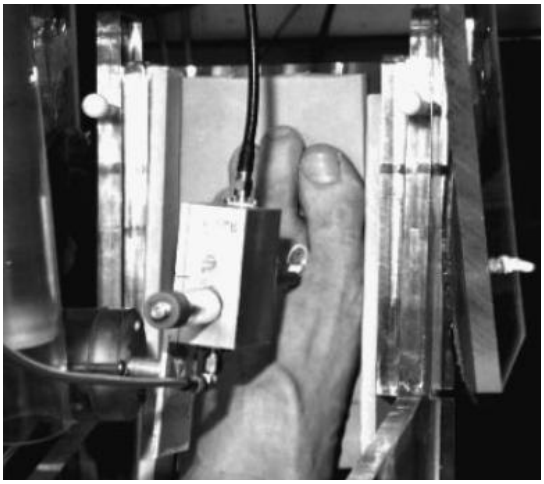

Figure 25: Platform to position and stabilize the foot for measurements of pO_2 (Swartz, 2004).

The increase in pO_2 in tumors induced by breathing carbogen (95% oxygen and 5% CO_2) was shown in several tumor lines using EPR spectroscopy and breathing

carbogen is also applied successfully into the clinic together with irradiation. For that reason, we used carbogen breathing in our study to increase tumor pO_2. Considering the use of EPR oximetry in human tumors and the use of carbogen breathing in clinical studies, we can consider the possibility of adapting our new method to measure oxygen consumption in human subjects. One limitation which remains to eradicate is the measurement deeper within the body. One possibility is to go to lower frequencies. The range of 300-700MHz seems most likely for this phase of development. At these frequencies the penetration of the exciting radiation can be up to 10-fold deeper than with the 1200 MHz spectrometer. The principal problem is to regain the sensitivity that will be lost by going down in frequency. Another possible approach is the use of an implanted resonator which is magnetically coupled to a surface resonator. This device will probably provide a useful signal/noise at depths of as much as 4cm and, after implantation, will be entirely non invasive (Swart, 1998; Li, 2010).

1.3. ^{19}F NMR imaging versus EPR oximetry

In our project thesis, two different techniques were used to measure tumor pO_2 and oxygen consumption of tumor cells. But what are really the differences between the two methods? What are the advantages and disadvantages of the methods?

EPR oximetry resolves pO_2 of less than 1 mmHg, is reproducible over time, and is not affected by the local environment. The method can make measurements for periods of hours or more, make repeated measurements from the same sites for periods of years, and make multiple simultaneously measurements (Swartz, 2004). Work has been done in animal models to validate EPR oximetry for monitoring radiation response, and it has begun to be applied in humans (see EPR oximetry and clinical applications). However, an important limitation of the EPR oximetry technique is that it is unable to resolve microscopic heterogeneity in the pO_2 and in the oxygen consumption of tumors. EPR imaging involves long acquisition times that are not suited to the sampling that is required with our protocol (see below). For that reason, we applied the protocol (breathing challenge) with ^{19}F NMR imaging to provide a paramagnetic map of pO_2 and oxygen consumption of tumors and, the method was successfully used to provide maps and to probe heterogeneity of tumor pO_2 and oxygen consumption.

The major application of ^{19}F NMR oximetry to oncology has been in the evaluation of tumor oxygenation and the effects of approaches to overcome tumor

hypoxia and enhance the response to irradiation. ^{19}F NMR oximetry is currently the only methodology from which absolute *in vivo* tumor pO_2 maps can be derived in a reasonable acquisition time. Despite this, this method presents some limitations. In the As_2O_3 study, the pO_2 values before and after treatment measured by EPR oximetry differ from that observed by ^{19}F NMR imaging. Indeed as already mentioned by other studies, the basal tumor pO_2 measured by ^{19}F NMR oximetry are systematically higher than those reported by EPR oximetry. These high PFC pO_2 results would predict very little radiobiological hypoxia, a prediction that is clearly at variance with our results showing radioresistance in the tumor model. One reason for this discrepancy could be the presence of a systemic error in the ^{19}F NMR measurement. Tumor pO_2 maps are derived from quantitative ^{19}F T_1 relaxation maps of the HFB by interpolation onto a calibration curve. This curve is usually derived *in vitro* from ^{19}F NMR T_1 measurement of pure PFC emulsion equilibrated to different oxygen tension using nitrogen, air or oxygen. Temperature can also give rise to a significant source of error in absolute pO_2 determination since PFCs depend on temperature. A 2°C error in tumor temperature can lead to an error of 12mmHg in tissue pO_2 (Robinson and Griffiths, 2003). Another reason of higher pO_2 values observed by ^{19}F NMR oximetry can be explained by the fact that HFB is a lipophilic structure in which oxygen is more soluble resulting in higher local oxygen concentration. Moreover, the sample size in EPR ($10mm^3$) is smaller compared to ^{19}F NMR oximetry (whole tumor). However, the method is repeatable and minimally invasive. ^{19}F NMR oximetry generates pO_2 maps with a good spatial resolution, repeatable measurements, reveals heterogeneity in a precise manner, as well as the dynamic changes in oxygen pertinent to acute interventions. HFB is inexpensive and commercially available at high purity, and its associated toxicity has been well characterized. The oxygen consumption rates (k values) of tumors, measured by ^{19}F NMR oximetry, were higher than those measured by EPR oximetry. This discrepancy is also probably due to the same reasons as mentioned above. EPR and ^{19}F NMR imaging seem complementary methods to evaluate tumors pO_2 and oxygen consumption. Indeed, EPR oximetry is a good marker of the response of tumors to radiotherapy and ^{19}F NMR imaging provides parametric maps which underline the heterogeneity of pO_2 inside the tumors and thereby could identify potential resistant zones.

In the current state, HFB administration seems not applicable to clinical studies due to the invasiveness of its administration. In counterpart, the use of perfluorocarbons

(PFCs) (intravenous administration) like blood substitutes in humans makes it feasible to use it as contrast agent for MRI into clinic. PFCs are synthetic compounds made of fluorine atoms replacing hydrogen atoms. The replacement of hydrogen with fluorine yields a rigid molecule with a dense electronic sheath that gives a "Scotch-guard like effect" at the molecular level. PFCs are highly hydrophobic and chemically inert compounds that cannot be metabolized *in vivo*. They are immiscible in water and can dissolve gases such as oxygen and carbon dioxide; they carry oxygen by direct solubility. The combination of biologic inertness with superior oxygen and carbon dioxide solubilities promotes the concept of PFC as viable red blood cell substitute (Cohn, 2009; Riess 2005). PFCs provide a simple and elegant, efficacious and immediate, safe and cost-effective mean of temporally augmenting oxygen delivery in patients at risk of tissue hypoxia or ischemia. Such emulsions offer a new potential strategy for reducing allogeneic blood transfusion during surgery and also prove useful in cardiopulmonary bypass surgery (Riess, 1998). However, at the current time, no clinical trials are ongoing in the United States with a PFC as blood substitute. Indeed, most of PFCs did not show appreciable beneficial effects. In the current state, PFCs do not appear to be a likely technology platform for a viable blood substitute. Moreover, compared to HFB, the majority of PFCs is sequestered in the liver and spleen and the amount taken up by the tumor is often insufficient for determination of the tumor pO_2. Intravenous administration also tends to deliver PFC emulsion to well perfused tumor regions where it is sequestered in macrophages around the blood vessels, and thus reports relatively high pO_2 values. Intravenously administered PFC emulsion has impaired access to the poorly vascularised areas that are likely to be radiobiologically hypoxic (Robinson and Griffiths, 2003). By contrast, direct intratumoral administration of PFCs has been shown to give lower pO_2 values. In this situation, the PFCs do appear to be interrogating poorly vascularised tumor regions that are hypoxic, and thus afford a more realistic tumor hypoxic profile. As mentioned above, intratumoral administration of PFCs is relatively invasive to apply it in humans. However, in oncology, processes like biopsy and others are also invasive, so further experiments will be interesting to perform and apply this method for clinical use. We should also mention that PFCs are not always safety and can induce some adverse effects which differ between them.

Electron paramagnetic resonance imaging (EPRI) could be an alternative to map the tumor oxygen consumption. EPRI has been widely used to map the distribution and

metabolism of paramagnetic species in *in vivo* biological system. The mapping of oxygen concentration using EPR imaging involves the use of spectral-spatial imaging techniques where the image contains not only spatial information but also the spectral information. The method requires stepped field gradients and the resulting image has information in one, two, or three spatial dimensions and one spectral dimension (Kuppusamy, 1998). EPRI can reproducibly and robustly measure pO_2 *in vivo* and has been validated for hypoxia measurements through correlation with pO_2 histography and with BOLD (Elas, 2003; Elas, 2006). EPRI presents a high sensitivity, resolution and offers the advantage of being able to take repeated measurements. However, data acquisition time is a major issue in EPRI. A reasonable CW (continuous wave)-3D spectral-spatial image takes ~30min (Kuppusamy, 1998) and it will be therefore not possible to measure the kinetics constants after the carbogen challenge. Moreover, for EPRI to be approved for human, safe concentrations and specific absorption rates must be developed for its contrast agents (Tatum, 2006). With Fourier Transform (FT)-EPRI, it is possible to peform data acquisition time in less than 3min, experiments are under development (Subramanian, 2002).

An alternative MRI technique for evaluating and mapping changes in tumor oxygenation status had already been used in humans with cancer (O'Connor, 2009). Molecular oxygen (O_2) is paramagnetic and therefore increases the proton longitudinal relaxation rate (R_1) of water containing dissolved oxygen. The measured change in R_1 ($=1/T_1$, where T_1 is the longitudinal relaxation time) induced by breathing oxygen is, proportional to the change in tissue oxygen concentration. Oxygen-induced increase in R_1 has the potential to provide non invasive measurement of change in tumor oxygen concentration. Consequently, the technique could be used as a potential method to measure and to map the oxygen consumption of tumor cells.

Comparative table of methods to measure oxygen consumption in vivo.

	EPR spectroscopy	***^{19}F NMR imaging***	***CW-EPRI***	***T_1-measurement MRI***
Time resolution	>20sec	Minutes (~1min)	Minutes (~30min)	Minutes (~1min)
Oxygen map	No	Yes	Yes	Yes
Oxygen consumption map	No	Yes	No	Yes
Invasiveness	Only sensor injection	Only sensor injection	Only sensor injection	No
Repeatability	Yes	Yes	Yes	Yes
Clinical use	Yes	No	No	Yes
Advantages	Sensitivity	pO_2 map	pO_2 map	pO_2 map
Disadvantages	No pO_2 map	Less sensitive	Acquisition time	Influence of flow To be developed and validated

2. Method to measure oxygen consumption *in vitro*

In the study which compares the different methods to measure the oxygen consumption *in vitro*, it is probably not correct to say that the Clark type electrode has the mentioned limitations in general. Indeed, the oxygen consumption of the electrode depends on the size probe of the working electrode, so it can be minimized to be smaller than the consumption of cells. Also stirring is not always necessary. A combined microelectrode with small-tip diameter had a fast response time, stable reading with good calibration linearity, low residual current signal, and low stirring effect (Lu and Yu, 2002). Dynamic monitoring of the effects of active agents on living cells is also possible with multiparametric sensor systems based on silicon or glass chip. The oxygen field effect transistor (O_2-FET) is a silicon based biohybrid microsensor. It is a combination of Clark-type dissolved oxygen electrode sensor and an ion sensitive field effect transistor

for pH measurement. The O_2-FET detects a pH change resulting from the reduction of oxygen molecules at a palladium noble metal electrode, surrounding an ion sensitive field effect transistor. Changes in pH are directly proportional to a pO_2 change. The O_2-FET is advantageous because of its possibility to measure pH and pO_2 at the same microspot, and because of its small size (cavity volume: 7µl). Moreover, the sensitivity and the selectivity of the sensors have to be investigated for a complete characterization of the sensors (Wiest, 2005).

3. Effects of As_2O_3

3.1. As_2O_3 and radiosensitivity

The effect of As_2O_3 on the tumor radiosensitivity was observed by regrowth delay measurements. To discriminate between an oxygen effect and a direct radiosensitizing effect by As_2O_3, we also irradiated a group of As_2O_3-treated mice whose legs had been temporally ligated to induce complete hypoxia at the time of irradiation. Tumors that were clamped during the irradiation time were not radiosensitized, which identifies the 'oxygen effect' as the major factor responsible for the radiosensitization of TLT tumors by As_2O_3, rather than an intrinsic direct radiosensitizing effect of the drug. The technique is useful to identify a possible radiosensitizing effect of the drug but a TCD 50 (tumor control dose 50) should be used to complete the method. The TCD 50 corresponds to the radiation dose required to control 50% of the tumors. The percentage of tumor control and normal tissue are sigmoidal (Figure 26). Below a minimum level of radiation, tumor control probability and normal tissue complications probability are low. There is a steep dose response for tumor control, increasing from 10% to 90% over 5 to 20 Gy. The dose that can be delivered to a tumor is limited by the probability of serious normal tissue complications. Therefore, the choice of tumor dose is based on the relative probability of tumor control and normal tissue complications. TCD 50 is thus very sensitive to small changes in the effectiveness of radiotherapy and seems a better mean to evaluate the effect of treatments on tumor radiosensitization.

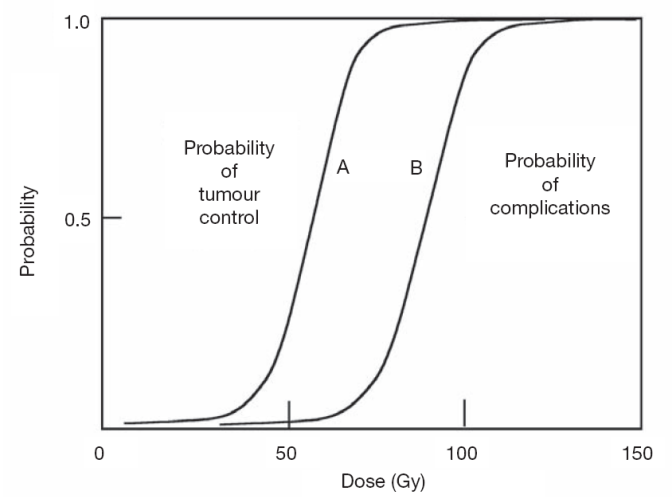

Figure 26: Tumor control probability (TCP) and the probability of normal tissue injury as a function of radiation. Curve A represents the TCP, curve B the probability of complications (Suntharalingam, 2005).

The effect of As_2O_3 as a radiosensitizer has been shown by different studies and has been explained by different mechanisms which have been extensively described in the thesis. In our study, we demonstrated that As_2O_3 could increase the radiation response by an oxygen effect. The timing schedule was very important since the radiosensitizing effect of As_2O_3 is observed 90min after the drug administration, at the time of maximal reoxygenation. The oxygen effect could be relevant in the clinic since As_2O_3 is already used to treat APL in humans and this effect should be considered since oxygen is the most radiosensitizing agent. Consequently, the reoxygenation of human tumors after As_2O_3 treatment should also be measured non invasively. The FMISO PET is a technique extensively used into clinic to image hypoxic cells and reoxygenation following radiation therapy. A good correlation of FMISO uptake with poor outcome to radiation and chemotherapy has also been demonstrated. Clinical EPR oximetry studies have been developed and EPR oximetry could be used in human subjects in the future (see EPR oximetry and clinical applications).

The radiosensitizing effect observed in our study has been observed after one single irradiation. In the clinic, the current conventional treatment regimens correspond to an administration of 2Gy twice a day, 5 times per week. Thus, it would be interesting to apply fractionated schedules and follow the clinical radiation protocol. Fractionated protocols have already been used into different preclinical studies with As_2O_3 as

pretreatment and showed that the drug had the potential to improve fractionated radiotherapy response (Griffin, 2005; Ning, 2006). But the proper dosing and frequency for clinical use of As_2O_3 in combination with radiation must be determined from our knowledge of the physiological and direct cellular effects of As_2O_3.

A potential clinical advantage of the combination of a sensitizing agent and radiation can only be foreseen if the potentiation of radiation response is higher in tumors than in normal tissues in the radiation field, indicating that the therapeutic ratio of the combined treatment is above unity. Since As_2O_3 is used to treat APL in humans and since As_2O_3 was identified as a powerful radiosensitizing agent, we can consider its potential use into clinical trials. For that purpose, it is necessary to obtain more preclinical data. First, it would be necessary to test the dose-response to As_2O_3 in terms of efficacy to sensitize radiation therapy. Second, the potential toxicity of As_2O_3 when combined with radiation therapy should be evaluated. For this purpose, we should determine whether As_2O_3 is responsible for toxicity to early or late responding tissues. Toxicity on normal early-responding tissues will be measured by the intestinal crypt regeneration assay and toxicity on normal late-responding tissue will be measured by the late leg contracture assay (Jordan, 2006).

3.2. As_2O_3 and healthy tissues

The As_2O_3 effects seem to be targeted specifically on the tumor. Indeed, several preclinical studies showed no accumulation of As_2O_3 in different tissues like muscle, liver, skin and brain. As_2O_3 seems to accumulate essentially in the tumor. The possible explanation of the accumulation of As_2O_3 in the tumor may be due to the specific microenvironment of the tumor. A low pH, hypoxic condition and an important oxidative stress contribute to the target effects of As_2O_3 on the tumor (Griffin, 2005). As_2O_3 was shown to decrease the tumor perfusion and this effect was not observed in muscle, skin and kidney (Lew, 1999; Griffin, 2000). To be sure that As_2O_3 does not act on healthy tissues, it should be interesting to measure the oxygen consumption of different healthy tissues like muscle after treatment. As_2O_3 administration also appears to show no signs of toxicity on healthy tissues. Indeed, no obvious signs of toxicity in terms of the loss of body weight were observed (Ning, 2006). In our study, the toxicity is not a major problem since the short term treatment is limited to the period of radiotherapy. Moreover, most anti-cancer agents present problems of toxicity.

3.3. Effects of As_2O_3 on mitochondrial respiratory chain

Our study showed that As_2O_3 has a profound effect on tumor oxygenation but it was not because of an increase in tumor blood flow but because of a decrease in tumor cell oxygen consumption. The increase in tumor oxygenation resulted in an important enhancement in the sensitivity of tumors to irradiation. To explain a possible mechanism by which As_2O_3 could decrease the oxygen consumption of tumor cells, we measured the GSH content in TLT and LLC cells. Our results showed a significant decrease in the GSH content in both cell lines. This decrease in GSH could be a possible mechanism by which As_2O_3 decrease the oxygen consumption of tumor cells. Indeed, a decrease in GSH content enhances the ROS level in the cells which acts on the mitochondrial respiratory chain by inhibiting the mitochondrial respiration. To better understand the mechanisms by which As_2O_3 acts on oxygen consumption, it would be interesting to measure the ROS level in the cells and to measure the effects of As_2O_3 with and without N-acetyl cystein (an antioxidant) which has been demonstrated to counteract the As_2O_3-effects. To further investigate the role of the mitochondrial respiration chain in As_2O_3 action, it could also be interesting to use sub-clone of mitochondrial respiration-deficient cells from different tumor cells. Due to the lack of mitochondrial respiration, the respiration-deficient cell line will depend on glycolysis as the energy source and will produced less ROS. If the mitochondrial respiratory function is important for the action of As_2O_3, these cells would be relatively resistant to the drug (Pelicano, 2003). We should also mention that a third tumor model, FSAII tumors, was also tested in our study. The results showed a decrease in oxygen consumption *in vitro* of tumor cells and a decrease in GSH level after As_2O_3 treatment. However, the tumor pO_2 was unchanged after administration of As_2O_3. Currently, we cannot explain this discrepancy between the results but further studies are needed to better understand the data.

3.4. Paradoxical effects of As_2O_3: carcinogenesis and anticancer

Arsenic contamination of drinking water is a public health issue worldwide and chronic exposure can cause cancer as well as non-cancer disease such as hyperkeratosis, cardiovascular disease, hypertension, liver and kidney disorders. However, it has proven difficult to induce tumors after arsenic exposure alone in rodents. Studies only implicate arsenic as a co-carcinogen. For example, in mice, arsenic can enhance the carcinogenicity

of ultraviolet radiation. In spite of its carcinogenic effects, arsenic is also known as a novel promising anticancer agent. As_2O_3 was reintroduced as an anticancer agent after reports emerged from China of the success of an As_2O_3-containing solution for the treatment of APL. When administered intravenously to APL patients, As_2O_3 induced complete remission in 73% of the untreated patients and 52% in the patients with relapsed or refractory APL. Several observations established in this initial study were confirmed in subsequent studies. Adverse effects were mild and reversible on cessation of the drug (Figure 27). In the United States, clinical investigations led to its approval by the US Food and Drug Administration in September 2000 for the treatment of relapsed and refractory APL (Cui, 2008).

Side Effects	Frequency (%)
Skin dryness, itching, or erythematous changes	26.7 (4/15)
Headache	6.7 (1/15)
EKG change	
(1) low-flat T-wave	6.7 (1/15)
(2) sinal tachycardia and I^0 A-V inductive block	6.7 (1/15)
Nausea, vomiting, or loss of appetite accompanied with lassitude	26.7 (4/15)
Liver function*	
GPT increased	6.7 (1/15)
GOT increased	13.3 (2/15)
AKP increased	13.3 (2/15)
γ-GTP increased	6.7 (1/15)
Total bilirubin increased	6.7 (1/15)
Enlargement of salivary gland†	6.7 (1/15)
Thyrophyma without thyroidism†‡	6.7 (1/15)
Arthralgia or musculogia	13.3 (2/15)
Teeth ache	13.3 (2/15)
Oral ulcer	6.7 (1/15)
Hemorrhage of teeth, nose, or skin	13.3 (2/15)

Figure 27: Main side effects with As_2O_3 treatment in APL (Shen, 1997).

However, clinical studies have shown difficulties to demonstrate the effects of As_2O_3 on solid tumors. As_2O_3 has been trialed in numerous cancers like liver, pancreatic, gastric and ovarian cancer; but the results are not yet available or mostly are refractory to current therapies (Dilda, 2007). Thus, more studies are needed to understand the different mechanisms by which As_2O_3 acts on solid tumors. But we demonstrated the relevance of the potential use of As_2O_3 as a co-treatment for radiation therapy in view of the impact of the drug on tumor oxygenation and radiation sensitivity, and the need for further preclinical characterization.

References list

Ai,Z., Lu,W. and Qin,X. Arsenic trioxide induces gallbladder carcinoma cell apoptosis via downregulation of Bcl-2, Biochem.Biophys.Res.Commun., *348:* 1075-1081, 2006.

Al-Hallaq,H.A., River,J.N., Zamora,M., Oikawa,H. and Karczmar,G.S. Correlation of magnetic resonance and oxygen microelectrode measurements of carbogen-induced changes in tumor oxygenation, Int.J.Radiat.Oncol.Biol.Phys., *41:* 151-159, 1998.

Amellem,O., Loffler,M. and Pettersen,E.O. Regulation of cell proliferation under extreme and moderate hypoxia: the role of pyrimidine (deoxy)nucleotides, Br.J.Cancer, *70:* 857-866, 1994.

An,H. and Lin,W. Quantitative measurements of cerebral blood oxygen saturation using magnetic resonance imaging, J.Cereb.Blood Flow Metab, *20:* 1225-1236, 2000.

An,H. and Lin,W. Impact of intravascular signal on quantitative measures of cerebral oxygen extraction and blood volume under normo- and hypercapnic conditions using an asymmetric spin echo approach, Magn Reson.Med., *50:* 708-716, 2003.

Ansiaux,R., Baudelet,C., Jordan,B.F., Beghein,N., Sonveaux,P., De,W.J., Martinive,P., Gregoire,V., Feron,O. and Gallez,B. Thalidomide radiosensitizes tumors through early changes in the tumor microenvironment, Clin.Cancer Res., *11:* 743-750, 2005.

Ansiaux,R., Baudelet,C., Jordan,B.F., Crokart,N., Martinive,P., Dewever,J., Gregoire,V., Feron,O. and Gallez,B. Mechanism of Reoxygenation after Antiangiogenic Therapy Using SU5416 and Its Importance for Guiding Combined Antitumor Therapy, Cancer Res., *66:* 9698-9704, 2006.

Ansiaux,R., Dewever,J., Gregoire,V., Feron,O., Jordan,B.F. and Gallez,B. Decrease in tumor cell oxygen consumption after treatment with vandetanib (ZACTIMA; ZD6474) and its effect on response to radiotherapy, Radiat.Res., *172:* 584-591, 2009.

Bahlis,N.J., Cafferty-Grad,J., Jordan-McMurry,I., Neil,J., Reis,I., Kharfan-Dabaja,M., Eckman,J., Goodman,M., Fernandez,H.F., Boise,L.H. and Lee,K.P. Feasibility and correlates of arsenic trioxide combined with ascorbic acid-mediated depletion of intracellular glutathione for the treatment of relapsed/refractory multiple myeloma, Clin.Cancer Res., *8:* 3658-3668, 2002.

Baudelet,C. and Gallez,B. How does blood oxygen level-dependent (BOLD) contrast correlate with oxygen partial pressure (pO2) inside tumors?, Magn Reson.Med., *48:* 980-986, 2002.

Baudelet,C. and Gallez,B. Cluster analysis of BOLD fMRI time series in tumors to study the heterogeneity of hemodynamic response to treatment, Magn Reson.Med., *49:* 985-990, 2003.

Baudelet,C. and Gallez,B. Effect of anesthesia on the signal intensity in tumors using BOLD-MRI: comparison with flow measurements by Laser Doppler flowmetry and

oxygen measurements by luminescence-based probes, Magn Reson.Imaging, *22:* 905-912, 2004a.

Baudelet,C., Ansiaux,R., Jordan,B.F., Havaux,X., Macq,B. and Gallez,B. Physiological noise in murine solid tumours using T2*-weighted gradient-echo imaging: a marker of tumour acute hypoxia?, Phys.Med.Biol., *49:* 3389-3411, 2004b.

Bellance,N., Lestienne,P and Rossignol,R. Mitochondria : from bioenergetics to the metabolic regulation of carcinogenesis, Front.Biosc., *14:* 4015-4034, 2009.

Bentzen,L., Keiding,S., Nordsmark,M., Falborg,L., Hansen,S.B., Keller,J., Nielsen,O.S. and Overgaard,J. Tumour oxygenation assessed by 18F-fluoromisonidazole PET and polarographic needle electrodes in human soft tissue tumours, Radiother.Oncol., *67:* 339-344, 2003.

Bertout,J.A., Patel,S.A. and Simon,M.C. The impact of O2 availability on human cancer, Nat.Rev.Cancer, *8:* 967-975, 2008.

Biaglow,J., Dewhirst,M., Leeper,D., Burd,R. and Tuttle,S. Factors controlling oxygen utilization, Adv.Exp.Med.Biol., *566:* 317-323, 2005.

Biaglow,J.E., Manevich,Y., Leeper,D., Chance,B., Dewhirst,M.W., Jenkins,W.T., Tuttle,S.W., Wroblewski,K., Glickson,J.D., Stevens,C. and Evans,S.M. MIBG inhibits respiration: potential for radio- and hyperthermic sensitization, Int.J.Radiat.Oncol.Biol.Phys., *42:* 871-876, 1998.

Biswas,S., Zhao,X., Mone,A.P., Mo,X., Vargo,M., Jarjoura,D., Byrd,J.C. and Muthusamy,N. Arsenic trioxide and ascorbic acid demonstrate promising activity against primary human CLL cells in vitro, Leuk.Res., 2010.

Bornstein,J., Sagi,S., Haj,A., Harroch,J. and Fares,F. Arsenic Trioxide inhibits the growth of human ovarian carcinoma cell line, Gynecol.Oncol., *99:* 726-729, 2005.

Boucher,Y., Baxter,L.T. and Jain,R.K. Interstitial pressure gradients in tissue-isolated and subcutaneous tumors: implications for therapy, Cancer Res., *50:* 4478-4484, 1990.

Boucher,Y. and Jain,R.K. Microvascular pressure is the principal driving force for interstitial hypertension in solid tumors: implications for vascular collapse, Cancer Res., *52:* 5110-5114, 1992.

Boushel,R. and Piantadosi,C.A. Near-infrared spectroscopy for monitoring muscle oxygenation, Acta Physiol Scand., *168:* 615-622, 2000.

Boushel,R., Langberg,H., Olesen,J., Gonzales-Alonzo,J., Bulow,J. and Kjaer,M. Monitoring tissue oxygen availability with near infrared spectroscopy (NIRS) in health and disease, Scand.J.Med.Sci.Sports, *11:* 213-222, 2001.

Braun,R.D., Lanzen,J.L. and Dewhirst,M.W. Fourier analysis of fluctuations of oxygen tension and blood flow in R3230Ac tumors and muscle in rats, Am.J.Physiol, *277:* H551-H568, 1999.

Braun,R.D., Lanzen,J.L., Snyder,S.A. and Dewhirst,M.W. Comparison of tumor and normal tissue oxygen tension measurements using OxyLite or microelectrodes in rodents, Am.J.Physiol Heart Circ.Physiol, *280:* H2533-H2544, 2001.

Brizel,D.M., Dodge,R.K., Clough,R.W. and Dewhirst,M.W. Oxygenation of head and neck cancer: changes during radiotherapy and impact on treatment outcome, Radiother.Oncol., *53:* 113-117, 1999.

Brown,J.M. and Giaccia,A.J. The unique physiology of solid tumors: opportunities (and problems) for cancer therapy, Cancer Res., *58:* 1408-1416, 1998.

Brown,J.M. and Wilson,W.R. Exploiting tumour hypoxia in cancer treatment, Nat.Rev.Cancer, *4:* 437-447, 2004.

Bugger,H., Chemnitius,J.M. and Doenst,T. Differential changes in respiratory capacity and ischemia tolerance of isolated mitochondria from atrophied and hypertrophied hearts, Metabolism, *55:* 1097-1106, 2006.

Burd,R., Wachsberger,P.R., Biaglow,J.E., Wahl,M.L., Lee,I. and Leeper,D.B. Absence of Crabtree effect in human melanoma cells adapted to growth at low pH: reversal by respiratory inhibitors, Cancer Res., *61:* 5630-5635, 2001.

Burd,R., Lavorgna,S.N., Daskalakis,C., Wachsberger,P.R., Wahl,M.L., Biaglow,J.E., Stevens,C.W. and Leeper,D.B. Tumor oxygenation and acidification are increased in melanoma xenografts after exposure to hyperglycemia and meta-iodo-benzylguanidine, Radiat.Res., *159:* 328-335, 2003.

Cai,X., Yu,Y., Huang,Y., Zhang,L., Jia,P.M., Zhao,Q., Chen,Z., Tong,J.H., Dai,W. and Chen,G.Q. Arsenic trioxide-induced mitotic arrest and apoptosis in acute promyelocytic leukemia cells, Leukemia, *17:* 1333-1337, 2003.

Cardenas-Navia,L.I., Richardson,R.A. and Dewhirst,M.W. Targeting the molecular effects of a hypoxic tumor microenvironment, Front Biosci., *12:* 4061-4078, 2007.

Cardenas-Navia,L.I., Mace,D., Richardson,R.A., Wilson,D.F., Shan,S. and Dewhirst,M.W. The pervasive presence of fluctuating oxygenation in tumors, Cancer Res., *68:* 5812-5819, 2008.

Carmeliet,P., Dor,Y., Herbert,J.M., Fukumura,D., Brusselmans,K., Dewerchin,M., Neeman,M., Bono,F., Abramovitch,R., Maxwell,P., Koch,C.J., Ratcliffe,P., Moons,L., Jain,R.K., Collen,D. and Keshert,E. Role of HIF-1alpha in hypoxia-mediated apoptosis, cell proliferation and tumour angiogenesis, Nature, *394:* 485-490, 1998.

Carmeliet,P. and Jain,R.K. Angiogenesis in cancer and other diseases, Nature, *407:* 249-257, 2000.

Chang,J.E., Voorhees,P.M., Kolesar,J.M., Ahuja,H.G., Sanchez,F.A., Rodriguez,G.A., Kim,K., Werndli,J., Bailey,H.H. and Kahl,B.S. Phase II study of arsenic trioxide and ascorbic acid for relapsed or refractory lymphoid malignancies: a Wisconsin Oncology Network study, Hematol.Oncol., *27:* 11-16, 2009.

Chaplin,D.J. and Hill,S.A. Temporal heterogeneity in microregional erythrocyte flux in experimental solid tumours, Br.J.Cancer, *71:* 1210-1213, 1995.

Chen,G.Q., Shi,X.G., Tang,W., Xiong,S.M., Zhu,J., Cai,X., Han,Z.G., Ni,J.H., Shi,G.Y., Jia,P.M., Liu,M.M., He,K.L., Niu,C., Ma,J., Zhang,P., Zhang,T.D., Paul,P., Naoe,T., Kitamura,K., Miller,W., Waxman,S., Wang,Z.Y., de,T.H., Chen,S.J. and Chen,Z. Use of arsenic trioxide (As2O3) in the treatment of acute promyelocytic leukemia (APL): I. As2O3 exerts dose-dependent dual effects on APL cells, Blood, *89:* 3345-3353, 1997.

Chen,K., Glockner,J.F., Morse,P.D. and Swartz,H.M. Effects of oxygen on the metabolism of nitroxide spin labels in cells, Biochemistry, *28:* 2496-2501, 1989.

Chen,Y.C., Lin-Shiau,S.Y. and Lin,J.K. Involvement of reactive oxygen species and caspase 3 activation in arsenite-induced apoptosis, J.Cell Physiol, *177:* 324-333, 1998.

Cheng,B., Yang,X., An,L., Gao,B. and Liu,X. Arsenic trioxide-induced apoptosis of Hep-2 cell line through modulating intracellular glutathione (GSH) level, Auris Nasus Larynx, *37:* 89-94, 2010.

Christen,T. Mesures *in vivo* de l'oxygénation sanguine et tissulaire par IRM; applications à l'étude de l'hypoxie tumorale chez le rat, Thesis, p91-111, 2009.

Chun,Y.J., Park,I.C., Park,M.J., Woo,S.H., Hong,S.I., Chung,H.Y., Kim,T.H., Lee,Y.S., Rhee,C.H. and Lee,S.J. Enhancement of radiation response in human cervical cancer cells in vitro and in vivo by arsenic trioxide (As2O3), FEBS Lett., *519:* 195-200, 2002.

Cohade,C. and Wahl,R.L. Applications of positron emission tomography/computed tomography image fusion in clinical positron emission tomography-clinical use, interpretation methods, diagnostic improvements, Semin.Nucl.Med., *33:* 228-237, 2003.

Cohn,C.S. and Cushing,M.M. Oxygen therapeutics: perfluorocarbons and blood substitute safety, Crit Care Clin., *25:* 399-414, Table, 2009.

Collingridge,D.R., Young,W.K., Vojnovic,B., Wardman,P., Lynch,E.M., Hill,S.A. and Chaplin,D.J. Measurement of tumor oxygenation: a comparison between polarographic needle electrodes and a time-resolved luminescence-based optical sensor, Radiat.Res., *147:* 329-334, 1997.

Cristofanilli,M., Yamamura,Y., Kau,S.W., Bevers,T., Strom,S., Patangan,M., Hsu,L., Krishnamurthy,S., Theriault,R.L. and Hortobagyi,G.N. Thyroid hormone and breast carcinoma. Primary hypothyroidism is associated with a reduced incidence of primary breast carcinoma, Cancer, *103:* 1122-1128, 2005.

Crokart,N., Radermacher,K., Jordan,B.F., Baudelet,C., Cron,G.O., Gregoire,V., Beghein,N., Bouzin,C., Feron,O. and Gallez,B. Tumor radiosensitization by antiinflammatory drugs: evidence for a new mechanism involving the oxygen effect, Cancer Res., *65:* 7911-7916, 2005.

Crokart,N., Jordan,B.F., Baudelet,C., Cron,G.O., Hotton,J., Radermacher,K., Gregoire,V., Beghein,N., Martinive,P., Bouzin,C., Feron,O. and Gallez,B. Glucocorticoids modulate

tumor radiation response through a decrease in tumor oxygen consumption, Clin.Cancer Res., *13:* 630-635, 2007.

Cui,X., Kobayashi,Y., Akashi,M. and Okayasu,R. Metabolism and the paradoxical effects of arsenic: carcinogenesis and anticancer, Curr.Med.Chem., *15:* 2293-2304, 2008.

Dai,J., Weinberg,R.S., Waxman,S. and Jing,Y. Malignant cells can be sensitized to undergo growth inhibition and apoptosis by arsenic trioxide through modulation of the glutathione redox system, Blood, *93:* 268-277, 1999.

Dalton,W.S. Targeting the mitochondria: an exciting new approach to myeloma therapy. Commentary re: N. J. Bahlis et al., Feasibility and correlates of arsenic trioxide combined with ascorbic acid-mediated depletion of intracellular glutathione for the treatment of relapsed/refractory multiple myeloma. Clin. Cancer Res., 8: 3658-3668, 2002, Clin.Cancer Res., *8:* 3643-3645, 2002.

Dang,C.V., Kim,J.W., Gao,P and Yustein,J. The interface between MYC and HIF in cancer, Nat.Rev.Cancer, *8:* 51-56, 2008.

Davison,K., Cote,S., Mader,S. and Miller,W.H. Glutathione depletion overcomes resistance to arsenic trioxide in arsenic-resistant cell lines, Leukemia, *17:* 931-940, 2003.

De Thé,T.H., Chomienne,C., Lanotte,M., Degos,L. and Dejean,A. The t(15;17) translocation of acute promyelocytic leukaemia fuses the retinoic acid receptor alpha gene to a novel transcribed locus, Nature, *347:* 558-561, 1990.

Denko,N.C. Hypoxia, HIF1 and glucose metabolism in the solid tumour, Nat.Rev.Cancer, *8:* 705-713, 2008.

Desquiret,V., Gueguen,N., Malthiery,Y., Ritz,P. and Simard,G. Mitochondrial effects of dexamethasone imply both membrane and cytosolic-initiated pathways in HepG2 cells, Int.J.Biochem.Cell Biol., *40:* 1629-1641, 2008.

Dewhirst,M.W., Secomb,T.W., Ong,E.T., Hsu,R. and Gross,J.F. Determination of local oxygen consumption rates in tumors, Cancer Res., *54:* 3333-3336, 1994.

Dewhirst,M.W., Ong,E.T., Rosner,G.L., Rehmus,S.W., Shan,S., Braun,R.D., Brizel,D.M. and Secomb,T.W. Arteriolar oxygenation in tumour and subcutaneous arterioles: effects of inspired air oxygen content, Br.J.Cancer Suppl, *27:* S241-S246, 1996.

Dewhirst,M.W., Ong,E.T., Braun,R.D., Smith,B., Klitzman,B., Evans,S.M. and Wilson,D. Quantification of longitudinal tissue pO2 gradients in window chamber tumours: impact on tumour hypoxia, Br.J.Cancer, *79:* 1717-1722, 1999.

Dewhirst,M.W., Klitzman,B., Braun,R.D., Brizel,D.M., Haroon,Z.A. and Secomb,T.W. Review of methods used to study oxygen transport at the microcirculatory level, Int.J.Cancer, *90:* 237-255, 2000.

Dewhirst,M.W., Cao,Y. and Moeller,B. Cycling hypoxia and free radicals regulate angiogenesis and radiotherapy response, Nat.Rev.Cancer, *8:* 425-437, 2008.

Diepart,C., Jordan,B.F. and Gallez,B. A New EPR Oximetry Protocol to Estimate the Tissue Oxygen Consumption In Vivo, Radiat.Res., *172:* 220-225, 2009.

Dilda,P.J. and Hogg,P.J. Arsenical-based cancer drugs, Cancer Treat.Rev., *33:* 542-564, 2007.

Dunn,J.F., Zaim-Wadghiri,Y., Pogue,B.W. and Kida,I. BOLD MRI vs. NIR spectrophotometry. Will the best technique come forward?, Adv.Exp.Med.Biol., *454:* 103-113, 1998.

Durand,R.E. The influence of microenvironmental factors during cancer therapy, In Vivo, *8:* 691-702, 1994.

Durand,R.E. and LePard,N.E. Contribution of transient blood flow to tumour hypoxia in mice, Acta Oncol., *34:* 317-323, 1995.

Durand,R.E. Intermittent blood flow in solid tumours--an under-appreciated source of 'drug resistance', Cancer Metastasis Rev., *20:* 57-61, 2001.

Elas,M., Williams,B.B., Parasca,A., Mailer,C., Pelizzari,C.A., Lewis,M.A., River,J.N., Karczmar,G.S., Barth,E.D. and Halpern,H.J. Quantitative tumor oxymetric images from 4D electron paramagnetic resonance imaging (EPRI): methodology and comparison with blood oxygen level-dependent (BOLD) MRI, Magn Reson.Med., *49:* 682-691, 2003.

Elas,M., Ahn,K.H., Parasca,A., Barth,E.D., Lee,D., Haney,C. and Halpern,H.J. Electron paramagnetic resonance oxygen images correlate spatially and quantitatively with Oxylite oxygen measurements, Clin.Cancer Res., *12:* 4209-4217, 2006.

Elkind,M.M., Swain,R.W., Alescio,T., et al. Oxygen, nitrogen, recovery and radiation therapy. In Shalek R, ed: Cellular Radiation Biology, pp 442-466. Baltimore, MD, Williams and Wilkins, 1965.

Escobar,L., Salvador,C., Contreras,M. and Escamilla,J.E. On the application of the Clark oxygen electrode to the study of enzyme kinetics in apolar solvents: the catalase reaction, Anal.Biochem., *184:* 139-144, 1990.

Fang,J.S., Gillies,R.D. and Gatenby,R.A. Adaptation to hypoxia and acidosis in carcinogenesis and tumor progression, Semin.Cancer Biol., *18:* 330-337, 2008.

Feron,O. Pyruvate into lactate and back: from the Warburg effect to symbiotic energy fuel exchange in cancer cells, Radiother.Oncol., *92:* 329-333, 2009.

Fiat,D., Dolinsek,J., Hankiewicz,J., Dujovny,M. and Ausman,J. Determination of regional cerebral oxygen consumption in the human: 17O natural abundance cerebral magnetic resonance imaging and spectroscopy in a whole body system, Neurol.Res., *15:* 237-248, 1993.

Folkman,J. Role of angiogenesis in tumor growth and metastasis, Semin.Oncol., *29:* 15-18, 2002.

Frackowiak,R.S., Lenzi,G.L., Jones,T. and Heather,J.D. Quantitative measurement of regional cerebral blood flow and oxygen metabolism in man using 15O and positron emission tomography: theory, procedure, and normal values, J.Comput.Assist.Tomogr., *4:* 727-736, 1980.

Fukumura,D. and Jain,R.K. Tumor microvasculature and microenvironment: targets for anti-angiogenesis and normalization, Microvasc.Res., *74:* 72-84, 2007a.

Fukumura,D. and Jain,R.K. Tumor microenvironment abnormalities: causes, consequences, and strategies to normalize, J.Cell Biochem., *101:* 937-949, 2007b.

Fukumura,D. and Jain,R.K. Imaging angiogenesis and the microenvironment, APMIS, *116:* 695-715, 2008.

Gallez,B., De,M.C., Debuyst,R., Dejehet,F. and Dumont,P. Mutagenicity of nitroxyl compounds: structure-activity relationships, Toxicol.Lett., *63:* 35-45, 1992.

Gallez,B., Jordan,B.F., Baudelet,C. and Misson,P.D. Pharmacological modifications of the partial pressure of oxygen in murine tumors: evaluation using in vivo EPR oximetry, Magn Reson.Med., *42:* 627-630, 1999.

Gallez,B., Baudelet,C. and Jordan,B.F. Assessment of tumor oxygenation by electron paramagnetic resonance: principles and applications, NMR Biomed., *17:* 240-262, 2004.

Gallez,B. and Swartz,H.M. In vivo EPR: when, how and why?, NMR Biomed., *17:* 223-225, 2004.

Gambhir,S.S. Molecular imaging of cancer with positron emission tomography, Nat.Rev.Cancer, *2:* 683-693, 2002.

Gatenby,R.A. and Gillies,R.J. Why do cancers have high aerobic glycolysis?, Nat.Rev.Cancer, *4:* 891-899, 2004.

Gatenby,R.A. and Gillies,R.J. A microenvironmental model of carcinogenesis, Nat.Rev.Cancer, *8:* 56-61, 2008.

Gillies,R.J., Schornack,P.A., Secomb,T.W. and Raghunand,N. Causes and effects of heterogeneous perfusion in tumors, Neoplasia., *1:* 197-207, 1999.

Grad,J.M., Bahlis,N.J., Reis,I., Oshiro,M.M., Dalton,W.S. and Boise,L.H. Ascorbic acid enhances arsenic trioxide-induced cytotoxicity in multiple myeloma cells, Blood, *98:* 805-813, 2001.

Gredilla,R., Lopez,T.M., Portero-Otin,M., Pamplona,R. and Barja,G. Influence of hyper- and hypothyroidism on lipid peroxidation, unsaturation of phospholipids, glutathione system and oxidative damage to nuclear and mitochondrial DNA in mice skeletal muscle, Mol.Cell Biochem., *221:* 41-48, 2001.

Griffin,R.J., Lee,S.H., Rood,K.L., Stewart,M.J., Lyons,J.C., Lew,Y.S., Park,H. and Song,C.W. Use of arsenic trioxide as an antivascular and thermosensitizing agent in solid tumors, Neoplasia., *2:* 555-560, 2000.

Griffin,R.J., Monzen,H., Williams,B.W., Park,H., Lee,S.H. and Song,C.W. Arsenic trioxide induces selective tumour vascular damage via oxidative stress and increases thermosensitivity of tumours, Int.J.Hyperthermia, *19:* 575-589, 2003.

Griffin,R.J., Williams,B.W., Park,H.J. and Song,C.W. Preferential action of arsenic trioxide in solid-tumor microenvironment enhances radiation therapy, Int.J.Radiat.Oncol.Biol.Phys., *61:* 1516-1522, 2005.

Griffin,R.J., Williams,B.W., Bischof,J.C., Olin,M., Johnson,G.L. and Lee,B.W. Use of a fluorescently labeled poly-caspase inhibitor for in vivo detection of apoptosis related to vascular-targeting agent arsenic trioxide for cancer therapy, Technol.Cancer Res.Treat., *6:* 651-654, 2007.

Griffith,O.W. Determination of glutathione and glutathione disulfide using glutathione reductase and 2-vinylpyridine, Anal.Biochem., *106:* 207-212, 1980.

Griffiths,J.R. and Robinson,S.P. The OxyLite: a fibre-optic oxygen sensor, Br.J.Radiol., *72:* 627-630, 1999.

Han,Y.H., Kim,S.Z., Kim,S.H. and Park,W.H. Arsenic trioxide inhibits the growth of Calu-6 cells via inducing a G2 arrest of the cell cycle and apoptosis accompanied with the depletion of GSH, Cancer Lett., *270:* 40-55, 2008.

Hardee,M.E., Dewhirst,M.W., Agarwal,N. and Sorg,B.S. Novel imaging provides new insights into mechanisms of oxygen transport in tumors, Curr.Mol.Med., *9:* 435-441, 2009.

Harris,A.L. Hypoxia--a key regulatory factor in tumour growth, Nat.Rev.Cancer, *2:* 38-47, 2002.

Hattori,N., Bergsneider,M., Wu,H.M., Glenn,T.C., Vespa,P.M., Hovda,D.A., Phelps,M.E. and Huang,S.C. Accuracy of a method using short inhalation of (15)O-O(2) for measuring cerebral oxygen extraction fraction with PET in healthy humans, J.Nucl.Med., *45:* 765-770, 2004.

He,J., Beghein,N., Ceroke,P., Clarkson,R.B., Swartz,H.M. and Gallez,B. Development of biocompatible oxygen-permeable films holding paramagnetic carbon particles: evaluation of their performance and stability in EPR oximetry, Magn Reson.Med., *46:* 610-614, 2001.

He,X. and Yablonskiy,D.A. Quantitative BOLD: mapping of human cerebral deoxygenated blood volume and oxygen extraction fraction: default state, Magn Reson.Med., *57:* 115-126, 2007.

He,X., Zhu,M. and Yablonskiy,D.A. Validation of oxygen extraction fraction measurement by qBOLD technique, Magn Reson.Med., *60:* 882-888, 2008.

Helmlinger,G., Yuan,F., Dellian,M. and Jain,R.K. Interstitial pH and pO2 gradients in solid tumors in vivo: high-resolution measurements reveal a lack of correlation, Nat.Med., *3:* 177-182, 1997.

Helmlinger,G., Sckell,A., Dellian,M., Forbes,N.S. and Jain,R.K. Acid production in glycolysis-impaired tumors provides new insights into tumor metabolism, Clin.Cancer Res., *8:* 1284-1291, 2002.

Hennig,J., Speck,O., Koch,M.A. and Weiller,C. Functional magnetic resonance imaging: a review of methodological aspects and clinical applications, J.Magn Reson.Imaging, *18:* 1-15, 2003.

Hercbergs,A.A., Goyal,L.K., Suh,J.H., Lee,S., Reddy,C.A., Cohen,B.H., Stevens,G.H., Reddy,S.K., Peereboom,D.M., Elson,P.J., Gupta,M.K. and Barnett,G.H. Propylthiouracil-induced chemical hypothyroidism with high-dose tamoxifen prolongs survival in recurrent high grade glioma: a phase I/II study, Anticancer Res., *23:* 617-626, 2003.

Ho,S.Y., Chen,W.C., Chiu,H.W., Lai,C.S., Guo,H.R. and Wang,Y.J. Combination treatment with arsenic trioxide and irradiation enhances apoptotic effects in U937 cells through increased mitotic arrest and ROS generation, Chem.Biol.Interact., *179:* 304-313, 2009.

Hockel,M., Schlenger,K., Hockel,S. and Vaupel,P. Hypoxic cervical cancers with low apoptotic index are highly aggressive, Cancer Res., *59:* 4525-4528, 1999.

Hockel,M. and Vaupel,P. Tumor hypoxia: definitions and current clinical, biologic, and molecular aspects, J.Natl.Cancer Inst., *93:* 266-276, 2001a.

Hockel,M. and Vaupel,P. Biological consequences of tumor hypoxia, Semin.Oncol., *28:* 36-41, 2001b.

Holmgren,L., O'Reilly,M.S. and Folkman,J. Dormancy of micrometastases: balanced proliferation and apoptosis in the presence of angiogenesis suppression, Nat.Med., *1:* 149-153, 1995.

Howe,F.A., Robinson,S.P., McIntyre,D.J., Stubbs,M. and Griffiths,J.R. Issues in flow and oxygenation dependent contrast (FLOOD) imaging of tumours, NMR Biomed., *14:* 497-506, 2001.

Hunjan,S., Zhao,D., Constantinescu,A., Hahn,E.W., Antich,P.P. and Mason,R.P. Tumor oximetry: demonstration of an enhanced dynamic mapping procedure using fluorine-19 echo planar magnetic resonance imaging in the Dunning prostate R3327-AT1 rat tumor, Int.J.Radiat.Oncol.Biol.Phys., *49:* 1097-1108, 2001.

Hynes,J., Hill,R. and Papkovsky,D.B. The use of a fluorescence-based oxygen uptake assay in the analysis of cytotoxicity, Toxicol.In Vitro, *20:* 785-792, 2006a.

Hynes,J., Marroquin,L.D., Ogurtsov,V.I., Christiansen,K.N., Stevens,G.J., Papkovsky,D.B. and Will,Y. Investigation of drug-induced mitochondrial toxicity using fluorescence-based oxygen-sensitive probes, Toxicol.Sci., *92:* 186-200, 2006b.

Ilangovan,G., Li,H., Zweier,J.L., Krishna,M.C., Mitchell,J.B. and Kuppusamy,P. In vivo measurement of regional oxygenation and imaging of redox status in RIF-1 murine tumor: effect of carbogen-breathing, Magn Reson.Med., *48:* 723-730, 2002.

Ilangovan,G., Zweier,J.L. and Kuppusamy,P. Microximetry: simultaneous determination of oxygen consumption and free radical production using electron paramagnetic resonance spectroscopy, Methods Enzymol., *381:* 747-762, 2004.

Ilangovan,G., Osinbowale,S., Bratasz,A., Bonar,M., Cardounel,A.J., Zweier,J.L. and Kuppusamy,P. Heat shock regulates the respiration of cardiac H9c2 cells through upregulation of nitric oxide synthase, Am.J.Physiol Cell Physiol, *287:* C1472-C1481, 2004.

Intes,X. and Chance,B. Non-PET functional imaging techniques: optical, Radiol.Clin.North Am., *43:* 221-34, xii, 2005.

Jain,R.K. Molecular regulation of vessel maturation, Nat.Med., *9:* 685-693, 2003.

Jain,R.K. Normalization of tumor vasculature: an emerging concept in antiangiogenic therapy, Science, *307:* 58-62, 2005.

James,P.E., Jackson,S.K., Grinberg,O.Y. and Swartz,H.M. The effects of endotoxin on oxygen consumption of various cell types in vitro: an EPR oximetry study, Free Radic.Biol.Med., *18:* 641-647, 1995.

Jana,N.R. NSAIDs and apoptosis, Cell Mol.Life Sci., *65:* 1295-1301, 2008.

Jiang,X.H., Wong,B.C., Yuen,S.T., Jiang,S.H., Cho,C.H., Lai,K.C., Lin,M.C., Kung,H.F. and Lam,S.K. Arsenic trioxide induces apoptosis in human gastric cancer cells through up-regulation of p53 and activation of caspase-3, Int.J.Cancer, *91:* 173-179, 2001.

Jing,Y., Dai,J., Chalmers-Redman,R.M., Tatton,W.G. and Waxman,S. Arsenic trioxide selectively induces acute promyelocytic leukemia cell apoptosis via a hydrogen peroxide-dependent pathway, Blood, *94:* 2102-2111, 1999.

Jones,E.L. and Douple,E.B. The effect of in vivo GSH depletion on thermosensitivity, radiosensitivity and thermal radiosensitization, Int.J.Hyperthermia, *6:* 951-955, 1990.

Jordan,B.F., Baudelet,C. and Gallez,B. Carbon-centered radicals as oxygen sensors for in vivo electron paramagnetic resonance: screening for an optimal probe among commercially available charcoals, MAGMA., *7:* 121-129, 1998.

Jordan,B.F., Misson,P., Demeure,R., Baudelet,C., Beghein,N. and Gallez,B. Changes in tumor oxygenation/perfusion induced by the no donor, isosorbide dinitrate, in comparison with carbogen: monitoring by EPR and MRI, Int.J.Radiat.Oncol.Biol.Phys., *48:* 565-570, 2000.

Jordan,B.F., Gregoire,V., Demeure,R.J., Sonveaux,P., Feron,O., O'Hara,J., Vanhulle,V.P., Delzenne,N. and Gallez,B. Insulin increases the sensitivity of tumors to irradiation: involvement of an increase in tumor oxygenation mediated by a nitric oxide-dependent decrease of the tumor cells oxygen consumption, Cancer Res., *62:* 3555-3561, 2002.

Jordan,B.F., Sonveaux,P., Feron,O., Gregoire,V., Beghein,N., Dessy,C. and Gallez,B. Nitric oxide as a radiosensitizer: evidence for an intrinsic role in addition to its effect on oxygen delivery and consumption, Int.J.Cancer, *109:* 768-773, 2004.

Jordan,B.F., Crokart,N., Baudelet,C., Cron,G.O., Ansiaux,R. and Gallez,B. Complex relationship between changes in oxygenation status and changes in R*2: the case of insulin and NS-398, two inhibitors of oxygen consumption, Magn Reson.Med., *56:* 637-643, 2006a.

Jordan,B.F., Beghein,N., Crokart,N., Baudelet,C., Gregoire,V. and Gallez,B. Preclinical safety and antitumor efficacy of insulin combined with irradiation, Radiother.Oncol., *81:* 112-117, 2006b.

Jordan,B.F., Christian,N., Crokart,N., Gregoire,V., Feron,O. and Gallez,B. Thyroid status is a key modulator of tumor oxygenation: implication for radiation therapy, Radiat.Res., *168:* 428-432, 2007.

Jordan,B.F., Cron,G.O. and Gallez,B. Rapid monitoring of oxygenation by 19F magnetic resonance imaging: Simultaneous comparison with fluorescence quenching, Magn Reson.Med., *61:* 634-638, 2009.

Kang,Y.H. and Lee,S.J. Role of p38 MAPK and JNK in enhanced cervical cancer cell killing by the combination of arsenic trioxide and ionizing radiation, Oncol.Rep., *20:* 637-643, 2008.

Kelleher,D.K., Nauth,C., Thews,O., Krueger,W. and Vaupel,P. Localized hypothermia: impact on oxygenation, microregional perfusion, metabolic and bioenergetic status of subcutaneous rat tumours, Br.J.Cancer, *78:* 56-61, 1998.

Kessler,R.M. Imaging methods for evaluating brain function in man, Neurobiol.Aging, *24 Suppl 1:* S21-S35, 2003.

Khan,N., Williams,B.B., Hou,H., Li,H. and Swartz,H.M. Repetitive tissue pO2 measurements by electron paramagnetic resonance oximetry: current status and future potential for experimental and clinical studies, Antioxid.Redox.Signal., *9:* 1169-1182, 2007.

Kida,I., Yamamoto,T. and Tamura,M. Interpretation of BOLD MRI signals in rat brain using simultaneously measured near-infrared spectrophotometric information, NMR Biomed., *9:* 333-338, 1996.

Kim,J.H., Lew,Y.S., Kolozsvary,A., Ryu,S. and Brown,S.L. Arsenic trioxide enhances radiation response of 9L glioma in the rat brain, Radiat.Res., *160:* 662-666, 2003.

Kim,J.W., Gao,P. and Dang,C.V. Effects of hypoxia on tumor metabolism, Cancer Metastasis Rev., *26:* 291-298, 2007.

Kimberg,D.V., Loud,A.V. and Wiener,J. Cortisone-induced alterations in mitochondrial function and structure, J.Cell Biol., *37:* 63-79, 1968.

Koh,W.J., Rasey,J.S., Evans,M.L., Grierson,J.R., Lewellen,T.K., Graham,M.M., Krohn,K.A. and Griffin,T.W. Imaging of hypoxia in human tumors with [F-18]fluoromisonidazole, Int.J.Radiat.Oncol.Biol.Phys., *22:* 199-212, 1992.

Krause,B.J., Beck,R., Souvatzoglou,M. and Piert,M. PET and PET/CT studies of tumor tissue oxygenation, Q.J.Nucl.Med.Mol.Imaging, *50:* 28-43, 2006.

Krause,M.M., Brand,M.D., Krauss,S., Meisel,C., Vergin,H., Burmester,G.R. and Buttgereit,F. Nonsteroidal antiinflammatory drugs and a selective cyclooxygenase 2 inhibitor uncouple mitochondria in intact cells, Arthritis Rheum., *48:* 1438-1444, 2003.

Krohn,K.A., Link,J.M. and Mason,R.P. Molecular imaging of hypoxia, J.Nucl.Med., *49 Suppl 2:* 129S-148S, 2008.

Kudomi,N., Hayashi,T., Teramoto,N., Watabe,H., Kawachi,N., Ohta,Y., Kim,K.M. and Iida,H. Rapid quantitative measurement of CMRO(2) and CBF by dual administration of (15)O-labeled oxygen and water during a single PET scan-a validation study and error analysis in anesthetized monkeys, J.Cereb.Blood Flow Metab, *25:* 1209-1224, 2005.

Kuhajda,F.P. Fatty acid synthase and cancer: new application of an old pathway, Cancer Res., *66:* 5977-5980, 2006.

Kuppusamy,P., Afeworki,M., Shankar,R.A., Coffin,D., Krishna,M.C., Hahn,S.M., Mitchell,J.B. and Zweier,J.L. In vivo electron paramagnetic resonance imaging of tumor heterogeneity and oxygenation in a murine model, Cancer Res., *58:* 1562-1568, 1998.

Kuppusamy,P., Li,H., Ilangovan,G., Cardounel,A.J., Zweier,J.L., Yamada,K., Krishna,M.C. and Mitchell,J.B. Noninvasive imaging of tumor redox status and its modification by tissue glutathione levels, Cancer Res., *62:* 307-312, 2002.

Lammertsma,A.A., Jones,T., Frackowiak,R.S. and Lenzi,G.L. A theoretical study of the steady-state model for measuring regional cerebral blood flow and oxygen utilisation using oxygen-15, J.Comput.Assist.Tomogr., *5:* 544-550, 1981.

Lanzen,J.L., Braun,R.D., Ong,A.L. and Dewhirst,M.W. Variability in blood flow and pO2 in tumors in response to carbogen breathing, Int.J.Radiat.Oncol.Biol.Phys., *42:* 855-859, 1998.

Larochette,N., Decaudin,D., Jacotot,E., Brenner,C., Marzo,I., Susin,S.A., Zamzami,N., Xie,Z., Reed,J. and Kroemer,G. Arsenite induces apoptosis via a direct effect on the mitochondrial permeability transition pore, Exp.Cell Res., *249:* 413-421, 1999.

Lee,I., Glickson,J.D., Dewhirst,M.W., Leeper,D.B., Burd,R., Poptani,H., Nadal,L., McKenna,W.G. and Biaglow,J.E. Effect of mild hyperglycemia +/- meta-iodo-benzylguanidine on the radiation response of R3230 Ac tumors, Adv.Exp.Med.Biol., *530:* 177-186, 2003.

Lew,Y.S., Brown,S.L., Griffin,R.J., Song,C.W. and Kim,J.H. Arsenic trioxide causes selective necrosis in solid murine tumors by vascular shutdown, Cancer Res., *59:* 6033-6037, 1999.

Lew,Y.S., Kolozsvary,A., Brown,S.L. and Kim,J.H. Synergistic interaction with arsenic trioxide and fractionated radiation in locally advanced murine tumor, Cancer Res., *62:* 4202-4205, 2002.

Li,H., Hou,H., Sucheta,A., Williams,B.B., Lariviere,J.P., Khan,M.N., Lesniewski,P.N., Gallez,B. and Swartz,H.M. Implantable resonators--a technique for repeated measurement of oxygen at multiple deep sites with in vivo EPR, Adv.Exp.Med.Biol., *662:* 265-272, 2010.

Li,J.J., Tang,Q., Li,Y., Hu,B.R., Ming,Z.Y., Fu,Q., Qian,J.Q. and Xiang,J.Z. Role of oxidative stress in the apoptosis of hepatocellular carcinoma induced by combination of arsenic trioxide and ascorbic acid, Acta Pharmacol.Sin., *27:* 1078-1084, 2006.

Li,Y., Qu,X., Qu,J., Zhang,Y., Liu,J., Teng,Y., Hu,X., Hou,K. and Liu,Y. Arsenic trioxide induces apoptosis and G2/M phase arrest by inducing Cbl to inhibit PI3K/Akt signaling and thereby regulate p53 activation, Cancer Lett., *284:* 208-215, 2009.

Liu,H., Song,Y.,Worden,K.L., Jiang,X., Constantinescu,A., Mason,R.P. Noninvasive investigation of blood oxygenation dynamics of tumors by near infrared spectroscopy, Appl.Opt, *39(28):* 5231-43, 2000.

Liu,K.J., Gast,P., Moussavi,M., Norby,S.W., Vahidi,N., Walczak,T., Wu,M. and Swartz,H.M. Lithium phthalocyanine: a probe for electron paramagnetic resonance oximetry in viable biological systems, Proc.Natl.Acad.Sci.U.S.A, *90:* 5438-5442, 1993.

Loesberg,C., Van,R.H., Nooijen,W.J., Meijer,A.J. and Smets,L.A. Impaired mitochondrial respiration and stimulated glycolysis by m-iodobenzylguanidine (MIBG), Int.J.Cancer, *46:* 276-281, 1990.

Loesberg,C., Van,R.H., Romijn,J.C. and Smets,L.A. Mitochondrial effects of the guanidino group-containing cytostatic drugs, m-iodobenzylguanidine and methylglyoxal bis (guanylhydrazone), Biochem.Pharmacol., *42:* 793-798, 1991.

Lowry,O.H., Rosebrough,N.J., Farr,A.L. and Randall,R.J. Protein measurement with the Folin phenol reagent, J.Biol.Chem., *193:* 265-275, 1951.

Lu,R and Yu, T. Fabrication and evaluation of an oxygen microelectrode applicable to environmental engineering and science, J.Environ.Eng.Sci., *1:* 225-235, 2002.

Lunt,S.J., Chaudary,N. and Hill,R.P. The tumor microenvironment and metastatic disease, Clin.Exp.Metastasis, *26:* 19-34, 2009.

Maeda,H., Hori,S., Nishitoh,H., Ichijo,H., Ogawa,O., Kakehi,Y. and Kakizuka,A. Tumor growth inhibition by arsenic trioxide (As2O3) in the orthotopic metastasis model of androgen-independent prostate cancer, Cancer Res., *61:* 5432-5440, 2001.

Maeda,H., Hori,S., Ohizumi,H., Segawa,T., Kakehi,Y., Ogawa,O. and Kakizuka,A. Effective treatment of advanced solid tumors by the combination of arsenic trioxide and L-buthionine-sulfoximine, Cell Death.Differ., *11:* 737-746, 2004.

Marcu,L. and Olver,I. Tirapazamine: from bench to clinical trials, Curr.Clin.Pharmacol., *1:* 71-79, 2006.

Mason,R.P. Non-invasive physiology: 19F NMR of perfluorocarbons, Artif.Cells Blood Substit.Immobil.Biotechnol., *22:* 1141-1153, 1994.

Mason,R.P., Rodbumrung,W. and Antich,P.P. Hexafluorobenzene: a sensitive 19F NMR indicator of tumor oxygenation, NMR Biomed., *9:* 125-134, 1996.

Mason,R.P., Constantinescu,A., Hunjan,S., Le,D., Hahn,E.W., Antich,P.P., Blum,C. and Peschke,P. Regional tumor oxygenation and measurement of dynamic changes, Radiat.Res., *152:* 239-249, 1999.

Mason,R.P. Non-invasive assessment of kidney oxygenation: a role for BOLD MRI, Kidney Int., *70:* 10-11, 2006.

McIntyre,D.J.O., McCoy,C.L. and Griffiths,J.R. Tumour oxygenation measurements by 19F magnetic resonance imaging of perfluorocarbons, Curr.Sci. *76:* 753-762, 1999.

Mees,G., Dierckx,R., Vangestel,C. and Van De,W.C. Molecular imaging of hypoxia with radiolabelled agents, Eur.J.Nucl.Med.Mol.Imaging, *36:* 1674-1686, 2009.

Mellon,E.A., Beesam,R.S., Baumgardner,J.E., Borthakur,A., Witschey,W.R. and Reddy,R. Estimation of the regional cerebral metabolic rate of oxygen consumption with proton detected 17O MRI during precision 17O2 inhalation in swine, J.Neurosci.Methods, *179:* 29-39, 2009.

Miller,W.H., Jr., Schipper,H.M., Lee,J.S., Singer,J. and Waxman,S. Mechanisms of action of arsenic trioxide, Cancer Res., *62:* 3893-3903, 2002a.

Miller,W.H., Jr. Molecular targets of arsenic trioxide in malignant cells, Oncologist., *7 Suppl 1:* 14-19, 2002b.

Minn,H., Gronroos,T.J., Komar,G., Eskola,O., Lehtio,K., Tuomela,J., Seppanen,M. and Solin,O. Imaging of tumor hypoxia to predict treatment sensitivity, Curr.Pharm.Des, *14:* 2932-2942, 2008.

Mintun,M.A., Raichle,M.E., Martin,W.R. and Herscovitch,P. Brain oxygen utilization measured with O-15 radiotracers and positron emission tomography, J.Nucl.Med., *25:* 177-187, 1984.

Mishkin,S.Y., Pollack,R., Yalovsky,M.A., Morris,H.P. and Mishkin,S. Inhibition of local and metastatic hepatoma growth and prolongation of survival after induction of hypothyroidism, Cancer Res., *41:* 3040-3045, 1981.

Monzen,H., Griffin,R.J., Williams,B.W., Amano,M., Ando,S. and Hasegawa,T. Study of arsenic trioxide-induced vascular shutdown and enhancement with radiation in solid tumor, Radiat.Med., *22:* 205-211, 2004.

Moreno-Sanchez,R., Bravo,C., Vasquez,C., Ayala,G., Silveira,L.H. and Martinez-Lavin,M. Inhibition and uncoupling of oxidative phosphorylation by nonsteroidal anti-inflammatory drugs: study in mitochondria, submitochondrial particles, cells, and whole heart, Biochem.Pharmacol., *57:* 743-752, 1999.

Nias,A.H., Perry,P.M. and Photiou,A.R. Modulating the oxygen tension in tumours by hypothermia and hyperbaric oxygen, J.R.Soc.Med., *81:* 633-636, 1988.

Ning,S. and Knox,S.J. Optimization of combination therapy of arsenic trioxide and fractionated radiotherapy for malignant glioma, Int.J.Radiat.Oncol.Biol.Phys., *65:* 493-498, 2006.

Nordsmark,M., Bentzen,S.M. and Overgaard,J. Measurement of human tumour oxygenation status by a polarographic needle electrode. An analysis of inter- and intratumour heterogeneity, Acta Oncol., *33:* 383-389, 1994.

Nordsmark,M., Bentzen,S.M., Rudat,V., Brizel,D., Lartigau,E., Stadler,P., Becker,A., Adam,M., Molls,M., Dunst,J., Terris,D.J. and Overgaard,J. Prognostic value of tumor oxygenation in 397 head and neck tumors after primary radiation therapy. An international multi-center study, Radiother.Oncol., *77:* 18-24, 2005.

O'Connor,J.P., Naish,J.H., Parker,G.J., Waterton,J.C., Watson,Y., Jayson,G.C., Buonaccorsi,G.A., Cheung,S., Buckley,D.L., McGrath,D.M., West,C.M., Davidson,S.E., Roberts,C., Mills,S.J., Mitchell,C.L., Hope,L., Ton,N.C. and Jackson,A. Preliminary study of oxygen-enhanced longitudinal relaxation in MRI: a potential novel biomarker of oxygenation changes in solid tumors, Int.J.Radiat.Oncol.Biol.Phys., *75:* 1209-1215, 2009.

O'Hara,J.A., Hou,H., Demidenko,E., Springett,R.J., Khan,N. and Swartz,H.M. Simultaneous measurement of rat brain cortex PtO2 using EPR oximetry and a fluorescence fiber-optic sensor during normoxia and hyperoxia, Physiol Meas., *26:* 203-213, 2005.

Ogawa,S., Lee,T.M., Kay,A.R. and Tank,D.W. Brain magnetic resonance imaging with contrast dependent on blood oxygenation, Proc.Natl.Acad.Sci.U.S.A, *87:* 9868-9872, 1990.

Ohta,S., Meyer,E., Thompson,C.J. and Gjedde,A. Oxygen consumption of the living human brain measured after a single inhalation of positron emitting oxygen, J.Cereb.Blood Flow Metab, *12:* 179-192, 1992.

Ohta,S., Meyer,E., Fujita,H., Reutens,D.C., Evans,A. and Gjedde,A. Cerebral [15O]water clearance in humans determined by PET: I. Theory and normal values, J.Cereb.Blood Flow Metab, *16:* 765-780, 1996.

Okazawa,H. and Kudo,T. Clinical impact of hemodynamic parameter measurement for cerebrovascular disease using positron emission tomography and (15)O-labeled tracers, Ann.Nucl.Med., *23:* 217-227, 2009.

Padhani,A.R., Krohn,K.A., Lewis,J.S. and Alber,M. Imaging oxygenation of human tumours, Eur.Radiol., *17:* 861-872, 2007.

Pals,M.A. and Swartz,H.M. Oxygen-dependent metabolism of potential magnetic resonance contrast agents, Invest Radiol., *22:* 497-501, 1987.

Park,W.H., Seol,J.G., Kim,E.S., Hyun,J.M., Jung,C.W., Lee,C.C., Kim,B.K. and Lee,Y.Y. Arsenic trioxide-mediated growth inhibition in MC/CAR myeloma cells via cell cycle arrest in association with induction of cyclin-dependent kinase inhibitor, p21, and apoptosis, Cancer Res., *60:* 3065-3071, 2000.

Pekar,J., Ligeti,L., Ruttner,Z., Lyon,R.C., Sinnwell,T.M., van,G.P., Fiat,D., Moonen,C.T. and McLaughlin,A.C. In vivo measurement of cerebral oxygen consumption and blood flow using 17O magnetic resonance imaging, Magn Reson.Med., *21:* 313-319, 1991.

Pelicano,H., Feng,L., Zhou,Y., Carew,J.S., Hileman,E.O., Plunkett,W., Keating,M.J. and Huang,P. Inhibition of mitochondrial respiration: a novel strategy to enhance drug-induced apoptosis in human leukemia cells by a reactive oxygen species-mediated mechanism, J.Biol.Chem., *278:* 37832-37839, 2003.

Peters,K.B., Wang,H., Brown,J.M. and Iliakis,G. Inhibition of DNA replication by tirapazamine, Cancer Res., *61:* 5425-5431, 2001.

Pilkington,G.J., Parker,K. and Murray,S.A. Approaches to mitochondrially mediated cancer therapy, Semin.Cancer Biol., *18:* 226-235, 2008.

Pizer,E.S., Jackisch,C., Wood,F.D., Pasternack,G.R., Davidson,N.E. and Kuhajda,F.P. Inhibition of fatty acid synthesis induces programmed cell death in human breast cancer cells, Cancer Res., *56:* 2745-2747, 1996.

Poulsen,P.H., Smith,D.F., Ostergaard,L., Danielsen,E.H., Gee,A., Hansen,S.B., Astrup,J. and Gjedde,A. In vivo estimation of cerebral blood flow, oxygen consumption and glucose metabolism in the pig by [15O]water injection, [15O]oxygen inhalation and dual injections of [18F]fluorodeoxyglucose, J.Neurosci.Methods, *77:* 199-209, 1997.

Prehn,R.T. The inhibition of tumor growth by tumor mass, Cancer Res., *51:* 2-4, 1991.

Presley,T., Kuppusamy,P., Zweier,J.L. and Ilangovan,G. Electron paramagnetic resonance oximetry as a quantitative method to measure cellular respiration: a consideration of oxygen diffusion interference, Biophys.J., *91:* 4623-4631, 2006.

Raichle,M.E., MacLeod,A.M., Snyder,A.Z., Powers,W.J., Gusnard,D.A. and Shulman,G.L. A default mode of brain function, Proc.Natl.Acad.Sci.U.S.A, *98:* 676-682, 2001.

Rajendran,J.G., Wilson,D.C., Conrad,E.U., Peterson,L.M., Bruckner,J.D., Rasey,J.S., Chin,L.K., Hofstrand,P.D., Grierson,J.R., Eary,J.F. and Krohn,K.A. [(18)F]FMISO and [(18)F]FDG PET imaging in soft tissue sarcomas: correlation of hypoxia, metabolism and VEGF expression, Eur.J.Nucl.Med.Mol.Imaging, *30:* 695-704, 2003.

Reich,G. Near-infrared spectroscopy and imaging: basic principles and pharmaceutical applications, Adv.Drug Deliv.Rev., *57:* 1109-1143, 2005.

Reynolds,T.Y., Rockwell,S. and Glazer,P.M. Genetic instability induced by the tumor microenvironment, Cancer Res., *56:* 5754-5757, 1996.

Riess,J.G. and Krafft,M.P. Fluorinated materials for in vivo oxygen transport (blood substitutes), diagnosis and drug delivery, Biomaterials, *19:* 1529-1539, 1998.

Riess,J.G. Understanding the fundamentals of perfluorocarbons and perfluorocarbon emulsions relevant to in vivo oxygen delivery, Artif.Cells Blood Substit.Immobil.Biotechnol., *33:* 47-63, 2005.

Rijpkema,M., Kaanders,J.H., Joosten,F.B., van der Kogel,A.J. and Heerschap,A. Effects of breathing a hyperoxic hypercapnic gas mixture on blood oxygenation and vascularity of head-and-neck tumors as measured by magnetic resonance imaging, Int.J.Radiat.Oncol.Biol.Phys., *53:* 1185-1191, 2002.

Rischin,D., Peters,L., Hicks,R., Hughes,P., Fisher,R., Hart,R., Sexton,M., D'Costa,I. and von,R.R. Phase I trial of concurrent tirapazamine, cisplatin, and radiotherapy in patients with advanced head and neck cancer, J.Clin.Oncol., *19:* 535-542, 2001.

Rischin,D., Peter,L., O'Sullivan,B., Giralt,J., Fisher,R., Yuen,K., Trotti,A., Bernier, J., Bourhis, J., Ringash,J., Henke,M and Kenny,L., Tirapazamine, Cisplatin, and radiation versus cisplatin and radiation for advanced squamous cell carcinoma of the head and neck (TROG 02.02, headSTART): a phase III trial of the trans-tasman radiation oncology group, J.Clin.Oncol., *18:* 2989-2995, 2010.

Robinson,S.P., Collingridge,D.R., Howe,F.A., Rodrigues,L.M., Chaplin,D.J. and Griffiths,J.R. Tumour response to hypercapnia and hyperoxia monitored by FLOOD magnetic resonance imaging, NMR Biomed., *12:* 98-106, 1999.

Robinson,S.P., Rijken,P.F., Howe,F.A., McSheehy,P.M., van der Sanden,B.P., Heerschap,A., Stubbs,M., van der Kogel,A.J. and Griffiths,J.R. Tumor vascular architecture and function evaluated by non-invasive susceptibility MRI methods and immunohistochemistry, J.Magn Reson.Imaging, *17:* 445-454, 2003.

Robinson,S.P. and Griffiths,J.R. Current issues in the utility of 19F nuclear magnetic resonance methodologies for the assessment of tumour hypoxia, Philos.Trans.R.Soc.Lond B Biol.Sci., *359:* 987-996, 2004.

Rockwell,S., Dobrucki,I.T., Kim,E.Y., Marrison,S.T. and Vu,V.T. Hypoxia and radiation therapy: past history, ongoing research, and future promise, Curr.Mol.Med., *9:* 442-458, 2009.

Rodrigues,L.M., Howe,F.A., Griffiths,J.R. and Robinson,S.P. Tumor R2* is a prognostic indicator of acute radiotherapeutic response in rodent tumors, J.Magn Reson.Imaging, *19:* 482-488, 2004.

Rodriguez-Enriquez,S., Juarez,O., Rodriguez-Zavala,J.S. and Moreno-Sanchez,R. Multisite control of the Crabtree effect in ascites hepatoma cells, Eur.J.Biochem., *268:* 2512-2519, 2001.

Rofstad,E.K. Microenvironment-induced cancer metastasis, Int.J.Radiat.Biol., *76:* 589-605, 2000.

Ruan,K., Song,G. and Ouyang,G. Role of hypoxia in the hallmarks of human cancer, J.Cell Biochem., *107:* 1053-1062, 2009.

Sakata,K., Kwok,T.T., Murphy,B.J., Laderoute,K.R., Gordon,G.R. and Sutherland,R.M. Hypoxia-induced drug resistance: comparison to P-glycoprotein-associated drug resistance, Br.J.Cancer, *64:* 809-814, 1991.

Scheller,K. and Sekeris,C.E. The effects of steroid hormones on the transcription of genes encoding enzymes of oxidative phosphorylation, Exp.Physiol, *88:* 129-140, 2003.

Schmaltz,C., Hardenbergh,P.H., Wells,A. and Fisher,D.E. Regulation of proliferation-survival decisions during tumor cell hypoxia, Mol.Cell Biol., *18:* 2845-2854, 1998.

Sealy,R., Harrison,G.G., Morrell,D., Korrubel,J., Gregory,A., Barry,L., Blekkenhorst,G., Hering,E.R., Fataar,A.B. and Boniaszczuk,J. A feasibility study of a new approach to clinical radiosensitisation: hypothermia and hyperbaric oxygen in combination with pharmacological vasodilatation, Br.J.Radiol., *59:* 1093-1098, 1986.

Secomb,T.W., Hsu,R., Ong,E.T., Gross,J.F. and Dewhirst,M.W. Analysis of the effects of oxygen supply and demand on hypoxic fraction in tumors, Acta Oncol., *34:* 313-316, 1995.

Secomb,T.W., Hsu,R. and Dewhirst,M.W. Synergistic effects of hyperoxic gas breathing and reduced oxygen consumption on tumor oxygenation: a theoretical model, Int.J.Radiat.Oncol.Biol.Phys., *59:* 572-578, 2004.

Seddon,B.M., Honess,D.J., Vojnovic,B., Tozer,G.M. and Workman,P. Measurement of tumor oxygenation: in vivo comparison of a luminescence fiber-optic sensor and a polarographic electrode in the p22 tumor, Radiat.Res., *155:* 837-846, 2001.

Semenza,G.L., Shimoda,L.A. and Prabhakar,N.R. Regulation of gene expression by HIF-1, Novartis.Found.Symp., *272:* 2-8, 2006.

Shannon,A.M., Bouchier-Hayes,D.J., Condron,C.M. and Toomey,D. Tumour hypoxia, chemotherapeutic resistance and hypoxia-related therapies, Cancer Treat.Rev., *29:* 297-307, 2003.

Shao,Q.S., Ye,Z.Y., Ling,Z.Q. and Ke,J.J. Cell cycle arrest and apoptotic cell death in cultured human gastric carcinoma cells mediated by arsenic trioxide, World J.Gastroenterol., *11:* 3451-3456, 2005.

Shen,Z.X., Chen,G.Q., Ni,J.H., Li,X.S., Xiong,S.M., Qiu,Q.Y., Zhu,J., Tang,W., Sun,G.L., Yang,K.Q., Chen,Y., Zhou,L., Fang,Z.W., Wang,Y.T., Ma,J., Zhang,P., Zhang,T.D., Chen,S.J., Chen,Z. and Wang,Z.Y. Use of arsenic trioxide (As2O3) in the treatment of acute promyelocytic leukemia (APL): II. Clinical efficacy and pharmacokinetics in relapsed patients, Blood, *89:* 3354-3360, 1997.

Shen,Z.Y., Tan,L.J., Cai,W.J., Shen,J., Chen,C., Tang,X.M. and Zheng,M.H. Arsenic trioxide induces apoptosis of oesophageal carcinoma in vitro, Int.J.Mol.Med., *4:* 33-37, 1999.

Shen,Z.Y., Shen,J., Cai,W.J., Hong,C. and Zheng,M.H. The alteration of mitochondria is an early event of arsenic trioxide induced apoptosis in esophageal carcinoma cells, Int.J.Mol.Med., *5:* 155-158, 2000.

Shen,Z.Y., Shen,J., Li,Q.S., Chen,C.Y., Chen,J.Y. and Yi,Z. Morphological and functional changes of mitochondria in apoptotic esophageal carcinoma cells induced by arsenic trioxide, World J.Gastroenterol., *8:* 31-35, 2002.

Shen,Z.Y., Shen,W.Y., Chen,M.H., Shen,J. and Zeng,Y. Reactive oxygen species and antioxidants in apoptosis of esophageal cancer cells induced by As2O3, Int.J.Mol.Med., *11:* 479-484, 2003.

Shen,Z.Y., Zhang,Y., Chen,J.Y., Chen,M.H., Shen,J., Luo,W.H. and Zeng,Y. Intratumoral injection of arsenic to enhance antitumor efficacy in human esophageal carcinoma cell xenografts, Oncol.Rep., *11:* 155-159, 2004.

Shoemaker,J.P. and Dagher,R.K. Remissions of mammary adenocarcinoma in hypothyroid mice given 5-fluorouracil and chloroquine phosphate, J.Natl.Cancer Inst., *62:* 1575-1578, 1979.

Siim,B.G., van Zijl,P.L. and Brown,J.M. Tirapazamine-induced DNA damage measured using the comet assay correlates with cytotoxicity towards hypoxic tumour cells in vitro, Br.J.Cancer, *73:* 952-960, 1996.

Simoes,R.V., gado-Goni,T., Lope-Piedrafita,S. and Arus,C. 1H-MRSI pattern perturbation in a mouse glioma: the effects of acute hyperglycemia and moderate hypothermia, NMR Biomed., *23:* 23-33, 2010.

Simon,N., Jolliet,P., Morin,C., Zini,R., Urien,S. and Tillement,J.P. Glucocorticoids decrease cytochrome c oxidase activity of isolated rat kidney mitochondria, FEBS Lett., *435:* 25-28, 1998.

Smolkova,K., Bellance,N., Scandurra,F., Genot,E., Gnaiger,E., Plecita-Hlavata,L., Jezek,P. and Rossignol,R. Mitochondrial bioenergetic adaptations of breast cancer cells to aglycemia and hypoxia, J.Bioenerg.Biomembr., *42:* 55-67, 2010.

Snyder,S.A., Lanzen,J.L., Braun,R.D., Rosner,G., Secomb,T.W., Biaglow,J., Brizel,D.M. and Dewhirst,M.W. Simultaneous administration of glucose and hyperoxic gas achieves greater improvement in tumor oxygenation than hyperoxic gas alone, Int.J.Radiat.Oncol.Biol.Phys., *51:* 494-506, 2001.

Soengas,M.S., Alarcon,R.M., Yoshida,H., Giaccia,A.J., Hakem,R., Mak,T.W. and Lowe,S.W. Apaf-1 and caspase-9 in p53-dependent apoptosis and tumor inhibition, Science, *284:* 156-159, 1999.

Soignet,S.L., Maslak,P., Wang,Z.G., Jhanwar,S., Calleja,E., Dardashti,L.J., Corso,D., DeBlasio,A., Gabrilove,J., Scheinberg,D.A., Pandolfi,P.P. and Warrell,R.P., Jr. Complete remission after treatment of acute promyelocytic leukemia with arsenic trioxide, N.Engl.J.Med., *339:* 1341-1348, 1998.

Somasundaram,S., Rafi,S., Hayllar,J., Sigthorsson,G., Jacob,M., Price,A.B., Macpherson,A., Mahmod,T., Scott,D., Wrigglesworth,J.M. and Bjarnason,I. Mitochondrial damage: a possible mechanism of the "topical" phase of NSAID induced injury to the rat intestine, Gut, *41:* 344-353, 1997.

Song,Y., Kim,J.G., Mason,R.P., and Liu,H. Investigation of rat breast tumour oxygen consumption by near-infrared spectroscopy, J.Phys.D:Appl.Phys, *38:* 2682-2690, 2005.

Subramanian,S., Yamada,K., Irie,A., Murugesan,R., Cook,J.A., Devasahayam,N., Van Dam,G.M., Mitchell,J.B. and Krishna,M.C. Noninvasive in vivo oximetric imaging by radiofrequency FT EPR, Magn Reson.Med., *47:* 1001-1008, 2002.

Sumi,D., Shinkai,Y. and Kumagai,Y. Signal transduction pathways and transcription factors triggered by arsenic trioxide in leukemia cells, Toxicol.Appl.Pharmacol., *244:* 385-392, 2010.

Swartz,H.M. and Clarkson,R.B. The measurement of oxygen in vivo using EPR techniques, Phys.Med.Biol., *43:* 1957-1975, 1998.

Swartz,H.M. Measuring real levels of oxygen in vivo: opportunities and challenges, Biochem.Soc.Trans., *30:* 248-252, 2002.

Swartz,H.M. Using EPR to measure a critical but often unmeasured component of oxidative damage: oxygen, Antioxid.Redox.Signal., *6:* 677-686, 2004a.

Swartz,H.M., Khan,N., Buckey,J., Comi,R., Gould,L., Grinberg,O., Hartford,A., Hopf,H., Hou,H., Hug,E., Iwasaki,A., Lesniewski,P., Salikhov,I. and Walczak,T. Clinical applications of EPR: overview and perspectives, NMR Biomed., *17:* 335-351, 2004b.

Swietach,P., Patiar,S., Supuran,C.T., Harris,A.L. and Vaughan-Jones,R.D. The role of carbonic anhydrase 9 in regulating extracellular and intracellular ph in three-dimensional tumor cell growths, J.Biol.Chem., *284:* 20299-20310, 2009.

Tailor,D.R., Baumgardner,J.E., Regatte,R.R., Leigh,J.S. and Reddy,R. Proton MRI of metabolically produced H2 17O using an efficient 17O2 delivery system, Neuroimage., *22:* 611-618, 2004.

Tannock,I.F. The relation between cell proliferation and the vascular system in a transplanted mouse mammary tumour, Br.J.Cancer, *22:* 258-273, 1968.

Tatum,J.L., Kelloff,G.J., Gillies,R.J., Arbeit,J.M., Brown,J.M., Chao,K.S., Chapman,J.D., Eckelman,W.C., Fyles,A.W., Giaccia,A.J., Hill,R.P., Koch,C.J., Krishna,M.C., Krohn,K.A., Lewis,J.S., Mason,R.P., Melillo,G., Padhani,A.R., Powis,G., Rajendran,J.G., Reba,R., Robinson,S.P., Semenza,G.L., Swartz,H.M., Vaupel,P., Yang,D., Croft,B., Hoffman,J., Liu,G., Stone,H. and Sullivan,D. Hypoxia: importance in tumor biology, noninvasive measurement by imaging, and value of its measurement in the management of cancer therapy, Int.J.Radiat.Biol., *82:* 699-757, 2006.

Taylor,N.J., Baddeley,H., Goodchild,K.A., Powell,M.E., Thoumine,M., Culver,L.A., Stirling,J.J., Saunders,M.I., Hoskin,P.J., Phillips,H., Padhani,A.R. and Griffiths,J.R. BOLD MRI of human tumor oxygenation during carbogen breathing, J.Magn Reson.Imaging, *14:* 156-163, 2001.

Teicher,B.A., Holden,S.A., al-Achi,A. and Herman,T.S. Classification of antineoplastic treatments by their differential toxicity toward putative oxygenated and hypoxic tumor subpopulations in vivo in the FSaIIC murine fibrosarcoma, Cancer Res., *50:* 3339-3344, 1990.

Theodossiou,C., Skrepnik,N., Robert,E.G., Prasad,C., Axelrad,T.W., Schapira,D.V. and Hunt,J.D. Propylthiouracil-induced hypothyroidism reduces xenograft tumor growth in athymic nude mice, Cancer, *86:* 1596-1601, 1999.

Thews,O., Kelleher,D.K., Hummel,M. and Vaupel,P. Can tumor oxygenation be improved by reducing cellular oxygen consumption, Adv.Exp.Med.Biol., *471:* 525-532, 1999.

Thomlinson,R.H. and Gray,L.H. The histological structure of some human lung cancers and the possible implications for radiotherapy, Br.J.Cancer, *9:* 539-549, 1955.

Tietze,F. Enzymic method for quantitative determination of nanogram amounts of total and oxidized glutathione: applications to mammalian blood and other tissues, Anal.Biochem., *27:* 502-522, 1969.

Tredan,O., Galmarini,C.M., Patel,K. and Tannock,I.F. Drug resistance and the solid tumor microenvironment, J.Natl.Cancer Inst., *99:* 1441-1454, 2007.

Vander Heiden,M.G., Cantley,L.C. and Thompson,C.B. Understanding the Warburg effect: the metabolic requirements of cell proliferation, Science, *324:* 1029-1033, 2009.

Vaupel,P., Kallinowski,F. and Okunieff,P. Blood flow, oxygen and nutrient supply, and metabolic microenvironment of human tumors: a review, Cancer Res., *49:* 6449-6465, 1989.

Vaupel,P., Schlenger,K., Knoop,C. and Hockel,M. Oxygenation of human tumors: evaluation of tissue oxygen distribution in breast cancers by computerized O2 tension measurements, Cancer Res., *51:* 3316-3322, 1991.

Vaupel,P., Thews,O. and Hoeckel,M. Treatment resistance of solid tumors: role of hypoxia and anemia, Med.Oncol., *18:* 243-259, 2001.

Vaupel,P. and Harrison,L. Tumor hypoxia: causative factors, compensatory mechanisms, and cellular response, Oncologist., *9 Suppl 5:* 4-9, 2004a.

Vaupel,P., Mayer,A. and Hockel,M. Tumor hypoxia and malignant progression, Methods Enzymol., *381:* 335-354, 2004b.

Vaupel,P. Tumor microenvironmental physiology and its implications for radiation oncology, Semin.Radiat.Oncol., *14:* 198-206, 2004c.

Vaupel,P. The role of hypoxia-induced factors in tumor progression, Oncologist., *9 Suppl 5:* 10-17, 2004d.

Vaupel,P. and Mayer,A. Hypoxia and anemia: effects on tumor biology and treatment resistance, Transfus.Clin.Biol., *12:* 5-10, 2005.

Vaupel,P. and Mayer,A. Hypoxia in cancer: significance and impact on clinical outcome, Cancer Metastasis Rev., *26:* 225-239, 2007.

Verrax,J., Delvaux,M., Beghein,N., Taper,H., Gallez,B. and Buc,C.P. Enhancement of quinone redox cycling by ascorbate induces a caspase-3 independent cell death in

human leukaemia cells. An in vitro comparative study, Free Radic.Res., *39:* 649-657, 2005.

Vikram,D.S., Zweier,J.L. and Kuppusamy,P. Methods for noninvasive imaging of tissue hypoxia, Antioxid.Redox.Signal., *9:* 1745-1756, 2007.

Von Heimburg,H.D., Hemmrich,K., Zachariah,S., Staiger,H. and Pallua,N. Oxygen consumption in undifferentiated versus differentiated adipogenic mesenchymal precursor cells, Respir.Physiol Neurobiol., *146:* 107-116, 2005.

Von Pauwel,P.J., von Roemeling,R.R., Gatzemeier,U., Boyer,M., Elisson,L.O., Clark,P., Talbot,D., Rey,A., Butler,T.W., Hirsh,V., Olver,I., Bergman,B., Ayoub,J., Richardson,G., Dunlop,D., Arcenas,A., Vescio,R., Viallet,J. and Treat,J. Tirapazamine plus cisplatin versus cisplatin in advanced non-small-cell lung cancer: A report of the international CATAPULT I study group. Cisplatin and Tirapazamine in Subjects with Advanced Previously Untreated Non-Small-Cell Lung Tumors, J.Clin.Oncol., *18:* 1351-1359, 2000.

Wang,Y., An,R., Dong,X., Pan,S., Duan,G. and Sun,X. Protein kinase C is involved in arsenic trioxide-induced apoptosis and inhibition of proliferation in human bladder cancer cells, Urol.Int., *82:* 214-221, 2009.

Warburg,O. On the origin of cancer cells, Science, *123:* 309-314, 1956.

Wen,B., Urano,M., Humm,J.L., Seshan,V.E., Li,G.C. and Ling,C.C. Comparison of Helzel and OxyLite systems in the measurements of tumor partial oxygen pressure (pO2), Radiat.Res., *169:* 67-75, 2008.

Wiest,J., Schmidhuber,M., Ressler,J., Scholz,A., Brischwein,M., Wolf,B. Cell based assays for diagnostic and therapy on multiparametric biosensor chips with an intelligent mobile lab, IFMBE Proc., *10:* 132-135, 2005.

Williams,B.B., Khan,N., Zaki,B., Hartford,A., Ernstoff,M.S. and Swartz,H.M. Clinical electron paramagnetic resonance (EPR) oximetry using India ink, Adv.Exp.Med.Biol., *662:* 149-156, 2010.

Wojtczak,L. The Crabtree effect: a new look at the old problem, Acta Biochim.Pol., *43:* 361-368, 1996.

Woo,S.H., Park,I.C., Park,M.J., Lee,H.C., Lee,S.J., Chun,Y.J., Lee,S.H., Hong,S.I. and Rhee,C.H. Arsenic trioxide induces apoptosis through a reactive oxygen species-dependent pathway and loss of mitochondrial membrane potential in HeLa cells, Int.J.Oncol., *21:* 57-63, 2002.

Wroblewski,F. and Ladue,J.S. Lactic dehydrogenase activity in blood, Proc.Soc.Exp.Biol.Med., *90:* 210-213, 1955.

Wrutniak-Cabello,C., Casas,F. and Cabello,G. Thyroid hormone action in mitochondria, J.Mol.Endocrinol., *26:* 67-77, 2001.

Xia,M., Kodibagkar,V., Liu,H. and Mason,R.P. Tumour oxygen dynamics measured simultaneously by near-infrared spectroscopy and 19F magnetic resonance imaging in rats, Phys.Med.Biol., *51:* 45-60, 2006.

Xiao,Y.F., Liu,S.X., Wu,D.D., Chen,X. and Ren,L.F. Inhibitory effect of arsenic trioxide on angiogenesis and expression of vascular endothelial growth factor in gastric cancer, World J.Gastroenterol., *12:* 5780-5786, 2006.

Xiao,Y.F., Wu,D.D., Liu,S.X., Chen,X. and Ren,L.F. Effect of arsenic trioxide on vascular endothelial cell proliferation and expression of vascular endothelial growth factor receptors Flt-1 and KDR in gastric cancer in nude mice, World J.Gastroenterol., *13:* 6498-6505, 2007.

Xie,L.X., Lin,X.H., Li,D.R., Chen,J.Y., Hong,C.Q. and Du,C.W. Synergistic therapeutic effect of arsenic trioxide and radiotherapy in BALB/C nude mice bearing nasopharyngeal carcinoma xenografts, Exp.Oncol., *29:* 45-48, 2007.

Yablonskiy,D.A. and Haacke,E.M. Theory of NMR signal behavior in magnetically inhomogeneous tissues: the static dephasing regime, Magn Reson.Med., *32:* 749-763, 1994.

Yablonskiy,D.A. Quantitation of intrinsic magnetic susceptibility-related effects in a tissue matrix. Phantom study, Magn Reson.Med., *39:* 417-428, 1998.

Yeh,S.H., Liu,R.S., Wu,L.C., Yang,D.J., Yen,S.H., Chang,C.W., Yu,T.W., Chou,K.L. and Chen,K.Y. Fluorine-18 fluoromisonidazole tumour to muscle retention ratio for the detection of hypoxia in nasopharyngeal carcinoma, Eur.J.Nucl.Med., *23:* 1378-1383, 1996.

Yuan,J. and Glazer,P.M. Mutagenesis induced by the tumor microenvironment, Mutat.Res., *400:* 439-446, 1998.

Yuan,J., Narayanan,L., Rockwell,S. and Glazer,P.M. Diminished DNA repair and elevated mutagenesis in mammalian cells exposed to hypoxia and low pH, Cancer Res., *60:* 4372-4376, 2000.

Zhao,D., Constantinescu,A., Jiang,L., Hahn,E.W. and Mason,R.P. Prognostic radiology: quantitative assessment of tumor oxygen dynamics by MRI, Am.J.Clin.Oncol., *24:* 462-466, 2001a.

Zhao,D., Constantinescu,A., Hahn,E.W. and Mason,R.P. Tumor oxygen dynamics with respect to growth and respiratory challenge: investigation of the Dunning prostate R3327-HI tumor, Radiat.Res., *156:* 510-520, 2001b.

Zhao,D., Constantinescu,A., Hahn,E.W. and Mason,R.P. Differential oxygen dynamics in two diverse Dunning prostate R3327 rat tumor sublines (MAT-Lu and HI) with respect to growth and respiratory challenge, Int.J.Radiat.Oncol.Biol.Phys., *53:* 744-756, 2002.

Zhao,D., Jiang,L., Hahn,E.W. and Mason,R.P. Comparison of 1H blood oxygen level-dependent (BOLD) and 19F MRI to investigate tumor oxygenation, Magn Reson.Med., *62:* 357-364, 2009.

Zhao,X.S., Song,P.L., Sun,B., Jiang,H.C. and Liu,T.F. Arsenic trioxide inhibits metastatic potential of mouse hepatoma H22 cells in vitro and in vivo, Hepatobiliary.Pancreat.Dis.Int., *8:* 510-517, 2009.

Zhou,R., Bansal,N., Leeper,D.B. and Glickson,J.D. Intracellular acidification of human melanoma xenografts by the respiratory inhibitor m-iodobenzylguanidine plus hyperglycemia: a 31P magnetic resonance spectroscopy study, Cancer Res., *60:* 3532-3536, 2000.

Zhu,X.H., Shen,Y.L., Jing,Y.K., Cai,X., Jia,P.M., Huang,Y., Tang,W., Shi,G.Y., Sun,Y.P., Dai,J., Wang,Z.Y., Chen,S.J., Zhang,T.D., Waxman,S., Chen,Z. and Chen,G.Q. Apoptosis and growth inhibition in malignant lymphocytes after treatment with arsenic trioxide at clinically achievable concentrations, J.Natl.Cancer Inst., *91:* 772-778, 1999.

Zhu,X.H., Zhang,Y., Tian,R.X., Lei,H., Zhang,N., Zhang,X., Merkle,H., Ugurbil,K. and Chen,W. Development of (17)O NMR approach for fast imaging of cerebral metabolic rate of oxygen in rat brain at high field, Proc.Natl.Acad.Sci.U.S.A, *99:* 13194-13199, 2002.

Zhu,X., Zhang,X., Chen,W. Study of 17O NMR sensitivity and relaxation times of cerebral water in human at 7 tesla, Proc.Intl.Soc.Mag.Reson.Med.11, 2003.

Zhu,X.H., Zhang,N., Zhang,Y., Zhang,X., Ugurbil,K. and Chen,W. In vivo 17O NMR approaches for brain study at high field, NMR Biomed., *18:* 83-103, 2005.

Zhu,X.H., Zhang,Y., Zhang,N., Ugurbil,K. and Chen,W. Noninvasive and three-dimensional imaging of CMRO(2) in rats at 9.4 T: reproducibility test and normothermia/hypothermia comparison study, J.Cereb.Blood Flow Metab, *27:* 1225-1234, 2007.

Zhu,X.H., Zhang,N., Zhang,Y., Ugurbil,K. and Chen,W. New insights into central roles of cerebral oxygen metabolism in the resting and stimulus-evoked brain, J.Cereb.Blood Flow Metab, *29:* 10-18, 2009.

Ziegler,S.I. Positron emission tomography: principles, technology, and recent developments, Nuclear Physics A *752:* 679c-687c, 2005.